Graduate School ETD Form 9
(Revised 12/07)

PURDUE UNIVERSITY
GRADUATE SCHOOL
Thesis/Dissertation Acceptance

This is to certify that the thesis/dissertation prepared

By Shuning Li

Entitled
THREE-DIMENSIONAL IMAGE ANALYSIS FOR QUANTIFICATION OF TOOTH MOVEMENTS AND LANDMARK CHANGES

For the degree of Doctor of Philosophy

Is approved by the final examining committee:

Jie Chen (Co-chair)
Chair

Douglas Adams

Anil K. Bajaj (Co-chair)

Thomas R. Katona

Lauren Christopher

To the best of my knowledge and as understood by the student in the *Research Integrity and Copyright Disclaimer (Graduate School Form 20)*, this thesis/dissertation adheres to the provisions of Purdue University's "Policy on Integrity in Research" and the use of copyrighted material.

Approved by Major Professor(s): Jie Chen

Approved by: David C. Anderson 04/23/2013
Head of the Graduate Program Date

THREE-DIMENSIONAL IMAGE ANALYSIS FOR QUANTIFICATION OF TOOTH MOVEMENTS AND LANDMARK CHANGES

A Dissertation

Submitted to the Faculty

of

Purdue University

by

Shuning Li

In Partial Fulfillment of the

Requirements for the Degree

of

Doctor of Philosophy

May 2013

Purdue University

Indianapolis, Indiana

To my parents, my husband Anli, and my daughter Sophia

ACKNOWLEDGMENT

I would like to gratefully acknowledge my research advisor, Dr. Jie Chen, for his assistance, guidance, and supervision during the entire course of this research and dissertation work. Dr. Chen generously shared with me his research experience and showed me his pursuit of perfection in every single detail, for with I am always thankful.

I would like to thank my advisory committee members, Dr. Anil K. Bajaj, Dr. Douglas Adams, Dr. Thomas Katona, and Dr. Lauren Christopher for their time and insight during the completion of this dissertation.

I would like to extend my special thanks to Dr. Katherine Kula and Dr. Sean Shih-Yao Liu from Indiana University School of Dentistry for their valuable contributions and insightful discussions that led to successful completion of this research. Dr. Kula and Dr. Liu helped to manage the clinical part of this study from patient recruiting to patient treatment. They also provide important suggestions from the orthodontists' point of view.

I would also like to thank my co-workers, Mr. Feifei Jiang and Dr. Zeyang Xia, for their help and support during my Ph. D study. I thank Ms. Valerie Lim Diemer for assisting me in formatting this dissertation.

Finally, I would express my gratitude to my parents, my husband Anli for their support and encouragement during my life. I would like to specially thank my daughter, Sophia. She is my source of energy, and she is the reason that I can achieve this accomplishment.

TABLE OF CONTENTS

Page

Page

LIST OF TABLES

Table Page

Table Page

LIST OF FIGURES

Figure Page

Figure Page

Figure Page

ABSTRACT

Li, Shuning. Ph.D., Purdue University, May 2013. Three-dimensional Image Analysis for Quantification of Tooth Movements and Landmark Changes. Major Professors: Jie Chen, Purdue School of Engineering and Technology and Anil K. Bajaj, School of Mechanical Engineering.

Quantification of treatment outcomes (tooth displacement and bony changes) is the key to advance orthodontic research and improve clinical practices. Traditionally, treatment outcome were quantified by using two-dimensional (2D) cephalometric analysis. However, there are problems inherent in 2D analysis, such as tracing errors and inability to detect side-effects. Thus, a reliable three-dimensional (3D) image analysis method for treatment outcome quantification is of high interest.

Systematic 3D image analysis methods were developed for digital dental cast models and Cone-Beam Computed Tomography (CBCT) models. A typical analysis procedure includes image reconstruction, landmarks identification, coordinate system setup, superimposition, and displacement or change calculation. The specified procedures for maxillary teeth displacements and anatomical landmarks movements were presented and validated. The validation results showed that these procedures were accurate and reliable enough for clinical applications.

The 3D methods were first applied to a human canine retraction clinical study. The purposes of this study were to quantify canines and anchorage tooth movements, and to compare two commonly used canine retraction strategies, controlled tipping and translation. The canine results showed that (1) canine movements were linear with time;

(2) the initial load system was not the only factor that controlled the canine movement pattern; and (3) control tipping was significantly faster than translation. The anchorage tooth results showed that (1) anchorage losses occurred even with transpalatal arch (TPA); (2) there was no significant difference in anchorage loss between the two treatment strategies; and (3) compared with removable TPA, fixed TPA appliance can significantly reduce the amount of anchorage loss in the mesial-distal direction.

The second clinical application for the 3D methods was a mandibular growth clinical trial. The purposes of this study were to quantify skeletal landmark movements, and compare two widely used appliances, Herbst and MARA. The results showed that (1) the Herbst appliance caused mandibular forward movement with backward rotation; and (2) the treatment effects had no significant differences by using either Herbst or MARA appliances.

The two clinical applications validated the methods developed in this study to quantify orthodontic treatment outcomes. They also demonstrated the benefits of using the 3D methods to quantify orthodontic treatment outcomes and to test fundamental hypotheses. These 3D methods can easily be extended to other clinical cases. This study will benefit orthodontic patients, clinicians and researchers.

1. INTRODUCTION

1.1. Problem Statement

Orthodontics relies primarily on the clinical experiences of orthodontists. Many orthodontic theories in orthodontics were developed from trial and error assessments and best guesses, and have rarely been validated scientifically mainly because there is no reliable method to quantitatively evaluation treatment outcomes (e.g. tooth displacements and bony changes).

Traditionally, tooth displacements and bony changes were quantified with two-dimensional (2D) cephalometric analyses. With the introduction of radiologic imaging on live subjects in the 1930s, many kinds of cephalometric analyses have been developed, that are still in use [1]. The basis of the analyses is identification of anatomic structures as landmark points. These points are projected onto the sagittal plane and connected to form lines and contours that are measured to show the locations or the interrelations of the maxilla, mandible, skull base, and dentition. These measurements can be compared to established "normal" data, or to serial cephalograms longitudinally to assess the changes from treatment and/or growth. The disadvantages of 2D cephalometric analysis are tracing and landmark identification errors, and inability to detect side-effects, such as undesired displacement components, the displacement components in the directions perpendicular to the direction of movement. Desired tooth displacement components are those that move the tooth into its treatment target position, while undesired displacement components should be detected because their correction prolongs treatment time.

New three dimensional (3D) imaging technologies provide 3D views of anatomical structures. However, there are no widely accepted 3D representations of

clinical parameters and reliable methods of treatment outcomes quantification. Thus, 2D images are being extracted from the 3D scans for traditional clinical evaluations which do not fully utilize the rich information embedded in the 3D scan. With the development of modeling techniques, 3D digital models can be used to quantify treatment outcomes and to determine side-effects that are undetectable in 2D. Three dimensional approaches can be used to evaluate treatment strategies and orthodontic appliances and as the basis for evidence in the design of new appliances and treatment planning.

Thus, the goals of this study are to quantify orthodontic treatment outcomes and side effects by developing feasible 3D image analysis methods. This study will benefit the orthodontic patient, clinician and researcher.

1.2. Anatomical Nomenclatures

The human skull anatomical structures used in this study are shown in Figure 1.1:(a) a human skull; (b) some of the skeletal landmarks used in cephalometric analysis; (c) a maxillary dental cast; and (d) the superior view of the cranial base in a Cone-Beam Computed Tomography (CBCT) scan.

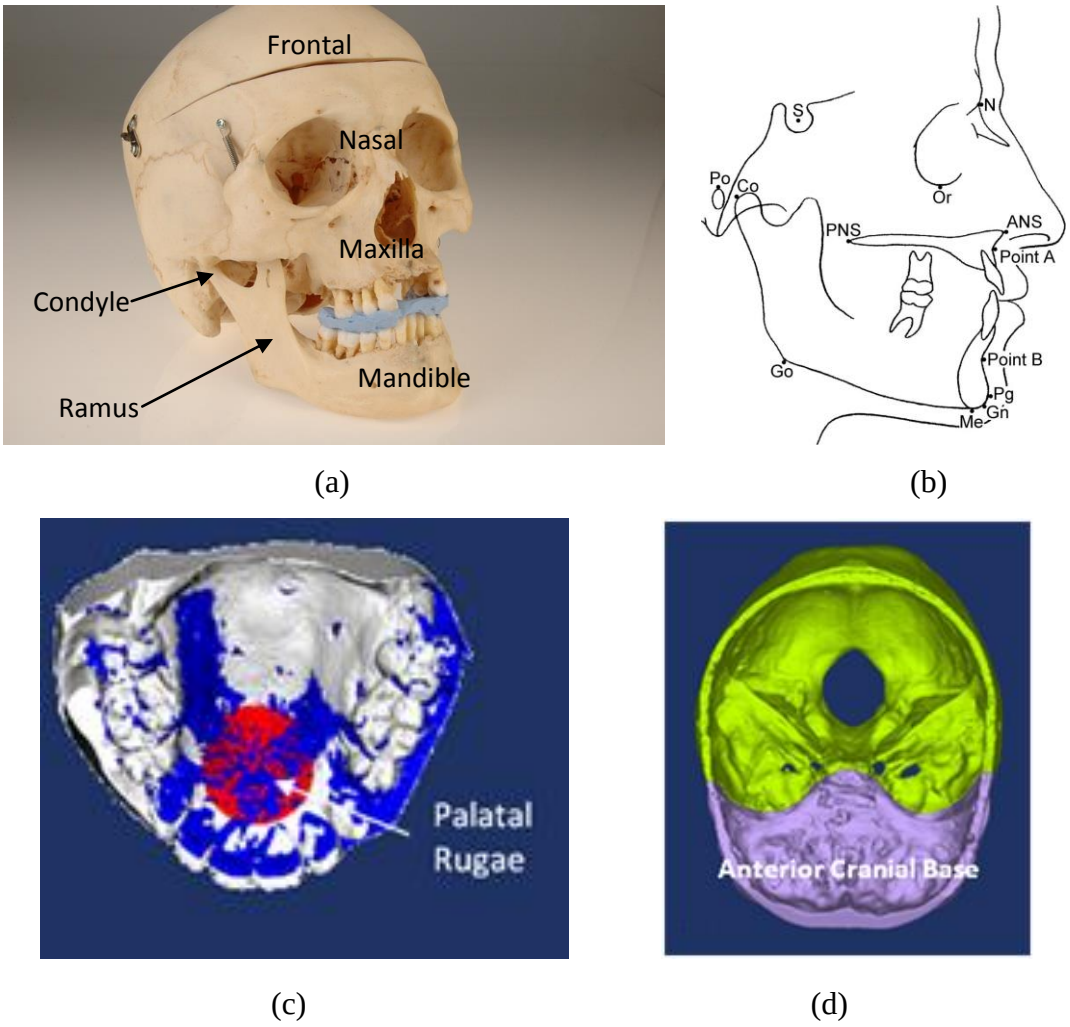

(a) (b)

(c) (d)

Figure 1.1. Anatomical nomenclatures.

1.3. Objectives

The overall goal of this study is to quantify orthodontic treatment outcomes and side-effects by using 3D image analysis methods, and to show the feasibility of using quantified treatment outcomes to test important hypotheses in orthodontics.

The specific objectives of this study are to

- Develop methods to quantify the 3D displacements of tooth and anatomical landmarks
- Experimentally assess the accuracy and variation of the displacement calculation

- Express the calculated results in conventional clinical terms and parameters
- Quantify treatment outcomes with the new methods, and
- Test some orthodontic hypotheses using two clinical cases.

1.4. Scopes of Study

1.4.1. 3D Image Analysis Methods (Chapter 3)

In Chapter 3, a general scheme for 3D image analysis is presented. The scheme includes image reconstruction, a coordinate system convention, superimposition, and anatomical change calculation. Based on the selection of 3D models and the clinical applications, three 3D image analysis procedures were developed, and their accuracy and reliability were validated.

1.4.2. 3D Image Analysis in a Canine Retraction Study (Chapter 4)

3D image analysis was applied to a canine retraction clinical trial. Two commonly used canine retraction strategies were implemented concurrently in patients. The movement of maxillary canines and anchorage teeth (1^{st} molars and 2^{nd} premolars) were quantified using the procedures presented in Chapter 3. Six hypotheses were proposed and tested. The hypotheses involved the relationship between canine movement and treatment time; the relationship between canine movements and orthodontic force systems; the comparison between two canine retraction strategies in terms of canine movement rate and anchorage loss; and the comparison between two anchorage control appliances.

1.4.3. 3D Image Analysis in a Mandibular Growth Study (Chapter 5)

3D image analysis was applied to a mandibular growth clinical trial. In this randomized controlled clinical trial, growing patients with mandibular deficiency were

treated by using either Mandibular Anterior Reposition Appliance (MARA) or Herbst appliances. The movements of selected skeletal landmarks were quantified. Two hypotheses were proposed and tested. One of the hypotheses was about the side-effects caused by the Herbst appliance, the other was about the landmark movements associated with the two appliances.

2. LITERATURE REVIEW

2.1. Medical Imaging in Orthodontics

Medical imaging is an important tool with a large number of applications in orthodontics. Orthodontists can use it not only for clinical diagnosis, but also for treatment planning and outcome evaluation. It helps researchers understand malocclusion and the relationships between important craniofacial structures.

Orthodontists, dentists, and researchers have been relying on medical imaging to diagnose malocclusion and to plan treatment. The extraoral methods include panoramic radiographs, cephalometric radiographs, digital dental cast and Cone-Beam Computed Tomography (CBCT).

2.1.1. Panoramic Radiographs

Panoramic radiography, also called orthopantomogram (OPG) is a simplified extraoral procedure to visualize maxilla and mandible on a single image [2-3] (Figure 2.1).

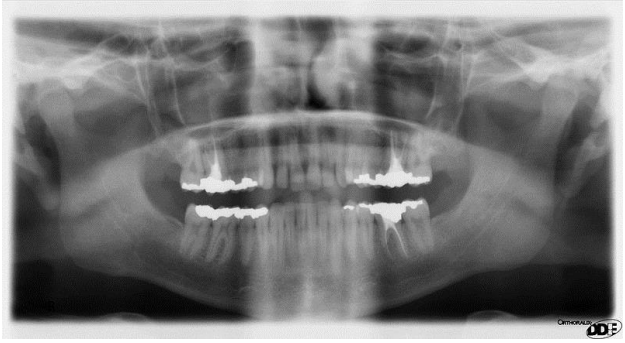

Figure 2.1. Panoramic radiographs.

Panoramic radiographs show a 2D view of a half-circle from ear to ear. The most important advantage of panoramic radiographs is the broader coverage of facial bones and teeth than conventional intraoral radiographs [4-7]. A panoramic radiograph is often taken at the first visit to provide information for diagnosis and treatment planning. It can be used to (1) determine the status of the impacted wisdom teeth; (2) help find the cause of dental pain; (3) assess the placement of dental implant; (4) detect caries. However, it has limitations of panoramic radiographs, such as blurring, distortion, and variations in horizontal image magnification, leading to a relatively poor definition of the structures compared to intraoral radiographs.

2.1.2. Cephalometric Analysis

Many early studies focused on 2D cephalometric analysis. Several analyses, based on different sets of measurements, have been developed [8-11]. The Downs (1956) analysis uses the Frankfort horizontal (FH) as its reference plane [1, 8]. It relates the central incisors to each other and to the occlusal and mandibular planes (Figure 2.2 (a)). The Steiner (1960) analysis uses the sella-nasion cranial base plane as its central reference [1, 9]. Steiner described the chin position relative to the mandible and the relationship between the occlusal plane and the sella-nasion. He also related the maxillary and mandibular central incisors to their respective bones in both linear and angular measures (Figure 2.2 (b)). Basic definitions and descriptions in the Steiner analysis are used today. The Ricketts (1961) analysis also used the Frankfort horizontal as its reference plane [1, 10]. He defined and measured the facial contour by comparing the N-Pg plane to the FH-A perpendicular (Figure 2.2 (c)).

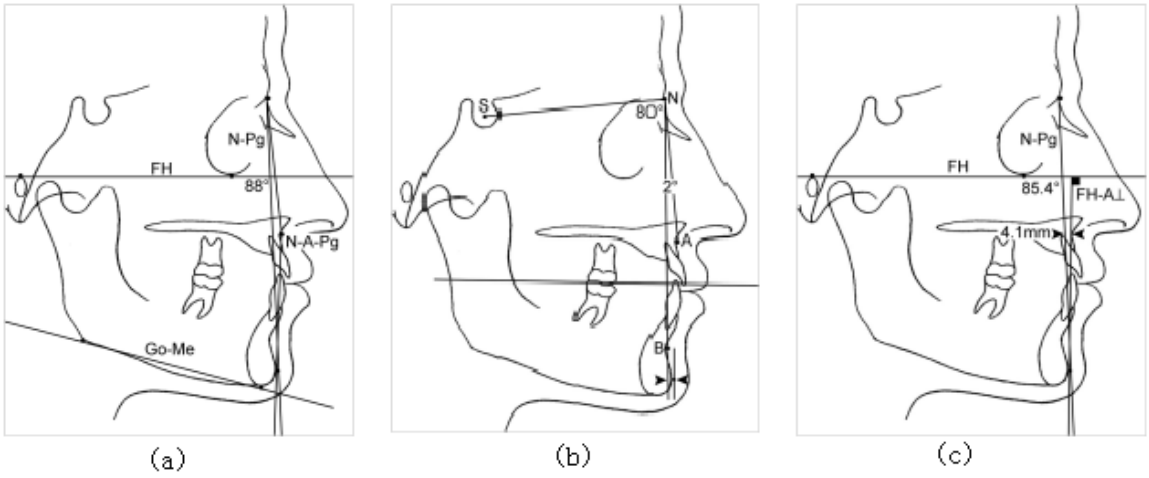

Figure 2.2. Cephalometric analysis [1].
(a) Downs analysis, (b) Steiner analysis, and (c) Ricketts analysis

Superimposition of serial cephalograms is used to trace an individual's facial changes due to growth and/or orthodontic treatment at different time points [12-13]. The changes are from a combination of growth and orthodontic treatment in patients receiving orthodontic therapy [11]. The most commonly used method to assess the overall change pattern of the face was suggested by Steiner [14]. This method superimposed on anterior cranial base along the sella-nasion (SN) line and registered at sella (Figure 1.1 (b)). In traditional "best-fit" method, maxillary analysis was done by superimposing along the palatal plane from anterior nasal spine (ANS, Figure 1.1 (b)) to posterior nasal spine (PNS, Figure 1.1 (b)) with registration at ANS. Mandibular superimposition was on the lower border of the mandible with registration at the chin [15-16]. Björk and Skieller examined maxillary and mandibular growth by using metallic implants inserted into the jaws as fixed references [17-19]. Their studies showed that the "best-fit" method had problems when applied to growing patient. The superimposition method they proposed was called "structural" method [20-21], which chose stable structures, such as the anterior cranial base and the anterior portion of the chin as references for superimposition. Figure 2.3 show the three major cephalometric superimpositions. Figure 2.3 (a) is superimposition on anterior cranial base along the SN line. This superimposition shows the overall change patterns of the face. Figure 2.3 (b) is superimposition on maxilla, and it shows the maxillary teeth changes relative to maxilla.

Figure 2.3 (c) is superimposition on mandible. This superimposition shows changes in condyle (Figure 1.1 (a)) and mandibular teeth relative to the mandible.

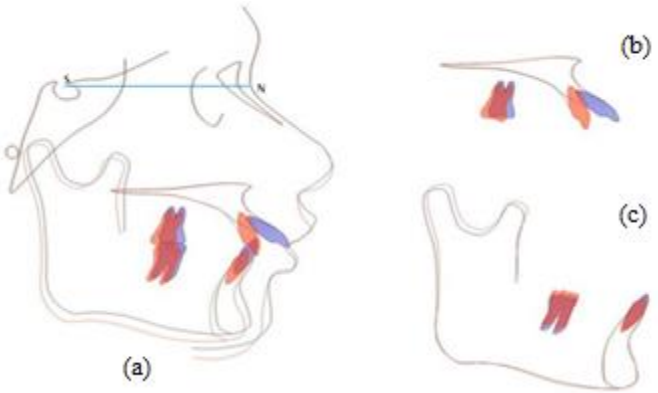

Figure 2.3. Three major cephalometric superimpositions [11].

Although 2D cephalometric analyses are widely used, they have several limitations [1, 22] They are (1) unable to reveal details in the complex 3D structures; (2) inconsistent due to head misalignments; (3) unable to take into account the left-right asymmetry of the head; (4) inconsistent in landmark location and identification; and (5) prone to errors in manual data collection and processing.

2.1.3. Three-dimensional (3D) Imaging

3D techniques overcome some of the limitations of 2D methods and imaging technologies have been developed to acquire, visualize, and quantify information from Cone-Beam Computed Tomography (CBCT).

2.1.3.1. Digital Dental Casts

Dental casts are the traditional 3D dental records for measuring clinical outcomes. It is widely used to identify changes in the dental arch. Several groups developed methods to analyze 3D tooth displacements with dental casts [23-26]. Commer et al. (2000) have measured tooth displacements by laser scanning plastic casts [23]. Their

measurements showed a maximum deviation of about 0.2 mm, but they relied on artificial reference points. In reality, however, it is a serious challenge to find clear and stable reference surfaces and points.

Ashmore et al. (2002) have developed a mathematical method for superimposing 3D data obtained from selected landmarks on longitudinally collected dental casts to describe maxillary first molar movement during headgear treatment [24]. They used the palatal rugae as landmarks to align the models, and expressed the displacement in an anatomically derived coordinate system. They calculated a rotation matrix by using only 4 landmark points per molar. Because of the close spatial positions of the 4 points, minor measurement errors can significantly impact the accuracy of rotation calculations.

Keilig et al. (2003) have used the surface-to-surface algorithm to determine tooth displacements [25]. This algorithm is equivalent to the minimization of the distance between the two surfaces. The casts were digitized either with a coordinate measurement table (COMT) or with a 3D laser scanner. The palatal rugae (Figure 1.1 (c)) of the initial model were used as the reference to align the initial and final models. The paper didn't provide detailed information about the coordinate system set-up. Although it is claimed that the complete crown surface was used to calculate tooth displacement, the figures only show the top surfaces of the crowns. So the displacement calculation was only based on the points on the top surfaces. This could work for posterior teeth with large and complicated occlusal surfaces, but not for anterior teeth with small and simple surfaces.

Cha et al. (2007) have compared 3D digital model superimposition with 2D cephalometric superimposition [26]. They used a laser scanner and reverse modeling software to obtain the 3D models. The palatal rugae region was chosen as a reference, and 3D surface-to-surface matching was used to superimpose the pre- and post-treatment scans. They chose the coordinate system defined by Ashmore et al. [24] to express the displacement components. They concluded that the mean incisor and molar movement measurements did not differ statistically between the superimpositions. They suggested

that 3D digital model superimposition is clinically as reliable as cephalometric superimpositions for assessing orthodontic tooth movement. They only calculated the translations of one landmark point, without involving rotations.

There are two major shortcomings in previously reported methods using digital dental casts. First, in many methods the calculations are based on the locations of certain landmark points, thus the accuracy is questionable. Second, rotation or tipping is not considered or calculated accurately. Furthermore, most studies were based on typodonts, thus variation among patients were not assessed. The precision and reproducibility of the landmarks was a main challenge, and there were no methods to improve the landmark identification process. Displacement calculation, based on surface matching, was a better approach. However, this requires that the digital casts have large, stable and accurate surfaces. These issues are addressed in this study.

2.1.3.2. Cone-beam Computed Tomography (CBCT)

CBCT can provide 3D images of the jaws and teeth, so it is increasingly used in the clinic, and because of the higher accuracy and richer information, many researchers turn to CBCT models for 3D analysis. The work can be placed in three categories: accuracy and reliability assessment, 3D superimposition, and treatment evaluation.

- Accuracy and Reliability Assessment

Lamichane et al. (2009) have developed a method to produce 2D cephalograms from CBCT images [22] to build a bridge between 2D and 3D. They designed a radiographic phantom with known dimensions, and took lateral and frontal cephalograms and CBCT scan of it. Landmarks on the cephalograms were traced and measured both manually and digitally. Orthogonal and perspective projections were generated from the CBCT scan, and lateral and frontal cephalograms based on the projections were created by using Dolphin 10. The results showed that the perspective lateral image constructed

from CBCT scan was accurate enough to be used in place of a traditional 2D cephalogram. They only used 3D images to do 2D analysis in.

Sherrard et al. (2010) evaluated the accuracy and reliability of tooth and root length measurement by using CBCT images [27]. They took CBCT scans of seven fresh porcine heads at three different resolutions, 0.2, 0.3, and 0.4 mm. Two periapical radiographs were also taken for the selected incisors and premolars. The CBCT scans were processed, and tooth and root length were derived by using Dolphin imaging software. The periapical radiographs of each tooth were imported into ImageTool software to measure the tooth and root length. All the measurement results were compared with actual measurements of the teeth by using digital calipers. Based on the results, they suggested that CBCT measurements were more accurate and reliable than periapical measurements for tooth and root length. Measurements from higher resolution scans had even better reliabilities. The main reason was that the periapical scans in the clinic might not be parallel.

Hassan et al. (2010) have investigated the influence of CBCT scan and reconstruction parameters [28]. The parameters they tested were scan field, mouth opening, voxel size, and segmentation threshold. Twenty-five patients were randomly assigned into three groups to take CBCT scans with different settings. The results indicated that the recommended setting to gain better quality scans was to use medium or small scan fields in an open-mouth position with a small voxel size. The segmentation threshold value was determined by the histogram of each model. Results showed that the maxilla threshold values varied more than the mandible ones, meaning that mandible region has better image quality than maxilla region in the same scan. One of the potential explanations was that the cortical bone in the mandible is thicker than in maxilla. The varied thin maxilla cortical bone creates significant artifacts in the 3D model.

- Superimposition

Superimposition is an important method for orthodontists to trace the growth and treatment related craniofacial changes. Early studies showed the potential of CBCT superimposition to assess the changes from both growth and orthodontic treatment in patients receiving orthodontic therapy.

Cevidances et al. (2007 and 2009) have used CBCT models to assess mandibular changes of both adult after orthognathic surgery [29] and in growing patients [30]. In the adults study, the before and after treatment models were superimposed on cranial base (Figure 1.1 (d)); while in the growing patients study, the superimposition was on anterior cranial base (Figure 1.1 (d)). The results of both studies suggested that 3D superimposition can be used to identify the magnitude and direction of mandibular displacement. The displacement calculation results in these studies only provided average shape changes of the structures since the shape changes in mandibular rami (Figure 1.1 (a)) and condyle (Figure 1.1 (a)) were not uniform. Average changes cannot give enough information to quantify the mandibular changes. The authors also didn't provide an explanation on the choice of the different superimposition regions in the two studies.

Choi et al. (2010) have introduced a method using the mutual information theory to superimpose 3D CBCT models [31]. This method does not depend on 3D surface models, and the registration aligned the before- and after-treatment gray level CBCT data sets. It is claimed that subvoxel level accuracy can be obtained and that the registration process was highly robust. There was no accuracy or reliability assessment for this method.

Tai et al. (2010) have developed a superimposition method by using surface-based registration [32]. The samples were the before- and after-treatment CBCT scans of fourteen patients. The superimpositions were done on cranial base (Figure 1.1 (d)), infraorbital margin, and corpus to show positional changes of bone and teeth relative to different stable structures. The image registration algorithm used in this study was

Iterative Closest Point (ICP). The results showed that ICP can be used to superimpose CBCT models. Of the three reference areas, cranial base was the most reliable surface for superimposition. However, this method only measured the distance changes between two positions of a landmark point without any angular change information.

Nada et al. (2011) have tested voxel based superimposition method on anterior cranial base and the zygomatic arches [33]. Sixteen pairs of 3D models were constructed from before and after treatment CBCT scans of adult dysgnathic patients. Each pair was registered on the anterior cranial base three times and on the left zygomatic arch twice. The authors concluded that voxel based image registration on both zones could be considered as an accurate and a reproducible method for CBCT superimposition. However, voxel-based algorithm needs longer computational time and is more computing intensive [34].

- Treatment Evaluation

Because CBCT is a useful tool in evaluating dental and skeletal changes such as tooth and anatomical landmark movements, it is important for assessing treatment outcomes.

Chen et al. (2009) have developed a method to calculate tooth displacement from two sets of CBCT images from the same subject [35]. To put the two models in an identifiable position, the superimposition was on the stable mandibular bony parts by using ICP algorithm. After superimposition, the six displacement components were calculated from the entries of the transformation matrix between the two positions of the same tooth. Experiments were designed to assess the accuracy and reliability of the method which was determined to be a feasible clinical method to quantify 3D tooth displacements.

Alves et al. (2011) used CBCT to assess the stability and behavior of mini-implant during upper molars intrusion [36]. CBCT scans were taken for each patient, one

at the beginning and the other one at the end of the treatment. To assess displacement, the distances of mini-implants' head and tail to coronal, sagittal and axial planes were measured on both scans. The measurements were actually done on a 2D cross-section of the CBCT scans, and rotation information cannot be obtained.

Since conventional 2D cephalometric analysis has been used by the orthodontists for several decades, researchers also made efforts to extend this method to 3D models. Cho et al. (2009) have presented a 3D cephalometric analysis system with coordinate system, landmarks, and dental and skeletal analysis parameters [37]. This system was based on the 2D analyses and studies, and it was a first step to extent analysis into 3D. However, in this system, many measurements still needed to be made on a projected plane, and it didn't provide a method to do superimposition.

There are many articles about the latest developments and applications of CBCT images. Since CBCT is still relatively new to orthodontics, many studies focused on validating its accuracy and on the processing of 3D images, e.g. different algorithms for superimpositions. However, treatment outcome evaluation was still done visually or in 2D. Clinical 3D treatment outcomes assessments and side-effect quantifications are still needed.

3D studies use digital casts or CBCT images, each with its advantages and disadvantage. CBCT images are more accurate and they can provide more information, but there is radiation dose concern. Dental casts can be obtained longitudinally at different treatment milestones. While the disadvantages of dental casts are: (1) the cumulative errors from multi-steps in making the cast; (2) the lack of root and bone information. So a better clinical approach is to integrate the two methods and streamline the process.

2.2. Orthodontic Tooth Movement

Orthodontic tooth movement is an important treatment outcome that can be used to evaluate treatment strategies and orthodontic appliances. In orthodontic treatment, the orthodontist always constructs an appliance to produce certain desired tooth movements. The efficiency of the desired tooth movement can be evaluated by using tooth movement rate. Typically an orthodontic load system is applied to the tooth to be moved by an appliance that is anchored by other teeth. Through activation, applying a force to the moving tooth will inevitably create a reaction force on the anchoring teeth also causing them to move. Methods have been developed to minimize anchorage loss, but their effects have not been documented due to a lack of reliable technology. The inability to quantify anchorage loss also affects the evaluation of clinical tooth displacement because the displacement has been measured using the anchorage tooth as the reference. When the anchorage tooth moves, it affects the accuracy. Therefore, quantification of anchorage loss is important.

2.2.1. Tooth Movement Rate

Tooth movement rate is the commonly used parameter to evaluate treatment efficiency. In animal studies, the relationship between the magnitude of force and tooth movement rate was investigated [38-41]. A mathematic model was also developed based on experimental studies in beagle dogs [42].

In human studies, besides comparing the effects of force magnitudes [43-45], movement rates were used to compare the treatment efficiency among different appliances [46-48], and different types of anchorage [49].

In the previous studies, tooth movement rate was quantified by using digital calipers [38-39, 47-48] or two-dimensional (2D) cephalometric analysis [49-50]. These methods can only provide linear or 2D measurements between landmarks. The off-plane movement and rotations are not assessed. These components are equally important because they characterize the side-effects.

2.2.2. Anchorage Control

Anchorage is defined as the resistance to unwanted tooth movement [16]. It is one of the most important factors in evaluating treatment outcome. Many different anchorage techniques have been designed in the past decades.

Teeth have been the most common anchors. In canine retraction treatment, traditionally, the typical anchorage involves the bonding of 2nd premolar, 1st molar and all anterior teeth [51]. This technique can be reinforced by adding a transpalatal arch (TPA) between the two 1st molars. TPA can also help reduce the rotation of molars [52]. However, this kind of intraoral technique is not always successful. Significant anchorage losses were observed in several studies [52-54]. The maximum anchorage loss observed in one study was more than 4.0mm [54].

Head gear is another widely used technique for anchorage control. It is able to provide absolute anchorage [16]. However, patient compliance is a big problem [55], especially when considering that many of the orthodontic patients are young children. The other concerns are undesired side effects on the maxillary complex and risk of injury [56-58].

With the development of bone implant techniques, mini-implants are gaining popularity for absolute anchorage. Orthodontic mini-implants were placed in locations such as alveolar bone [59], the retromolar region [60], the midpalatal region [61], and the lingual [62] and buccal [63] cortical plates. Studies focusing on comparing mini-implant with traditional anchorage control techniques were also found in current literature [49, 52]. The results showed that implant can provide a better anchorage control and increase the canine movement rate.

3. METHODOLOGY

The commonly used three-dimensional (3D) methods to record clinical tooth displacement and bony changes are Cone-Beam Computed Tomography (CBCT) scans and digital dental casts. Methods have been developed to quantify tooth and bone changes using these records [25, 29-30, 35-36, 64]. A general scheme for 3D image analysis usually has four major steps (Figure 3.1).

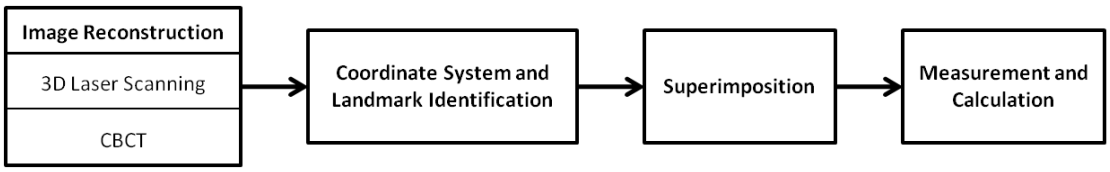

Figure 3.1. A general scheme for 3D image analysis.

The first step is to scan the casts or patients and reconstruct the raw images or data sets. During this step, 3D objects may be created and the images or models may be reoriented to a standard position. The outcomes of this step are the 3D digital models which can be used to quantify tooth movement and bony changes.

The second step is to setup coordinate systems and identify landmark points. An appropriate coordinate system is essential to 3D analysis. It can simplify the analysis process and make the final outcomes more meaningful and useful. As in 2D cephalometric analysis, landmark identification is the base for all analysis in 3D. Accurate and consistent landmarks contribute much to analysis accuracy.

The third step is to superimpose 3D models. After this step, the models are in comparable positions, and the treatment and/or growing related changes can be traced.

The last step is to calculate the changes between different models or to quantify the parameters clinicians want through measuring important anatomical markers on the superimposed model.

Based on 3D models and clinical case selection, the technical details of 3D image analysis methods may be quite different. However, the general scheme is the same. In this study, maxillary digital dental casts were used to quantify canine movement; and Cone-Beam Computed Tomography (CBCT) models were chosen for quantification of both maxillary anchorage loss and skeletal landmark movement.

3.1. Image Reconstruction

3.1.1. 3D Laser Scanning of Dental Cast

To digitize dental casts, a 3D scan of the casts was performed using an OPTIX 400S® (3D Digital Corp., Sandy Hook, CT, US) 3D laser scanner (Figure 3.2). The highest resolution (0.06 mm) was used to get the best representation of the surfaces [65].

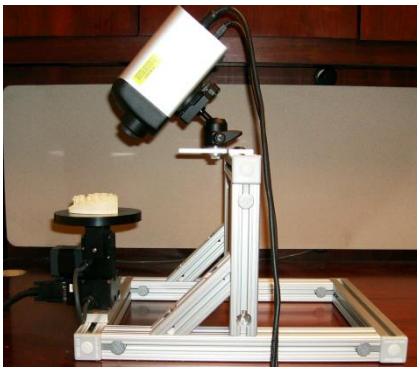

Figure 3.2. OPTIX 400S® 3D laser scanner.

The entire model was reconstructed from seven to nine images taken from different directions, Figure 3.3. For the seven images, images a and b were from the occlusal surfaces of the teeth and the palatal area, each one focuses on one side; image c was taken from the front to cover the outside surfaces of the incisors; images d and e were focused on the left buccal surfaces, and similarly images f and g were of the right buccal. Occasionally, one or two images were added to improve quality. The images had overlapping regions for registration and merging.

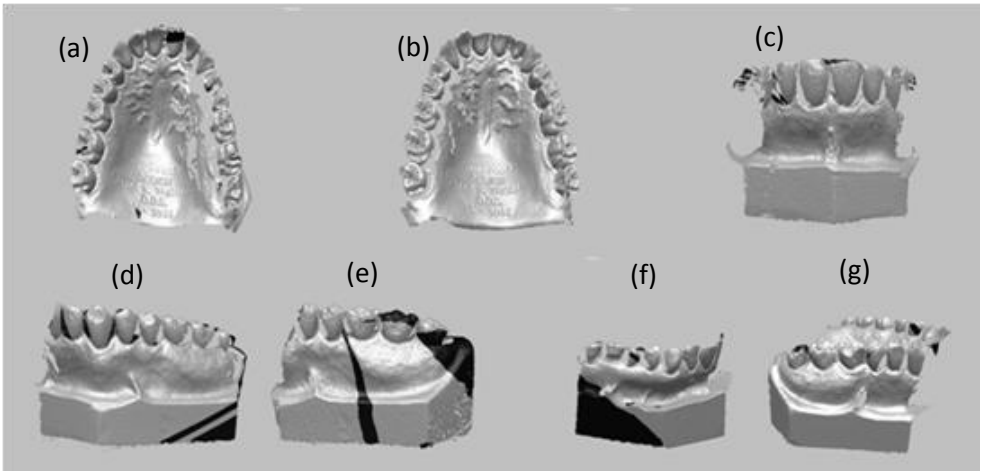

Figure 3.3. Seven images taken from different directions.

The reconstruction was done with RapidForm® (INUS Technology Inc., Seoul, South Korea), reverse engineering software. There are two steps in model reconstructing, registrating and merging [66]. Registration is the process that aligns two or more shells on the basis of the coordinate of a fixed shell. It calculates the exact position of each shell by utilizing some common geometric features between them. These geometric features, also called corresponding points, are specified by the user. After registration, the shells which have been aligned are merged together. During the merging process, overlapped regions on the shells are removed effectively and neighboring boundaries are stitched together with newly added polygons. The result and accuracy of shells are still maintained after merging.

3.1.2. Cone-Beam Computed Tomography (CBCT)

CBCT, also known as Cone-Beam Volumetric Tomography (CBVT), has become widely used in orthodontics. CBCT scanners can image the mandible and maxilla at the same time, thus the patient only needs to be exposed one time for both jaws. The CBCT machine used in both of the presented studies is i-CAT® (Imaging Science International, Hatfield, PA). Based on the requirements of the applications, different resolutions and scanning times were selected. Because of concerns about radiation exposure, especially with young patients, the scans were generally only taken at the beginning and at the end of treatment.

The CBCT images were processed with MIMCS® (Materialise Group, Leuven, Belgium). Figure 3.4 shows a typical MIMICS® browser. In the default configuration, the images appear in a four-view window [67].

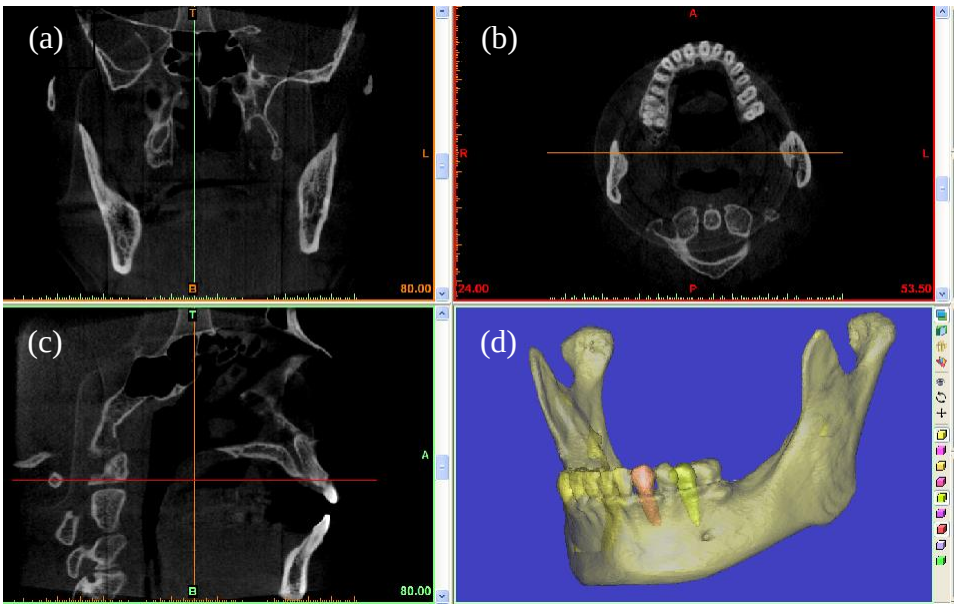

Figure 3.4. CBCT image shown in a MIMCS® window.
(a) coronal view, (b) axial view, (c) sagittal view, and (d) 3D view

Due to the complicated geometry and non-uniform density distribution of the bone and teeth, there is no automatic way to do segmentation. In this study, bone and

teeth were manually reconstructed by using the tools provided by MIMICS®. The first step was to set an appropriate threshold to make the segmentation object contain only those pixels between the upper and lower thresholding limits. If the threshold range is too large, the segmented object will contain much noise and there will be more operator intervention needed. If the threshold range is too small, some details may be lost. In this study, the criterion for thresholding was to cover as much as possible the region of interest. After threshold selection, the cross-sections of the CBCT images were carefully examined. Intervention was needed when clear boundaries were not observed in the cross-sections. After clarifying the boundaries and segmenting the structures of interests from the surrounding tissues, 3D objects were created.

3.2. Coordinate Systems

3.2.1. Coordinate Systems on Maxillary Digital Dental Casts

In the maxillary digital dental cast method to quantify canine movement, two coordinate systems were used: the global coordinate system (GCS) and the canine coordinate system (CCS). Both were defined on the pre-treatment cast. GCS was used to correlate the results with traditional cephalometrics; while CCS was used to show movements in the mesial-distal (M-D), buccal-lingual (B-L), and occlusal-gingival (O-G) directions, which are commonly used in the clinic.

GCS was a modified version of the coordinate system proposed by Ashmore *et al*. (2002) [24] and Cha *et al*. (2007) [26]. GCS was defined based on seven landmarks (Figure 3.5 (a)). The origin was at the crossing point of the median raphe and the base of the incisive papillae. The sagittal plane was made up of that origin and two arbitrary non-co-linear points on the mid-palatal suture. The horizontal plane was through the origin and parallel to the posterior occlusal plane. The posterior occlusal plane was constructed by connecting the two second premolar buccal cusp tips and two first molar mesial-buccal cusp tips using the principal component analysis best-fitting method [24, 26]. The

frontal plane included origin of GCS and was perpendicular to both the sagittal and horizontal planes. The intersections of the three planes form three axes defined as: x-axis, antero-posterior direction; z-axis, vertical direction; and y-axis, transverse direction. In the position shown in Figure 3.5 (b), the positive x points to the right; the positive y points to the posterior; and the positive z points superiorly.

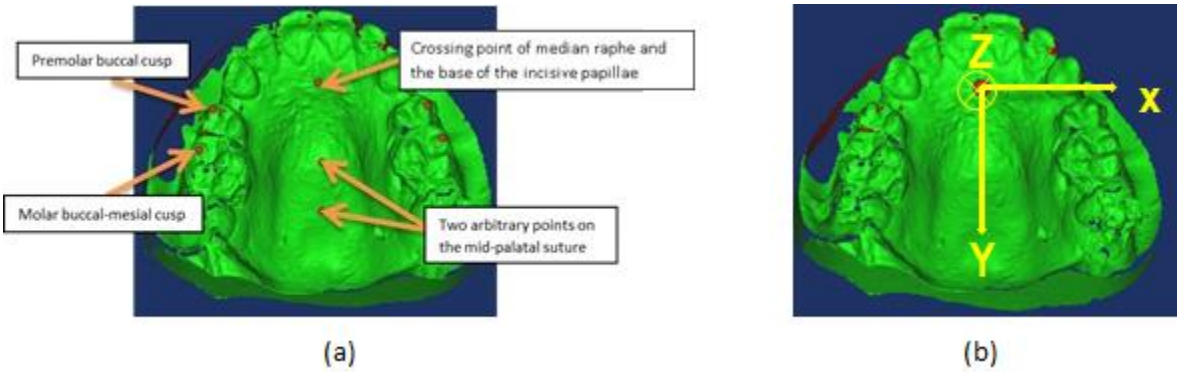

Figure 3.5. Global coordinate system (GCS) definitions.

CCS origin was defined at canine crown center, the bisection of its two proximal contact points (Figure 3.6). The x and y axes formed a plane that was parallel to the occlusal plane. On the left canine, Figure 3.7 (a), the positive x, y and z directions were in buccal, distal, and apical directions, respectively. On the right canine, Figure 3.7 (b), they were in buccal, mesial, and apical directions, respectively.

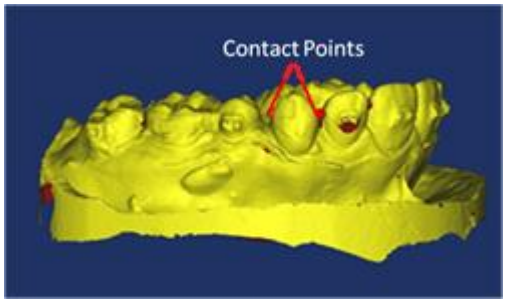

Figure 3.6. Definition of center of crown.

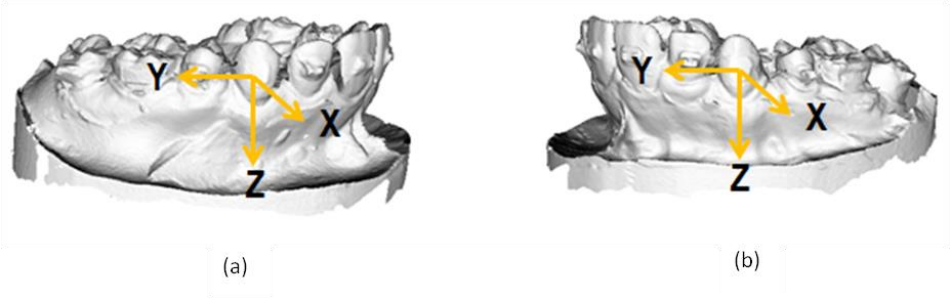

Figure 3.7. Canine coordinate system (CCS) definitions.

To be consistent, the displacement components on the right CCS were converted to be expressed on the left CCS. The clinically used terms that describe the displacements were shown in Table 3.1 and Figure 3.8.

Table 3.1. Displacement component definitions.

Translation		Rotation	
Positive x	Buccal	Positive x	Distal tipping
Negative x	Lingual	Negative x	Mesial tipping
Positive y	Distal	Positive y	Lingual tipping
Negative y	Mesial	Negative y	Buccal tipping
Positive z	Intrusion	Positive z	Crown mesial out
Negative z	Extrusion	Negative z	Crown mesial in

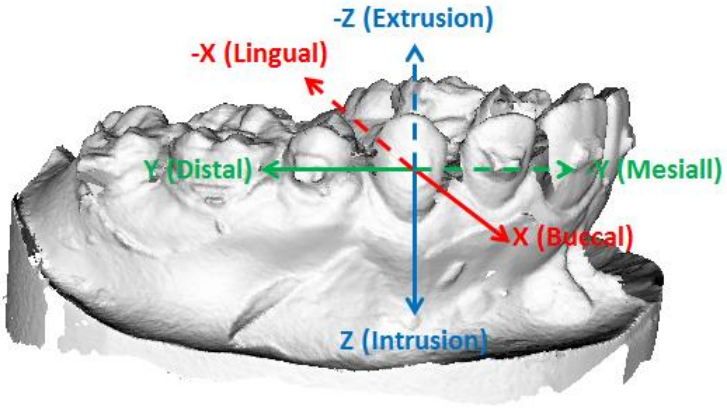

Figure 3.8. Left CCS and corresponding clinical terms.

The relationship between CCS and GCS was defined in 3.1, where x, y, and z are the unit vectors of the 3 axes in GCS; x', y', and z' are the unit vector of the 3 axes in CCS; and θ is the angle between the positive GCS y-axis direction and distal direction of each canine.

$$x' = \begin{bmatrix} \cos\theta & -\sin\theta & 0 \\ \sin\theta & \cos\theta & 0 \\ 0 & 0 & 1 \end{bmatrix} x;\ y' = \begin{bmatrix} \cos\theta & -\sin\theta & 0 \\ \sin\theta & \cos\theta & 0 \\ 0 & 0 & 1 \end{bmatrix} y;\ z' = z\ . \quad (3.1)$$

3.2.2. Coordinate Systems on CBCT Models

Before setting up the coordinate system on CBCT models, the patient's head in the scan must be in the standard anatomical position. To standardize head position, CBCT images were orientated in MIMICS®. A transverse reference plane was defined by connecting the Nasion (N) and the right and left frontozygomatic (FZ) points (Figure 3.9). The frontozygomatic point was defined as the most anterior point where the zygomatic bone and the zygomatic process of the frontal bone meet. The orientation was based on the transverse plane which needs to be perpendicular to skull sagittal plane. After reorientation, a coordinate system was assigned automatically by the software.

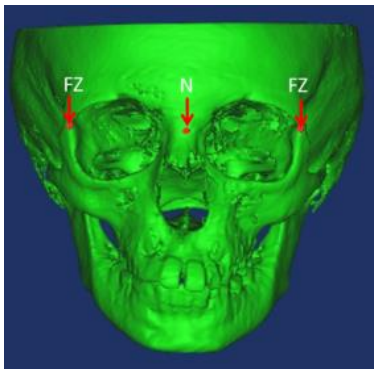

Figure 3.9. Landmarks to reorient head model in a standard position.

3.2.2.1. Coordinate System for Maxillary Tooth Movement Quantification

The coordinate system for maxillary tooth movement quantification, the Upper Jaw Coordinate System (UCS) was attached to the hard palate in pre-treatment upper jaw

model. The origin of UCS was at the incisive foramen; the three axes were parallel to the coordinate system axes assigned by the software. The UCS was shown in Figure 3.10.

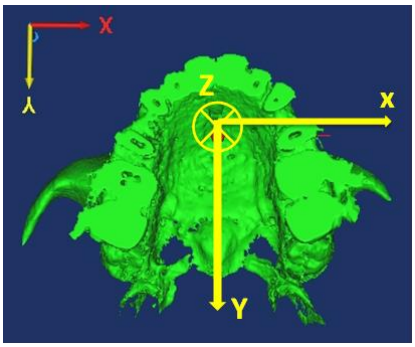

Figure 3.10. Upper jaw coordinate system (UCS) on CBCT.

3.2.2.2. Coordinate Systems for Skeletal Landmark Movement Quantification

There were two coordinate systems, the cranial base coordinate system (CBCS) and the mandible coordinate system (MCS), used to quantify skeletal landmark movements. Both were attached to the pre-treatment model. CBCS was used to show changes face relative to the cranial base, and MCS was used to quantify the absolute movements of the mandibular landmarks.

The origin of CBCS was at the nasion (N) point. The three axes were created according to the right-hand rule and defined as follows: the x-axis is parallel to the line connecting the right and left frontozygomatic points; the y-axis is perpendicular to the x-axis and parallel to the right Frankfort horizontal line; and the z-axis is perpendicular to the x and y axes (Figure 3.11). Their positive values are to the left of, posterior to, and superior to the Nasion point of the subject.

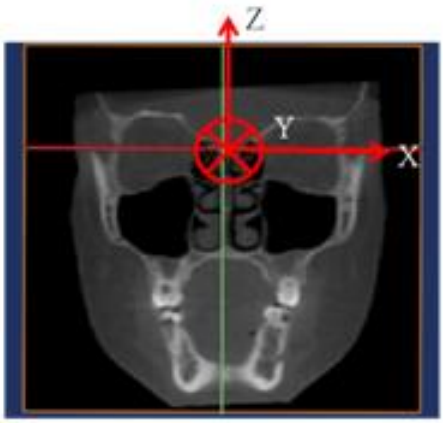

Figure 3.11. Cranial base coordinate system (CBCS).

To set up MCS, first, the mandible sagittal plane was established. It was based on the bisection point of the right and left inferior border of corpus points, the bisection point of the right and left gonion points, and the bisection point of right and left condylion points (Figure 3.12 (a)). The origin of MCS was at the pogonion (Pog) point. The MCS x-axis was perpendicular to the sagittal plane. Its y-axis was defined as the projection of the CBCS y-axis onto the MCS sagittal plane, perpendicular to the MCS x-axis. The MCS z-axis was perpendicular to MCS x- and y-axes, following the right-hand rule (Figure 3.12 (b)).

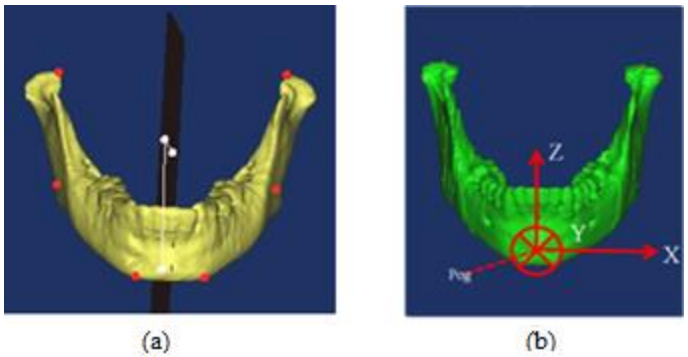

Figure 3.12. Mandibular sagittal plane and coordinate system (MCS).

3.3. Superimposition

There are three major 3D superimposition sites. One is superimposition on the anterior cranial base surface (Figure 3.13 (a)). Another is on the palatal rugae area for dental cast [68-69] (Figure 3.13 (b)); and on the anterior inner curve of the hard palate for CBCT models (Figure 3.13 (c)). The third is on a stable portion of the mandible that surrounds the inferior alveolar canal and the outer and inner cortical plates of the chin, excluding the region surrounding the B point and the inferior border of the chin (Figure 3.13 (d)). 2D and 3D superimpositions and their applications are summarized in Table 3.2.

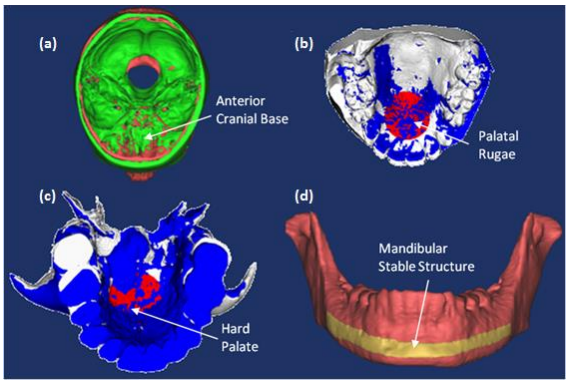

Figure 3.13. Three major 3D superimpositions.

Table 3.2. Comparison between 2D and 3D superimpositions.

2D Superimposition	3D Superimposition		Application
	Digital Dental Cast	CBCT	
anterior cranial base along the SN line		anterior cranial base surface	overall change patterns of the face
maxilla	palatal rugae area	anterior inner curve of the hard palate	maxillary teeth changes relative to maxilla
mandible		mandibular natural stable structure	condyle and mandibular teeth changes relative to mandible

The algorithm implemented for superimposition is called the Iterative Closest Point (ICP) method. ICP is a surface-based registration method that employs geometric optimization algorithm that precisely aligns the 3D polygon mesh data sets of the digital models [35, 70]. Using ICP for digital model superimposition handles the full six degree of freedom. The ICP method is also independent of shape representation, which handles images represented by different geometric elements (i.e., sets of points, line segments, parametric curves, implicit curves, triangles, parametric surfaces, or implicit surfaces).

The ICP algorithm works as follows: given two 3D point sets, find the transformation that brings one dataset into the best possible alignment with the other dataset. The key is to compute the optimal transformation [T] by iteratively finding a local minimum of a mean-square distance metric. In this implementation, the cost function is defined as the mean of the least distances from the vertices of one dataset to the other.

$$f(T) = \frac{1}{N}\sum_{i}\left\|x_i - Tp_i\right\|^2 \quad . \tag{3.2}$$

where T is a rigid transformation matrix, N is the number of points, x_i is a vertex of the first dataset and p_i is a vertex of the second dataset that is the closest to x_i. This process converges when the mean squared error (MSE) stops improving. The optimal transformation produces the minimum MSE that measures the difference of the two data sets in consecutive steps. The transformation matrix, T (3.3), between the data sets in two positions is the accumulative matrix calculated from the matrices of every step. The unit vectors representing coordinate axes in the first dataset are x, y, and z; and in second dataset they are x', y', and z'. The projections of x' on x, y and z axes are called direction cosines, $\cos\theta_{x'x}$, $\cos\theta_{x'y}$ and $\cos\theta_{x'z}$. Similarly, the projections of y' on x, y and z axes are $\cos\theta_{y'x}$, $\cos\theta_{y'y}$, and $\cos\theta_{z'z}$; and the projections of z' are $\cos\theta_{z'x}$, $\cos\theta_{z'y}$, and $\cos\theta_{z'z}$. d_x, d_x, and d_x are the three translation components.

$$T = \begin{bmatrix} \cos\theta_{x'x} & \cos\theta_{x'y} & \cos\theta_{x'z} & d_x \\ \cos\theta_{y'x} & \cos\theta_{y'y} & \cos\theta_{y'z} & d_y \\ \cos\theta_{z'x} & \cos\theta_{z'y} & \cos\theta_{z'z} & d_z \\ 0 & 0 & 0 & 1 \end{bmatrix}. \quad (3.3)$$

3.4. Anatomical Changes Calculation

After superimposition, the before-treatment model (BTM) and the post-treatment model (ATM) were in the comparable position. Then, the displacement of teeth and landmarks were calculated.

3.4.1. Tooth Displacement Calculation

The ICP program was used again to calculate the transformation matrix between the same tooth's pre- and post-treatment positions. The six components of the displacement can be calculated from the entities of the transformation matrix.

There are two types of coordinate system involved in this step, the coordinate system which is usually assigned by the image processing software (SCS), and the coordinate systems which were defined based on anatomical landmarks and structures (LCS). Based on the choice of 3D models and treatments, LCS could be one of the GCS, CCS, or UCS shown in Section 3.2.1 and 3.2.2.1.

To depict the 3D rotation, three angles were defined to delineate the angle "about x-axis", "about y-axis", and "about z-axis". Figure 3.14 shows the definition of the three angles, where XYZ is the LCS on the BTM, X'Y'Z' is the LCS on the ATM2. The about x-axis angle is approximately defined as the angle between the two z-axes projected onto the YZ plane in the LCS on the BTM; similarly the about y-axes angle is defined as the angle between the two z-axes projected on the ZX plane in the LCS on the BTM; while the about z-axis angle is defined as the angel between the two y-axes projected on the XY plane in the LCS on the BTM.

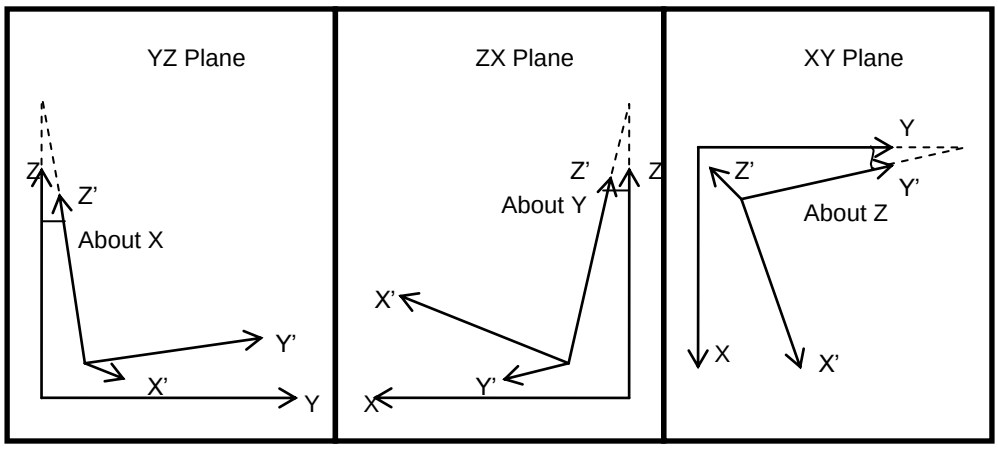

Figure 3.14. The definition of rotation angles in tooth displacement calculation.

A Matlab® (MathWorks, Natick, MA) script was used to do the calculation. The transformation matrix is the input of the script. The matrix is first applied to the definition of LCS in BTM, which means the coordinate of the origin, the direction vectors of the axes, to obtain the definition of the LCS in the aligned ATM on the same structure. Then, the transformation matrix between SCS and BTM LCS is calculated by using the definition of BTM LCS. The distance and rotation angles in BTM LCS are calculated by using the following equations.

$$O_2 = T \cdot O_1 \ . \tag{3.4}$$

$$x = \begin{bmatrix} x_1 \\ x_2 \\ x_3 \end{bmatrix} \qquad y = \begin{bmatrix} y_1 \\ y_2 \\ y_3 \end{bmatrix} \qquad z = \begin{bmatrix} z_1 \\ z_2 \\ z_3 \end{bmatrix} . \tag{3.5}$$

$$M_r = \begin{bmatrix} x^T \\ y^T \\ z^T \end{bmatrix} . \tag{3.6}$$

$$d = M_r \cdot (O_2 - O_1) \ . \tag{3.7}$$

$$x' = M_r \cdot R \cdot x \quad y' = M_r \cdot R \cdot y \quad z' = M_r \cdot R \cdot z \ . \tag{3.8}$$

$$x' = \begin{bmatrix} x_1' \\ x_2' \\ x_3' \end{bmatrix} \quad y' = \begin{bmatrix} y_1' \\ y_2' \\ y_3' \end{bmatrix} \quad z' = \begin{bmatrix} z_1' \\ z_2' \\ z_3' \end{bmatrix} . \tag{3.9}$$

$$\alpha = \tan^{-1}(z_2'/z_3') \ . \tag{3.10}$$

$$\beta = \tan^{-1}(z_1'/z_3') \ . \tag{3.11}$$

$$\gamma = \tan^{-1}(y_1'/y_2') \ . \tag{3.12}$$

where $\mathbf{O_1}$ is the origin of the LCS in BTM; $\mathbf{O_2}$ is the origin of the LCS in ATM; **T** is the transformation matrix between the two positions (Section 3.3, 3.3); $\mathbf{M_r}$ is the 3 x 3 rotation matrix between the LCS and the SCS in BTM; **x**, **y**, **z** are the unit vector of the 3-axis in the LCS in BTM; $\mathbf{x^T}$, $\mathbf{y^T}$, and $\mathbf{z^T}$ are the transposes of **x**, **y**, **z**; **d** is the vector in the LCS in BTM between $\mathbf{O_1}$ and $\mathbf{O_2}$; **x'**, **y'**, **z'** are the unit vector of the 3-axis in the LCS in ATM and are expressed in the LCS in BTM; **R** is a 3 x 3 rotation matrix between the two positions; and **α**, **β**, **γ** are the rotations about x-, y-, z-axis respectively. The three components of **d** represent the x, y, and z displacement respectively.

3.4.2. Landmark Displacement Calculation

Landmark displacement was calculated by using the coordinates of the same landmark in pre- and post-treatment positions. The calculation was done in either CBCS (displacement relative to cranial base) or MCS (displacement relative to mandible) (Section 3.2.2.2). The rotation of the vector between the coordinate system origin and the landmark, "about x-axis", "about y-axis", and "about z-axis", were defined in Figure 3.15. P_i and P_f are the pre- and post-positions of a landmark. P_i^{YZ}, P_i^{ZX}, and P_i^{XY} are the projections of P_i onto the YZ plane, ZX plane, and XY plane; and P_f^{YZ}, P_f^{ZX}, and P_f^{XY} are the projections of P_f onto the YZ plane, ZX plane, and XY plane. α, β, γ are the rotations about x-, y-, z-axis respectively. When the rotations of the vector between the coordinate system origin and the landmark are used later, they are called as the rotation of the corresponding landmark for simplification.

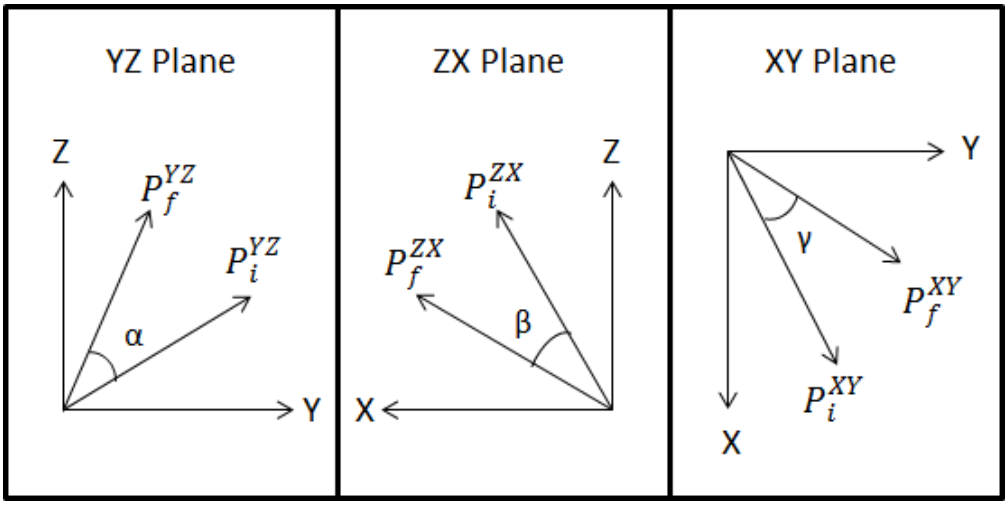

Figure 3.15. The definition of vector rotations in landmark displacement calculation.

The displacement of a landmark P was calculated by using the following equations.

$$d = P_f - P_i \ . \tag{3.13}$$

$$\alpha = \tan^{-1}(z_f/y_f) - \tan^{-1}(z_i/y_i) \ . \tag{3.14}$$

$$\beta = \tan^{-1}(x_f/z_f) - \tan^{-1}(x_i/z_i) \ . \tag{3.15}$$

$$\gamma = \tan^{-1}(y_f/x_f) - \tan^{-1}(y_i/x_i) \ . \tag{3.16}$$

where **d** is the translation vector between pre- and post-treatment positions; $\mathbf{P_i}$ is the landmark in pre-treatment position; $\mathbf{P_f}$ is the landmark in post-treatment position; $\mathbf{x_i}$, $\mathbf{y_i}$, and $\mathbf{z_i}$ are the x, y and z coordinates of $\mathbf{P_i}$; $\mathbf{x_f}$, $\mathbf{y_f}$, and $\mathbf{z_f}$ are the x, y and z coordinates of $\mathbf{P_f}$; and **α**, **β**, **γ** are the rotations of the vector between the origin and the landmark about x-, y-, z-axis respectively.

3.5. Quantification of Maxillary Tooth Movement

Based on the technical details presented in Section 3.1 to 3.4, the procedures used to quantify maxillary tooth movement by using digital dental casts and CBCT models are summarized in Figure 3.16 and 3.17.

The digital dental cast procedure (P1) started with the 3D laser digitizing of the dental casts which were then reconstructed into 3D models; then the GCS and CCS were defined on the pre-treatment model. Next, the pre- and post-treatment models were superimposed on the palatal rugae region; the last step was to calculate tooth movements based on the transformation matrix between the pre- and post-treatment positions of the tooth. Figure 3.16 showed the workflow.

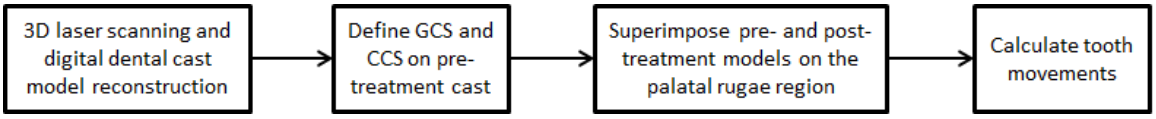

Figure 3.16. Workflow of digital dental cast procedure (P1).

The first step of the CBCT maxillary tooth movement procedure (P2) was to standardize the head position in the CBCT scans. The second step was to separate the upper jaw and the target teeth from the rest of the image, and to create 3D models. The third step was to define UCS on the pre-treatment upper jaw model. Next, the pre- and post-treatment models were superimposed on the anterior inner curve of the hard palate, followed by the calculation of the tooth movement. Figure 3.17 shows the workflow of P2.

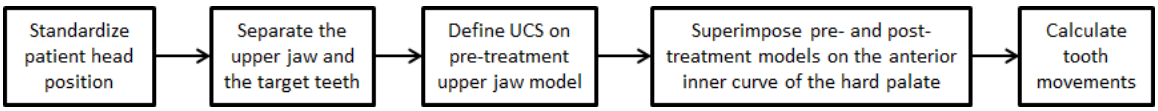

Figure 3.17. Workflow of CBCT maxillary tooth movement procedure (P2).

3.6. Quantification of Skeletal Landmark Movement

The skeletal landmark movement quantification procedure (P3) began with a standardized patient head position. Then, the quantification of landmark movements took two paths. One was performed relative to the anterior cranial base, the other relative to the mandibular stable structure. Figure 3.18 shows the workflow of P3. The anterior cranial base route consisted of defining CBCS, superimposing pre- and post-treatment

skull models, and calculating landmark movements relative to anterior cranial base. The mandible route involved setting up the mandible sagittal plane, defining MCS, superimposing pre- and post-treatment mandible models, and calculating landmark movements relative to the mandible stable structure.

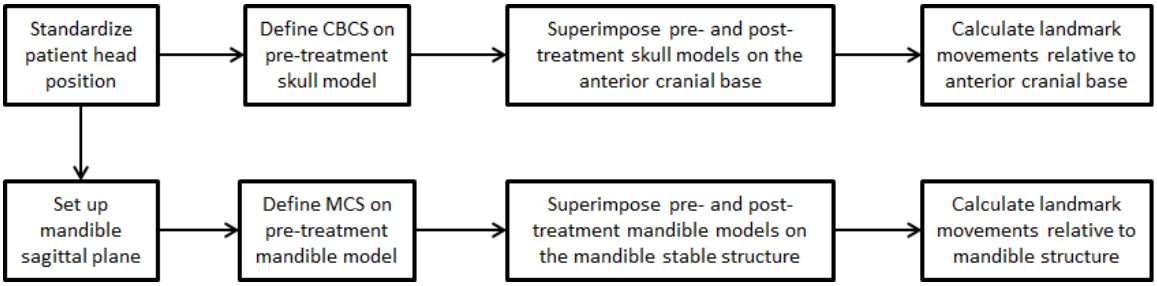

Figure 3.18. Workflow of CBCT skeletal landmark procedure (P3).

3.7. Validation

3.7.1. CBCT Model Consistency Validation

Since the CBCT scan settings were the same in all cases, the validation experiment was performed only for the segmentation process by repeating the process five times for an incisor, a canine, a premolar and a molar. In each process, the segmentation settings were the same, so the only potential source of error was the human interference when the tooth boundaries needed to be cleaned-up manually. After each segmentation process, the surface area and volume were measured using tools provided by MIMICS®. Table 3.3 shows the standard deviations in the measurements. Since they are all less than 0.4% of the average value, the variation between different segmentation models is small, and therefore it can be concluded that the 3D CBCT models are consistent.

Table 3.3. The means and standard deviations of five repetitive measurements.

		Incisor	Canine	Premolar	Molar
Volume (mm^3)	Ave.	379.98	528.45	408.11	913.84
	Std.	1.66	1.03	0.56	2.04
Surface Area (mm^2)	Ave.	355.67	494.85	437.40	973.98
	Std.	1.35	0.69	0.46	1.28

3.7.2. Quantification of Maxillary Tooth Movement Procedure Validation

3.7.2.1. Digital Dental Cast Procedure (P1) Validation

To assess the errors and variations in the digital dental cast procedure (P1), two experiments were performed [35]. In one, a single cast was digitized twice, each was reconstructed five times, and the canine displacements (which, in theory, should be zero) were calculated using P1. In the second experiment, two digital cast models were created from two scans of the same dental cast. The first cast model (considered to be the pre-treatment model) was constructed from the original scan. The second model (considered as the post-treatment model) was created after the left canine crown in the second scan was artificial moved according to each of the two prescribed displacement cases, Table 3.4. The canine displacements were calculated using P1 and compared with the prescribed values. The entire process repeated five times, and the errors and variations were assessed.

Table 3.4. Prescribed tooth displacements.

		Translation along	Rotation about
Experiment 1		0	0
Experiment 2	Case 1	z: 2.00mm	z: 5.00 °
	Case 2	z: 2.00mm	x: 5.00 ° y: 5.00 °

Estimations of errors and variations of P1 are shown in Tables 3.5 and 3.6. With a zero prescribed displacement in the first experiment, the maximum average calculated translation and rotation were 0.26 mm (± 0.06 mm) and 1.33 ° (± 0.08 °) (Table 3.5). These are considered as the noise level of P1. Any linear and angular displacements that are smaller than these would be considered unreliable. For case 1 in the second experiment, with a 2 mm and 5^o prescribed displacement, the average measured translation was 1.83 mm (± 0.08 mm) and 4.40 ° (± 0.08 °). For Case 2, with the prescribed 2 mm translation in the z direction and 5 ° prescribed rotations about the x and y axes, the calculated displacement components were 1.70 mm (± 0.05 mm) along the z axis, 6.29 ° (± 0.09 °) about the x axis, and 6.32 ° (± 0.07 °) about the y axis. The average errors were 10% and 13% in translation and rotation, respectively **(**Table 3.6**)**.

By using P1, all six displacement components relative to the palatal rugae region were quantified. The maximum standard deviations were 0.08 mm for translation and 0.10 ° for rotation. Since these variations are smaller than those that are clinically detectable, thus improves the quantification of tooth displacement, and thus it is the best estimates available. The maximum translational error was 0.37 mm, and the rotational error was 1.40 °, which are hard to detect visually in the clinic. The maximum translational error was 18.5% of the prescribed value, and the maximum rotational error was 28.0%, Table 3.6.

Table 3.5. Results for canines with zero prescribed displacement.

	Translation (mm)			Rotation (°)		
	x	y	z	x	y	z
1	0.24	-0.11	-0.15	1.36	-0.57	1.21
2	0.23	-0.29	-0.07	1.12	-0.62	1.36
3	0.34	-0.20	-0.16	1.33	-0.68	1.40
4	0.19	-0.09	-0.12	1.24	-0.48	1.29
5	0.30	-0.24	-0.12	1.28	-0.61	1.39
Average	0.26	-0.19	-0.13	1.26	-0.59	1.33
Standard deviation	0.06	0.08	0.04	0.10	0.08	0.08

Table 3.6. Results for canines with prescribed displacements.
(Tz: Translation along z axis; Rx, Ry, and Rz: Rotation about x, y, and z axes)

	Case 1		Case 2		
	Tz (mm)	Rz (°)	Tz (mm)	Rx (°)	Ry (°)
1	1.89	4.43	1.74	6.38	6.22
2	1.71	4.38	1.71	6.15	6.36
3	1.81	4.31	1.67	6.36	6.33
4	1.91	4.52	1.75	6.26	6.30
5	1.85	4.39	1.63	6.31	6.40
Average	1.83	4.41	1.70	6.29	6.32
Standard deviation	0.08	0.08	0.05	0.10	0.07
Error	0.17	0.59	0.30	1.29	1.32

3.7.2.2. CBCT Maxillary Tooth Movement Quantification Procedure (P2) Validation

To assess the errors and variations of CBCT maxillary tooth movement quantification procedure (P2), one volunteer was scanned with i-CAT® CBCT machine (resolution 0.25 mm) twice in two weeks with no orthodontic treatment. Two mandible models were created from the two sets of CBCT images. The first set was considered as pre-treatment (B1) and the second as post-treatment (A1) with no tooth displacement. A third model (A2) was created by artificially displacing left 2nd premolar and 1st molar of A1 to simulate displacements from orthodontic treatment. The teeth were digitally displaced individually by using the MIMICS software with prescribed displacements (Table 3.4). Similar to the validation process described in Section 3.7.2.1, two experiments were used. The first experiment was the 2nd premolar and 1st molar movement quantification with models B1 and A1, and no movement was expected. The second experiment was the movement quantification with models B1 and A2, and the calculated movements were compared with the prescribed displacements. For both experiments, the whole processes were repeated five times.

Estimations of errors and variations of P2 were shown in Tables 3.7-3.10. With a zero prescribed displacement in the first experiment, the maximum average calculated translation and rotation were 0.01 mm (± 0.06 mm) and 0.32 °(± 0.04 °) for 2nd premolars

(Tables**)**, and 0.04 mm (± 0.07 mm) and 0.09 ° (± 0.11 °) for 1st molars. The noise levels of P2 were 0.04 mm (± 0.07 mm) for translation and 0.32 ° (± 0.04 °) for rotation. Any linear and angular displacements that are smaller than these would be considered unreliable. For case 1 in the second experiment, with a 2 mm and 5° prescribed displacement, the average translations were 1.99 mm (± 0.06 mm) for 2nd premolar and 1.96 mm (± 0.07 mm) for 1st molar; and the average rotations were 4.74 ° (± 0.04 °) for 2nd premolar and 5.03 ° (± 0.03 °) for 1st molar. For Case 2, with the prescribed 2 mm translation in z axis and 5 ° prescribed rotations about the x and y axes, the calculated displacement components were 1.99 mm (± 0.06 mm) along z axis, 4.81 ° (± 0.10 °) about x axis, and 5.03 ° (± 0.07 °) about the y axis for 2nd premolar; and the calculated displacement components were 1.99 mm (± 0.07 mm) along z axis, 4.94 ° (± 0.10 °) about x axis, and 5.05 ° (± 0.03 °) about the y axis for 1st molar **(**Tables 3.9 and 3.10**)**.

By using P2, all six displacement components relative to the anterior inner curve of the hard palate were quantified. The maximum standard deviations were 0.07 mm for translation and 0.11 ° for rotation which are smaller than the displacement that are visually detectable clinically, thus providing improved quantification of tooth displacements. The accuracy is acceptable. The maximum translational error was 0.13 mm, and the rotational error was 0.30 °, which cannot be detected visually in the clinic. The maximum translational error was 6.5% of the prescribed value, and the maximum rotational error was 6.0%, Table 3.9 and 3.10, which were smaller than those obtained from the dental casts.

Table 3.7. Results for 2nd premolars with zero prescribed displacement.

	Translation (mm)			Rotation (°)		
	x	y	x	y	x	y
1	0.04	0.04	-0.02	0.15	-0.01	0.26
2	0.02	0.02	0.08	0.27	-0.02	0.34
3	0.02	-0.05	-0.05	0.02	-0.05	0.36
4	0.00	-0.01	-0.03	0.12	0.01	0.35
5	-0.02	0.04	0.06	0.27	0.02	0.28
Average	0.01	0.01	0.01	0.17	-0.01	0.32
Std	0.02	0.04	0.06	0.11	0.03	0.04

Table 3.8. Results for 1st molars with zero prescribed displacement.

	Translation (mm)			Rotation (°)		
	x	y	x	y	x	y
1	0.04	0.04	0.01	0.07	-0.05	-0.07
2	0.00	0.02	0.13	0.19	-0.06	0.01
3	0.02	-0.05	-0.04	-0.06	-0.09	0.02
4	0.00	-0.01	-0.01	0.04	-0.03	0.01
5	-0.02	0.04	0.10	0.19	-0.01	-0.05
Average	0.01	0.01	0.04	0.09	-0.05	-0.02
Std	0.02	0.04	0.07	0.11	0.03	0.04

Table 3.9. Results for 2nd premolars with prescribed displacements.
(Tz: Translation along z axis; Rx, Ry, and Rz: Rotation about x, y, and z axes)

	Case 1		Case 2		
	Tz (mm)	Rz (°)	Tz (mm)	Rx (°)	Ry (°)
1	2.02	4.80	2.01	4.83	5.03
2	1.92	4.71	1.92	4.71	5.05
3	2.05	4.70	2.05	4.96	5.08
4	2.03	4.71	2.03	4.86	5.02
5	1.94	4.77	1.95	4.72	4.99
Mean	1.99	4.74	1.99	4.81	5.04
Standard deviation	0.06	0.04	0.06	0.10	0.03
Error	0.01	0.26	0.01	0.19	0.04

Table 3.10. Results for 1st molars with prescribed displacements.
(Tz: Translation along z axis; Rx, Ry, and Rz: Rotation about x, y, and z axes)

	Case 1		Case 2		
	Tz (mm)	Rz (°)	Tz (mm)	Rx (°)	Ry (°)
1	1.99	5.09	2.02	4.95	5.04
2	1.87	5.01	1.90	4.83	5.06
3	2.04	5.00	2.07	5.08	5.09
4	2.01	5.00	2.04	4.98	5.03
5	1.90	5.07	1.93	4.84	5.01
Mean	1.96	5.03	1.99	4.94	5.05
Standard deviation	0.07	0.04	0.07	0.10	0.03
Error	0.04	0.03	0.01	0.06	0.05

3.7.3. Quantification of Skeletal Landmark Movement Validation

A human dry skull was used to validate the skeletal landmark movement quantification procedure (P3). Sixteen titanium balls (0.8mm in diameter) were glued to the dry skull at selected anatomical locations (Figure 3.19 (a)). Titanium balls served as landmarks to avoid potential identification errors. With maximum intercuspation, the dry skull was scanned using i-CAT® CBCT machine at 0.3 mm resolution in enhanced portrait mode. The mandible was then slightly (~8 mm) opened and a small amount of bite registration material (EXABITE II NDS® vinyl polysiloxane) (GC America Inc., Alsip, IL) was injected between the upper and lower dentitions (Figure 3.19 (b)). Then, a second CBCT scan was taken with the same settings. With different regions of superimposition, the displacements of the landmarks were quantified on the digital models of the closed and open jaw configurations.

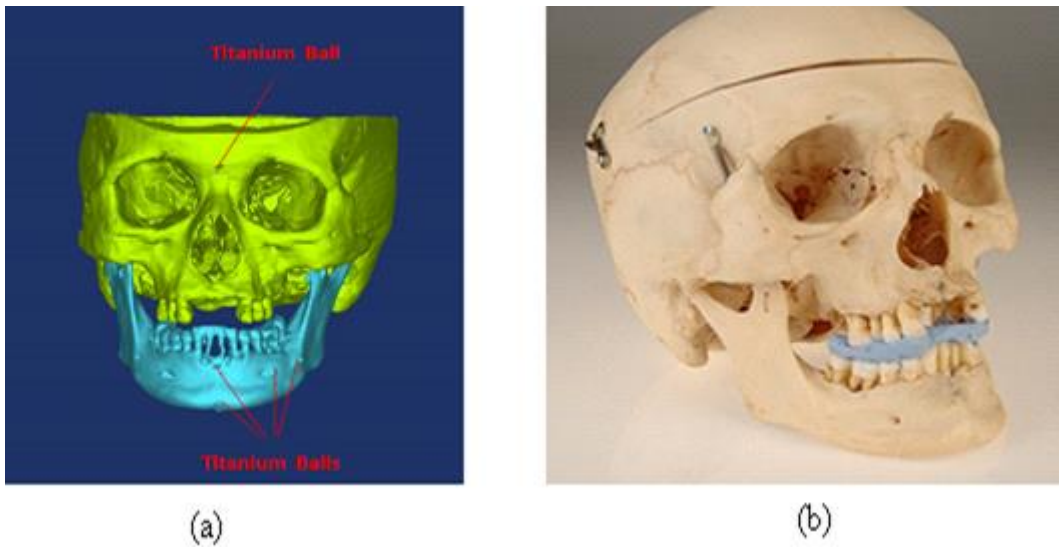

Figure 3.19. Dry skull.
(a) Dry skull CBCT scan with landmarks; (b) Dry skull with bite registration cr ème

Two whole skull digital models before (SK1) and after (SK2) jaw-opening were used for the cranial base superimposition. Two mandibular digital models before (MD1) and after (MD2) jaw-opening were used for the mandible superimposition.

To quantify the overall change of the face, SK1 and SK2 models were superimposed on the anterior cranial base; and the movements of all eleven landmarks were calculated relative to the Nasion (Figure 3.20). To quantify landmark movements relative to the mandible, MD1 and M2 were superimposed on the mandible stable structures; and the movements of eight mandible landmarks were calculated relative to pogonion (Pog). The entire process was repeated five times.

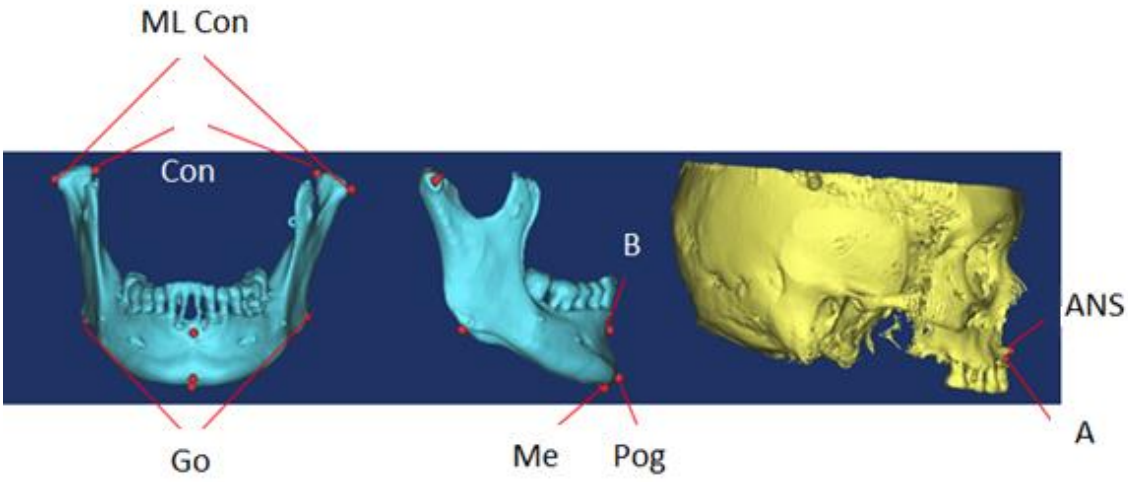

Figure 3.20. Landmarks.
ML Con: medial and lateral poles; Con: condylion; Go: gonion; B: B point; Pog: pogonion; Me: Menton; ANS: anterior nasal spine; and A: A point

The prescribed landmark movements relative to the anterior cranial base were obtained as follows: first, two whole skull digital models (SK1 and SK2) were superimposed by using the four markers glued on the anterior cranial base bones (Figure 3.21); second, the movements of each landmark were calculated by using the coordinates of the same point in the two models. The prescribe landmark movements relative anterior cranial base were shown in Table 3.11. When the second CBCT scan was taken with the mandible slightly open, the entire mandible was moved. So, ideally, there were no relative movements of the landmarks with superimposition on mandible. The prescribed landmark movements relative to the mandible were all zero.

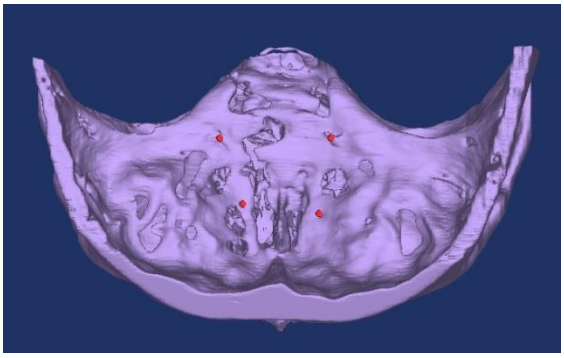

Figure 3.21. Four markers on anterior cranial base.

Table 3.11. Prescribe landmark movements relative to anterior cranial base (RL = left and right).

	Translation (mm)			Rotation (°)		
	x	y	z	x	y	z
B	8.19	2.00	1.00	-1.05	1.67	0.22
Pog	8.82	3.83	0.00	-2.37	1.80	1.31
Me	8.84	4.87	0.00	-2.97	1.71	1.59
R Go	3.50	4.24	1.00	-0.91	0.05	0.78
L Go	2.40	4.04	1.00	-1.14	0.30	0.89
R ML Con	0.05	0.24	0.00	-0.04	0.01	0.05
L ML Con	0.03	-0.05	0.00	0.01	0.01	-0.02
R Con	-0.07	-0.15	0.00	0.03	-0.02	-0.02
L Con	-0.02	-0.05	0.00	0.01	-0.01	-0.01
A	0.29	0.32	0.00	-0.18	0.10	0.13
ANS	0.30	0.16	0.00	-0.09	0.11	0.02

Estimations of errors and variations of P3 were shown in Tables 3.12-3.14. The maximum differences between the average calculated landmark movements and the prescribed movements relative to anterior cranial base were 0.94 mm (± 0.08 mm) for translation (R Con, z direction translation) and 0.63 ° (± 0.03 °) for rotation (R con, x direction rotation) (Tables 3.12 and 3.13). With zero prescribed movements relative to the mandible, the maximum absolute values of average calculated translation and rotation were 1.21 mm (± 0.15 mm) and 0.62 °(± 0.21 °) (Table 3.14).

Compared with the CBCT maxillary tooth movement quantification procedure (P2) whose validation results were shown in Section 3.7.2.2, the maximum standard deviations and errors were significantly increased for both translations and rotations. The maximum standard deviation for translations was increased from 0.07 mm to 0.62 mm, and for rotations was increased from 0.11 ° to 0.21 °. The maximum error for translations was increased from 0.13 mm to 1.45 mm, and for rotations was increased from 0.30 ° to 0.63 °. The main reason for the error and variation increase is the difficulty in identifying 3D landmark points accurately and consistently.

With P3, all six displacement components of the landmarks relative to the anterior cranial base region and mandible stable structure were quantified. The maximum standard deviations were 0.62 mm for translation and 0.21 ° for rotation. The variation is smaller than that is visually detectable clinically. The accuracy is acceptable. The maximum translational error was 0.94 mm, and the rotational error was 0.63 °, which are hard to detect visually in the clinic, Tables 3.13 and 3.14.

Table 3.12. Averages and standard deviations of landmark movements relative to anterior cranial base (RL = left and right).

	Translation (mm)			Rotation (°)		
	x	y	z	x	y	z
B	8.38 ± 0.24	2.35 ± 0.12	1.58 ± 0.04	-1.17 ± 0.06	1.54 ± 0.05	0.37 ± 0.03
Pog	8.95 ± 0.22	3.73 ± 0.08	0.77 ± 0.05	-2.23 ± 0.05	1.61 ± 0.03	1.27 ± 0.02
Me	9.16 ± 0.23	4.27 ± 0.07	0.01 ± 0.05	-2.6 ± 0.04	1.78 ± 0.03	1.34 ± 0.02
R Go	3.97 ± 0.38	4.64 ± 0.10	0.82 ± 0.06	-1.15 ± 0.01	0.18 ± 0.02	0.83 ± 0.04
L Go	2.82 ± 0.35	4.74 ± 0.07	1.28 ± 0.06	-1.31 ± 0.02	0.33 ± 0.06	1.04 ± 0.04
R ML Con	0.49 ± 0.45	0.08 ± 0.22	-0.36 ± 0.07	-0.19 ± 0.02	0.31 ± 0.07	-0.13 ± 0.09
L ML Con	0.36 ± 0.38	0.11 ± 0.17	0.45 ± 0.07	0.23 ± 0.04	-0.13 ± 0.1	-0.08 ± 0.08
R Con	-0.03 ± 0.45	-0.21 ± 0.21	0.95 ± 0.08	0.67 ± 0.03	-0.49 ± 0.1	-0.30 ± 0.09
L Con	-0.82 ± 0.41	-0.38 ± 0.18	0.15 ± 0.07	0.14 ± 0.04	-0.27 ± 0.11	0.17 ± 0.09
A	-0.13 ± 0.26	0.12 ± 0.21	-0.52 ± 0.02	-0.17 ± 0.11	0.12 ± 0.09	0.11 ± 0.06
ANS	0.09 ± 0.27	0.16 ± 0.22	0.40 ± 0.02	0.00 ± 0.12	-0.09 ± 0.1	0.08 ± 0.06

Table 3.13. The difference between the average calculated landmark movements and the prescribed movements relative to anterior cranial base.

	Translation (mm)			Rotation (°)		
	x	y	z	x	y	z
B	0.19	0.35	0.57	0.12	0.13	0.14
Pog	0.13	0.11	0.76	0.14	0.20	0.05
Me	0.32	0.61	0.00	0.37	0.06	0.26
R Go	0.46	0.39	0.18	0.24	0.12	0.05
L Go	0.41	0.69	0.28	0.17	0.03	0.15
R ML Con	0.43	0.16	0.37	0.16	0.30	0.18
L ML Con	0.32	0.15	0.45	0.21	0.15	0.06
R Con	0.04	0.07	0.94	0.63	0.47	0.29
L Con	0.81	0.34	0.15	0.12	0.27	0.18
A	0.42	0.20	0.52	0.01	0.02	0.02
ANS	0.22	0.01	0.40	0.08	0.20	0.06

Table 3.14. Averages and standard deviations of landmark movements relative to mandible (RL = left and right).

	Translation (mm)			Rotation (°)		
	x	y	z	x	y	z
B	0.37 ±0.01	-0.27 ±0.03	0.72 ±0.1	0.26 ±0.02	-0.13 ±0.03	-0.17 ±0.01
Me	0.60 ±0.05	-0.23 ±0.15	-0.05 ±0.05	0.04 ±0.09	0.43 ±0.01	-0.12 ±0.06
R Go	0.17 ±0.39	0.36 ±0.13	0.08 ±0.04	-0.09 ±0.06	-0.01 ±0.05	0.09 ±0.11
L Go	-0.16 ±0.25	0.18 ±0.2	0.57 ±0.05	0.04 ±0.07	-0.16 ±0.05	0.09 ±0.11
R ML Con	-0.75 ±0.62	0.20 ±0.18	-0.57 ±0.15	-0.32 ±0.09	0.18 ±0.18	0.3 ±0.15
L ML Con	-0.49 ±0.38	-0.38 ±0.07	0.21 ±0.15	0.31 ±0.04	-0.34 ±0.11	0.05 ±0.11
R Con	-0.80 ±0.61	-0.99 ±0.17	0.77 ±0.16	0.54 ±0.08	-0.62 ±0.21	0.00 ±0.15
L Con	-0.17 ±0.44	-0.48 ±0.11	-0.02 ±0.16	0.12 ±0.05	-0.35 ±0.14	0.26 ±0.12

4. IMAGE ANALYSIS IN CANINE RETRACTION STUDY

4.1. Introduction

Orthodontic space closure is a common procedure that requires the movement of a single tooth or a segment of teeth into edentulous spaces. Two treatment strategies are commonly used: (1) translation (TR), a one-step process or (2) controlled tipping (CT) followed by root correction, a two-step process. In this study, both strategies were implemented concurrently in patients who needed bilateral canine retraction. The study is intended to determine which strategy moves the canine faster into position with less side-effect.

A split mouth clinical experimental approach, approved by the Indiana University Institutional Review Board (IRB), was used with each patient. Randomly, one side received a segmental T-loop designed for controlled tipping, the other side for translation. Patients were scheduled for monthly appointments. A treatment interval (TI) was defined by milestones, i.e., a reduction of 1+ mm in the inter-bracket distance (IBD) of one side which was measured as the distance from the mesial aspect of the auxiliary tube of the 1st molar bracket to the distal aspect of the canine bracket. When a milestone was reached, a new T-loop was designed and reactivated for both sides.

The goal of this study was to (1) quantify the treatment outcomes and side effects, such as unwanted displacement and anchorage loss; (2) compare the two strategies in terms of treatment time and side effects.

4.2. Subjects

Fifteen patients (five male and ten female) participated in this split-mouth trial study at the Indiana University School of Dentistry graduate orthodontic clinic. The average age of the patients was 21.1 years, ranging from 14 to 47. These patients needed bilateral canine retractions to close extraction spaces as parts of their treatment plans. The average treatment period was 158.4 days, ranging from 75 to 357 days.

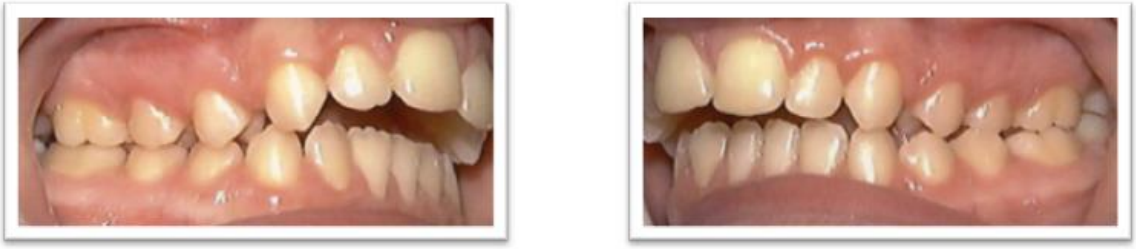

Figure 4.1. Pictures of a potential patient.

Maxillary dental casts were made before treatment and at each milestone; and a pair of Cone-beam Computed Tomography (CBCT) scans was taken before- and after-treatment for each patient. The casts were digitized with an OPTIX 400S® 3D laser scanner, and the digital models of the cast were reconstructed with reverse engineering software, Rapidform®. The CBCT images were taken with i-CAT®. The scan resolution was 0.25 mm, taken at 26.9s. The images were saved as DICOM (Digital Imaging and Communications in Medicine) format files and processed by the MIMCS® image processing software. Figure 4.2 shows the digital cast model and CBCT model.

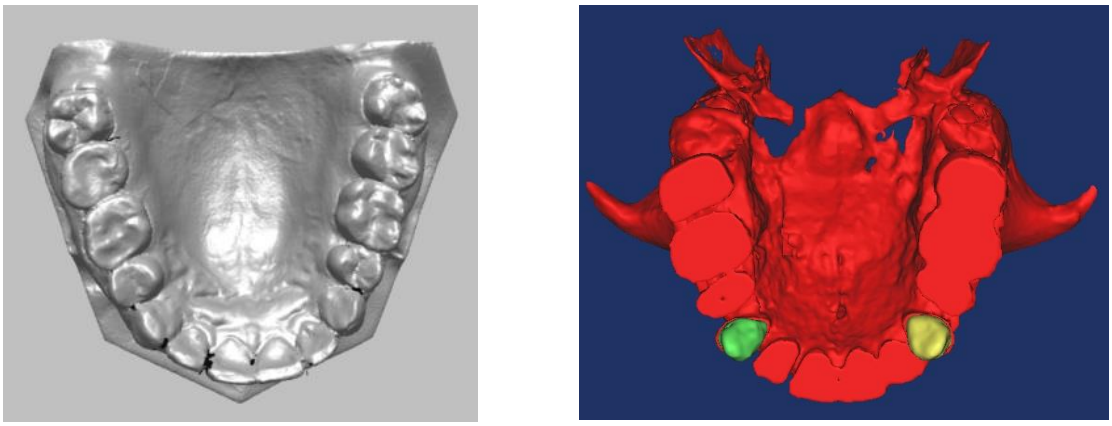

Figure 4.2. Dental cast and CBCT models.

4.3. Hypotheses and Parameters

The hypotheses for this study are:

H4.1: Canines move linearly with respect to time.

H4.2: Canine displacement pattern is uniquely controlled by the initial load system, including the moment force ratio (M/F).

H4.3: Control tipping/uprighting moves the canine into position faster than translation.

H4.4: There is no anchorage loss when a removable or fixed TPA appliance was applied.

H4.5: Control tipping/uprighting strategy causes greater anchorage loss than translation strategy.

H4.6: Fixed TPA reduces the amount of anchorage loss compared to removable TPA.

These hypotheses were tested with the following parameters:

Treatment interval (TI) displacement was the canine displacement within each TI. It was expressed in both global coordinate system (GCS, Section 3.2.1) and canine coordinate system (CCS, Section 3.2.1).

Resultant TI displacement was defined in 4.1, where RD_{TI} was the resultant displacement; x_{TI} and y_{TI} were the x and y direction translation components of corresponding TI displacement.

$$\mathrm{RD}_{TI} = \sqrt{\mathrm{x}_{TI}{}^2 + \mathrm{y}_{TI}{}^2}\,. \quad (4.1)$$

Resultant displacement was defined in 4.2, where RD was the resultant movement; x and y were the x and y direction translation components of corresponding displacement.

$$\mathrm{RD} = \sqrt{\mathrm{x}^2 + \mathrm{y}^2}\,. \quad (4.2)$$

Resultant Movement Rate is defined in 4.3, where RR was the resultant Movement Rate; RD was the resultant movement; and T was the number of days.

$$RR = \frac{RD}{T}\,. \quad (4.3)$$

Movement rate in distal-mesial direction was defined in Eq. 4.4, where DR was the movement rate in mesial/distal direction; y was the mesial/distal direction translation components of a displacement expressed in CCS (section 3.2.1); and T was the number of days.

$$DR = \frac{y}{T}\,. \quad (4.4)$$

First molar displacement was the displacement of 1st molar during the treatment. It was calculated from the before- and after-treatment CBCT models, and expressed in a rectangular coordinate system (UCS, Section 3.2.2.1) with six displacement components, three translations and three rotations.

Second premolar displacement was the displacement of 2nd premolar during the treatment. It was calculated by using the before- and after-treatment CBCT models, and expressed in a rectangular coordinate system (UCS, Section 3.2.2.1) with six displacement components, three translations and three rotations.

TI displacement, resultant TI displacement, resultant TI movement rate, and TI movement rate in distal-mesial direction are used to test the hypotheses related to canine

movement (**H4.1** to **H4.3**). First molar displacement and second premolar displacement are quantified for the hypotheses about anchorage loss (**H4.4** to **H4.6**).

4.4. Quantification of Canine Movement

4.4.1. Canine Displacement and Movement Rate Quantification

In each TI, two dental casts, one at the beginning (pre-TI) and one at the end (post-TI) were fabricated after alginate impression. Then the digital dental cast procedure (P1, Section 3.5 Figure 3.15) was used to calculate canine TI displacements and resultant TI displacements. After scanning and reconstructing, the two digital dental casts were aligned by overlapping the palatal (rugae) area. Next, the crowns of the canine in the two locations (pre-TI and post-TI) were aligned using the entire crown surface points. Transformation matrix between the two positions was calculated. Then the canine's six displacement components in terms of translation along and rotation about the three coordinate axes were computed from the entries of the transformation matrix [35] and expressed in both global coordinate system (GCS, Section 3.2.1) and canine coordinate system (CCS, Section 3.2.1). The process repeated for each of the TIs.

The resultant movement rates and movement rates in distal-mesial direction were determined by using Eq. 4.3 and 4.4 (Section 4.3). The displacements from the last treatment periods were not included because teeth movements were checked at patient's office visits while the canine displacement might stop sometimes within the period, which was not recorded. This means that if a patient had n TIs, then the movement rate was calculated based on the sum of the first (n-1) TI displacements.

The intrusion and extrusion are expected to be small and will be represented by the z-components in both GCS and CCS. Based on the coordinate system design, the z-components in CCS had the same value as the corresponding z-components in GCS.

The means and standard deviations of the TI displacements, resultant movement rates, movement directions, movement rates in distal-mesial direction and intrusions/extrusions were calculated. Differences in canine movement rates between controlled tipping side and translation side were compared with paired t-tests, since there was only one observation on each side for each subject. The equal-variance and normality assumptions were checked using normal probability plots (Figure 4.3). The normal probability plot was performed by using Matlab®. Differences were considered to be significant at $p<0.05$.

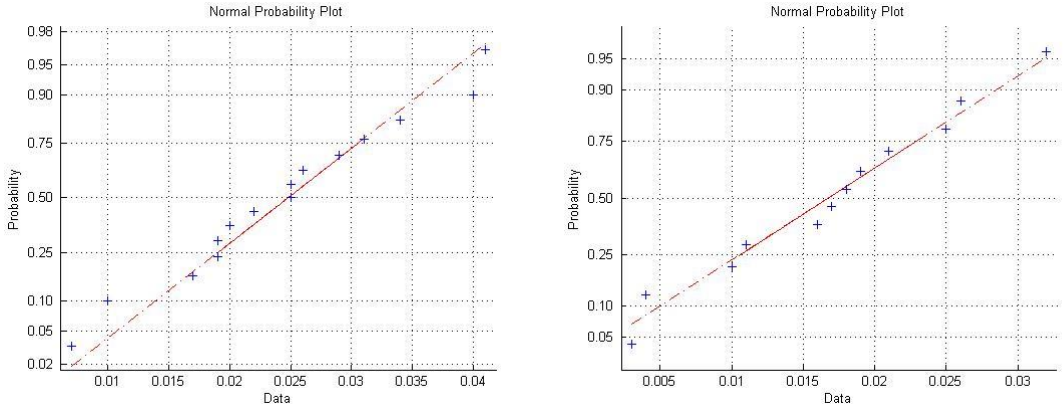

Figure 4.3. Normal probability plots for movement rate data.

4.4.2. Results and Discussion

4.4.2.1. Canines Movement and Treatment Time (**H4.1**)

In order to find the relationship between canine movement and treatment time, linear regressions were performed on resultant TI displacements with respect to treatment time (Figure 4.4). The determine factor R^2 were 0.0153 for controlled tipping, and 0 for translation, respectively.

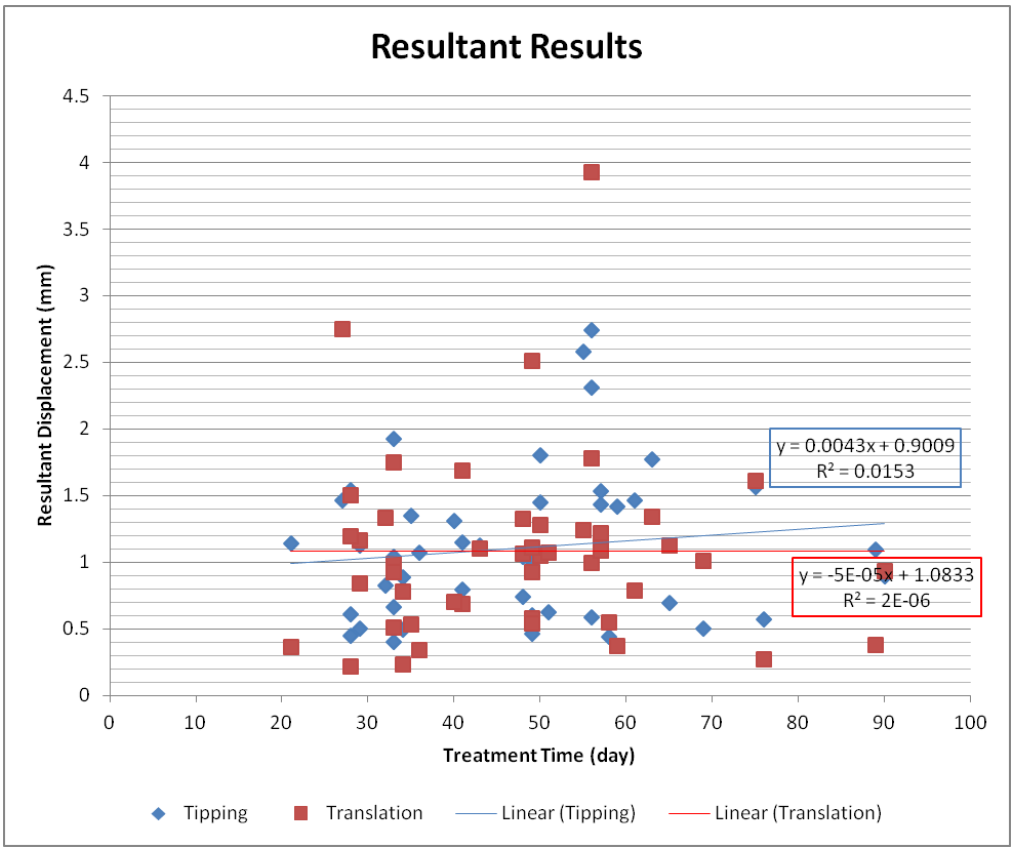

Figure 4.4. Relationship between resultant TI displacements and treatment time.

Studies on beagle dogs showed a four phase tooth movement [38, 41]: phase 1, initial tooth movement; phase 2, arrest of tooth movement; phase 3, acceleration of tooth movement; and phase 4, linear tooth movement. In the last phase of tooth movement, there was a linear relationship between tooth movement and treatment time. However, no human studies provided sufficient evidences to support this relationship in current literature [50]. In this study, the determined factors, R^2, were close to 0 for both translation and controlled tipping data. This means that the relationship between tooth movement and treatment time is highly nonlinear. There were several possible reasons to explain this nonlinear result. First, the tooth movement data collected much more frequently in animal studies (twice a week). This made it possible to observe the detailed changes in tooth movement. Second, the appliances used for tooth movement was segmental T-loop in this study. As teeth moved, the forces and moments provided by segmental T-loops changed. Patients' teeth movement might stop in the middle of a

treatment interval due to the force drop. Third, there was a large variation in tooth movement among patients.

4.4.2.2. Canine Movement Pattern and Orthodontic Force System (**H4.2**)

Teeth displacement pattern can be placed into three categories controlled tipping (CT), Translation (TR), and torque. Traditionally, the definition for CT was that as the tooth tips the root and crown move in the same direction; for TR was equal movement of crown and root; and for torque was that root apex moves further than crown [16].

Since tipping or translation was randomly assigned to each side, side is not a controlled parameter. To be consistent, all the displacement components were expressed in CCS on the left side (Section 3.2.1). There were two groups defined by the appliance design, CT group or TR group. Specific appliances were designed for either CT or TR. Each patient experienced multiple treatment intervals (TIs) defined by milestones. It is possible that one canine on one side might have small displacement which much less than 1 mm. After excluding the interval data with less than 0.3 mm mesial/distal displacements based on the translational noise level obtained from the digital dental cast procedure validation (Section 3.7.2.1), 78 data sets remained (42 data sets for CT and 36 for TR). The means and standard deviations of the canine displacement components were calculated (Tables 4.1-4.4).

A 3D tooth displacement consists of three translational and three rotational components. Translational components on the CT side were shown in Table 4.1. In the buccal/lingual direction, more TIs had buccal displacement than lingual (27 to 15 TIs). In mesial/distal direction, all the TIs have distal direction movements. In intrusion/extrusion direction, the number of TIs with intrusion displacement was very close to the number of TIs with extrusion displacement (20 to 22 TIs). The difference between the average buccal and lingual displacements was 0.1 mm; the difference between the average intrusion and extrusion displacements was 0.2 mm; while the difference between the average distal and mesial displacements was 1.0 mm.

Table 4.1. CT side translational components results.

(mm)	Buccal	Lingual	Distal	Mesial	Intrusion	Extrusion
No. of TIs	27	15	42	0	20	22
Minimum	0.0	0.0	0.4		0.0	0.0
Maximum	1.6	1.4	2.9		0.8	2.5
Average	0.4	0.5	1.0		0.3	0.5
Standard Deviation	0.3	0.4	0.6		0.2	0.6

CT side rotational components are shown in Table 4.2. In the distal/mesial direction, both distal and mesial tippings were observed. The number of TIs with distal tipping was greater than the number of TIs with mesial tipping (26 to 16 TIs). In the ligual/buccal direction, more lingual tipping TIs than buccal tipping TIs were observed (26 to 16 TIs). For rotation, the numbers of TI with mesial out/in rotations were very close (22 to 20 TIs).

Table 4.2. CT side rotational components results.

(°)	Distal tipping	Mesial tipping	Lingual tipping	Buccal tipping	Mesial out	Mesial in
No. of TIs	26	16	26	16	22	20
Minimum	0.0	0.2	0.1	0.1	0.1	0.2
Maximum	11.8	7.5	10.6	6.5	22.3	9.8
Average	2.9	2.8	3.2	2.7	3.0	2.4
Standard Deviation	2.9	1.8	2.6	2.1	4.7	2.3

Translational components on the TR side are shown in Table 4.3. In the buccal/lingual direction, more TIs had lingual displacement than buccal displacement (25 to 11 TIs). In the mesial/distal direction, the number of TIs with distal displacement was much greater than the number of TIs with mesial displacement (35 to 1 TIs). In intrusion/extrusion direction, the number of TIs with intrusion displacement was close to the number of TIs with extrusion displacement (15 to 21 TIs). The difference between the average buccal and lingual displacements was 0.1 mm; the difference between the average intrusion and extrusion displacements was 0.2 mm; while the difference between the average distal and mesial displacements was 0.7 mm.

Table 4.3. TR side translational components results.

(mm)	Buccal	Lingual	Distal	Mesial	Intrusion	Extrusion
No. of TIs	11	25	35	1	15	21
Minimum	1.0	0.0	2.5	0.3	0.0	0.0
Maximum	0.1	1.1	0.3	0.3	1.3	3.7
Average	0.4	0.5	1.0	0.3	0.3	0.5
Standard Deviation	0.3	0.3	0.5		0.4	0.8

Rotational components on the TR side are shown in Table 4.4. Among the rotation components, the number of TIs with distal tipping was the same to the number of TIs with mesial tipping (18 to 18 TIs). Similar observations can be found in the mesial out/in rotations (17 to 19 TIs). However, the difference of the number of TIs with lingual tipping and buccal tipping was more significant (15 to 21 TIs).

Table 4.4. TR side rotational components results.

(°)	Distal tipping	Mesial tipping	Lingual tipping	Buccal tipping	Mesial out	Mesial in
No. of TIs	18	18	15	21	17	19
Minimum	0.2	0.9	0.0	0.1	0.5	0.1
Maximum	13.5	9.2	7.6	7.6	8.2	10.7
Average	3.4	3.4	3.0	2.1	2.9	4.2
Standard Deviation	3.1	2.5	2.4	1.7	2.4	3.2

Under the controlled retraction load system, the canines moved generally distally. Relatively large lingual/buccal displacement components existed. Figure 4.5 showed that 36 of 42 TIs moved in the directions within 45 °to distal direction for TIs on the CT side. Figure 4.6 showed that 30 of 36 TIs moved in the directions within 45 °to distal direction for the TIs on the TR side.

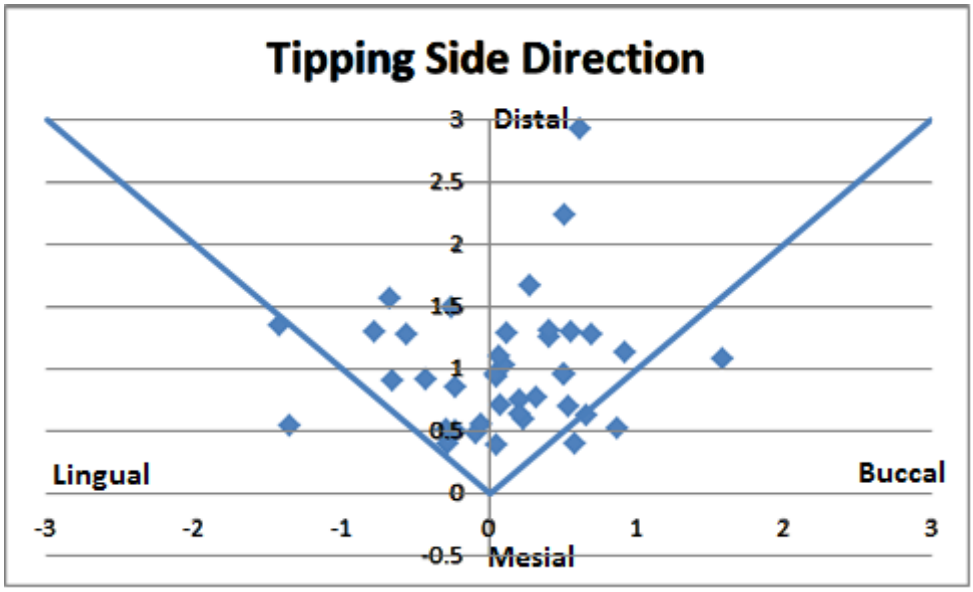

Figure 4.5. Tipping side displacement directions.

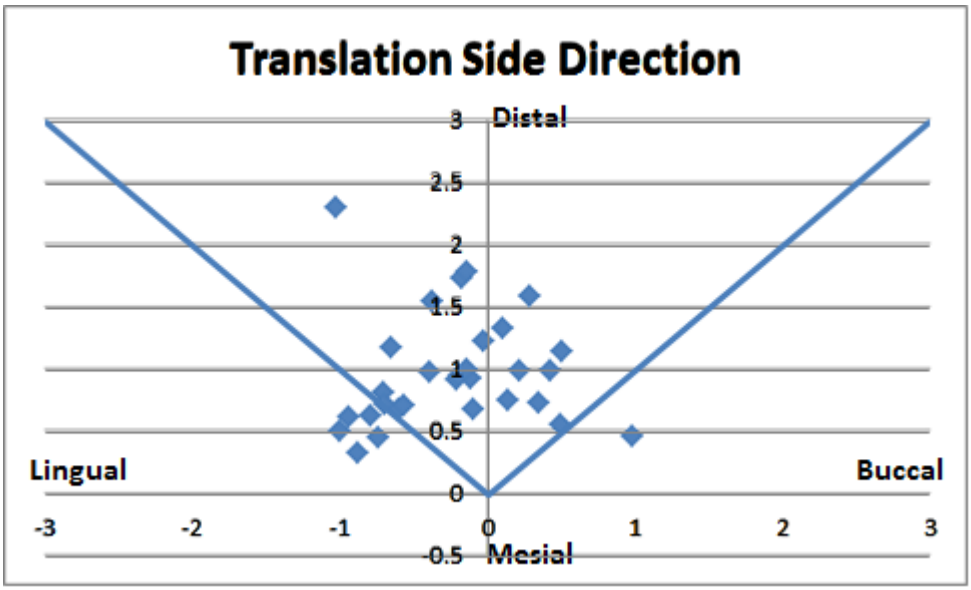

Figure 4.6. Translation side displacement directions.

The displacement reported was with respect to the CCS at the beginning of each TI. It is the absolute displacement as a result of the applied orthodontic load system. This displacement may not be intuitive clinically because the canine can only be evaluated

relative to the posterior segment, which may also move (anchorage loss) due to the treatment. However, the relative displacement components can be easily calculated by subtracting the displacement of the posterior segment from the displacement of the canine.

The magnitude of the tooth displacement is not the main focus of this part of the study because it is patient dependent and affected by the treatment time that varied significantly. For the purpose of this study, the displacement pattern, including tipping, translation and their directions as well as the movement direction are the focuses.

In this study, the force system applied on canines was well controlled. The initial load system consisted of a retraction force, an anti-tipping and an anti-rotation moment with minimum force and moment components in other directions. If hypothesis **H4.2** is valid, the canine displacement pattern should be consistent and the canine should move distally with either CT or TR. However, the canine displacements varied significantly in both displacement pattern and direction. With the retraction forces, the canines should move distally. This was true in most TIs, Tables 4.1 and 4.3. One TI had a mesial displacement due to mesial tipping. The displacement was only 0.30 mm, which was at the translational process error level. The buccal/lingual displacement could be in either direction because the initial force component in the direction was in either direction. Overall, the number of TIs with buccal displacement was almost the same as the number of TIs with lingual displacement (38 to 40). However, more controlled tipping side TIs had buccal displacement (64.29%), and more translation side TIs had lingual displacement (69.44%). The clear correlation between the direction of initial force and final displacement was not found. Interpersonal differences in terms of bone quality and initial tooth position relative to the neighboring teeth might contribute to the inconsistency. The results showed that a specified patient tended to have either buccal or lingual displacement for all of his/her TIs. Eleven of all 15 patients had more than 66.7% of their TIs moving in either buccal or lingual direction. When considering the PIs with larger displacements, this trend was more obvious. Among the 11 patients who had TIs

with greater than 0.5 mm buccal or lingual displacements, 6 patients had all TIs with the either buccal or lingual direction, and another 3 patients had more than 66.7% of their TIs moving in either buccal or lingual direction.

In this study, the canine displacement pattern was defined based on mesial/distal tipping angles, Table 4.5. The displacement pattern classification results were shown in Table 4.6. Under the CT treatment strategy, 52.4% TI resulted in controlled tipping; 14.3% were translation; and the other 33.3% were torque. Under the TR strategy, 16.7% TI were actually translation; 41.7% were controlled tipping; and the other 41.7% were torque. According to our hypothesis, when certain load system was applied, canine movement should be consistent. Our results failed support the theory strongly. The initial load system does not dictate the final canine displacement pattern, meaning there are other key factors controlling the clinical outcomes. The possible factors include: 1) initial alignment of the tooth to the alveolar bone; 2) the geometric constraints at the root; 3) the alveolar bone quality; 4) the bone modeling and remodeling cycles; and 5) personal biological reaction to the load. The behavior of the segmental T-Loop also contributed the variation. Previous study showed that the load system of the T-loop changed significantly as the canine moved. The changes varied greatly among individual, which may contribute to the large displacement variation. In general, the M/F in the retraction direction increases as the canine is retracted. Since the M/F for TR is higher than CT, it is expected that TR side will have higher M/F than the CT side, meaning that higher possibility to have torque. This has been demonstrated in our study. The TR side has 42% torque while the CT side has 33%. Further studies will be focused on the effects of other factors.

Table 4.5. Canine displacement pattern definition.

Controlled Tipping	Translation	Torque
> 1 °Distal tipping	≤ 1° Distal tipping or ≤ 1° Mesial tipping	> 1 °Mesial tipping

Table 4.6. Canine displacement pattern classification.

	Controlled Tipping		Translation		Torque	
	37		12		29	
	Tipping	Translation	Tipping	Translation	Tipping	Translation
Number	22	15	6	6	14	15
%	52.4	41.7	14.3	16.7	33.3	41.7

When segmental T-loops were used, the variations of the canine displacement components were large although the initial load system was well-controlled. In orthodontic practice, the load system may not be well controlled as reported in this study, thus larger variation in canine movement may be expected. However, the results are only for segmental T-loops. Different level of variation is expected with other type of appliances. The displacement reported was with respect to the CS at the beginning of each TI. It is the absolute displacement as a result of the applied orthodontic load system. This displacement may not be intuitive clinically because the canine can only be evaluated relative to the posterior segment, which may also move (anchorage loss) due to the treatment. However, the relative displacement components can be easily calculated by subtracting the displacement of the posterior segment from the displacement of the canine.

4.4.2.3. Canine Movement Rate (**H4.3**)

The resultant movement rates were shown in Figure 4.7. The rate for controlled tipping (CT) canines ranged between 0.007 and 0.036 mm/day; and for translation (TR) ranged between 0.007 and 0.034 mm/day. The movement rate difference varies among patients (between 0.0007 and 0.0205 mm/day). The movement directions varied from -60.3° to 58.7° with an average being 17.28° (± 20.81°) (Figure 4.8). Positive moving direction angle implied that tooth moved in buccal and distal direction; while negative angle implied that tooth moved in lingual and distal direction. Three CT and one TR canines had the magnitude of the angles greater than 45°.

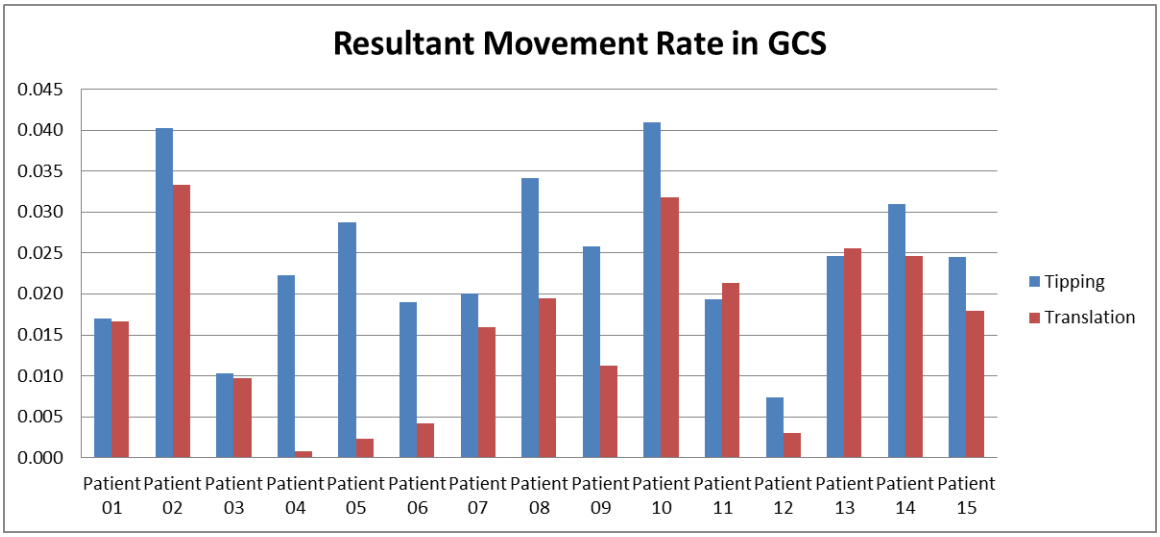

Figure 4.7. Canine resultant movement rate results in GCS.

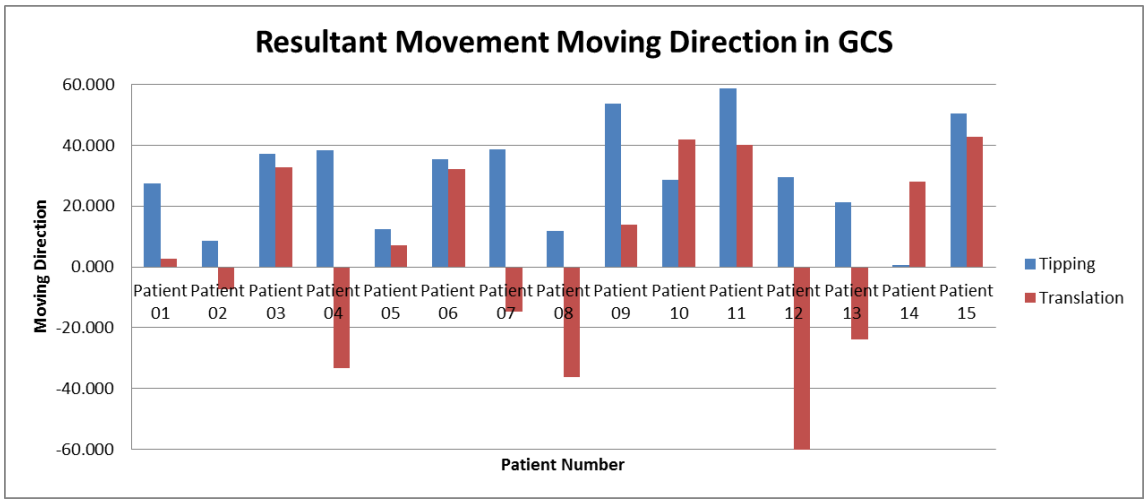

Figure 4.8. Canine resultant movement directions in GCS.

Distal-mesial movement rates are shown in Figure 4.9. The rate for controlled tipping ranged between 0.007 and 0.041 mm/day; and for translation ranged between 0.000 and 0.035 mm/day. The movement rate difference varies among patients (between 0.0000 and 0.0266 mm/day).

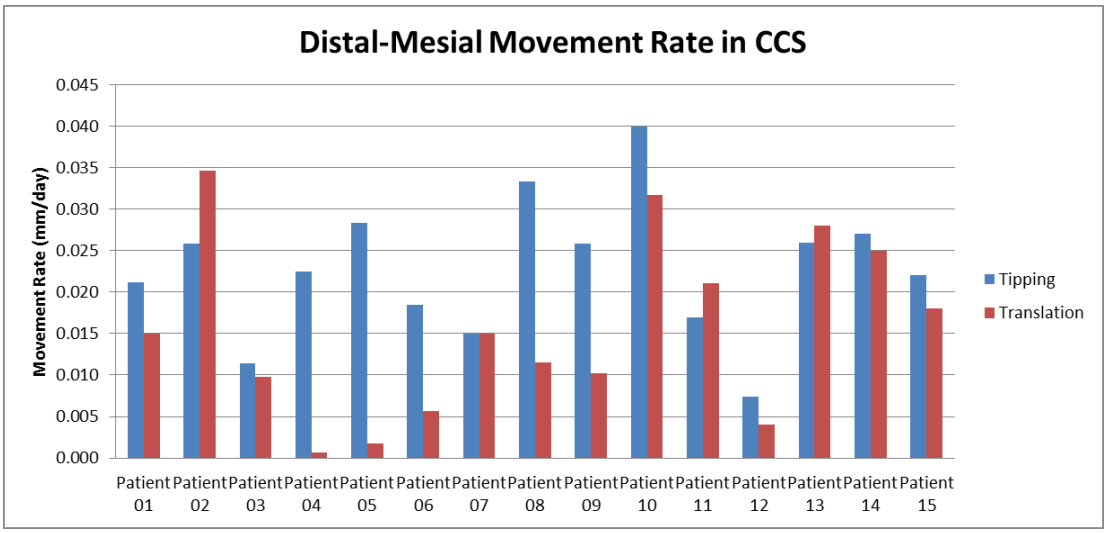

Figure 4.9. Canine distal-mesial direction movement rate results in CCS.

Except movements on occlusal plane (x and y direction movements), canines also have intrusions and extrusions (movements in z direction). Figure 4.10 showed the intrusions and extrusions results. Positive values are intrusions; and negatives are extrusions. For CT, eight patients had intrusions, and the other seven had extrusions. The maximum intrusion value was 0.65mm, and the maximum extrusion value was 1.20mm. For TR, five patients had intrusions, and the other ten had extrusions. The maximum intrusion value was 1.48mm, and the maximum extrusion value was 1.89mm.

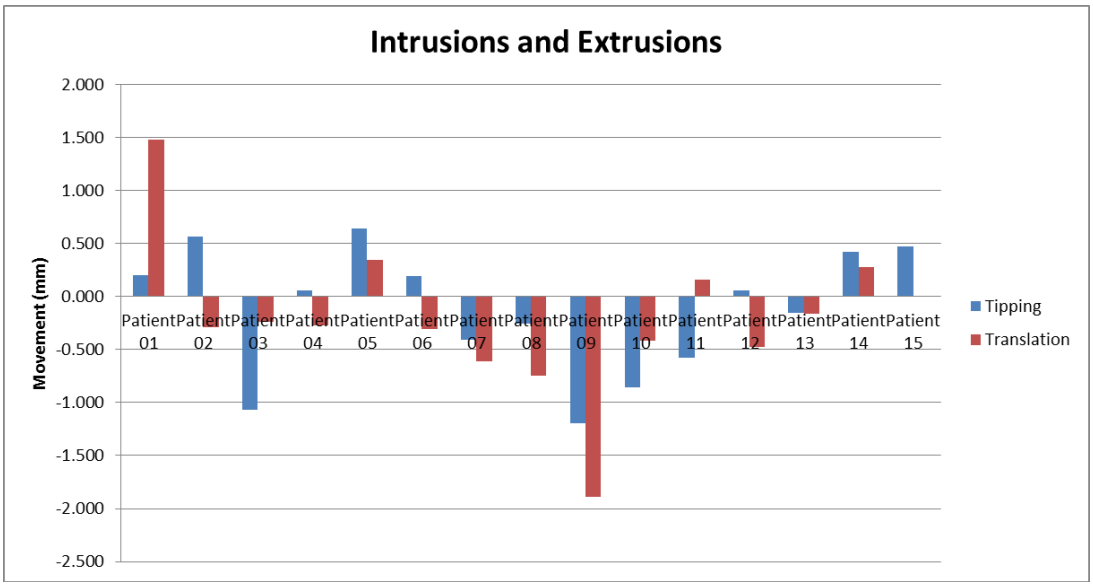

Figure 4.10. Intrusions and extrusions (Positive: intrusion; Negative: extrusion).

To estimate the averages and variations of the movement rates, the means and standard deviations shown in Table 4.7. For both resultant movement rates in GCS and distal/mesial direction movement rates in CCS, CT T-loops moved canines 41.7% and 40.9% faster than TRT-loops, respectively. In general, the differences were statistically significant.

Table 4.7. Movement Rates Statistical Analysis Results (mm/day).

	Tipping		Translation		Difference		p-value
	Mean	Standard Deviation	Mean	Standard Deviation	Mean	Standard Deviation	
GCS	0.024	0.010	0.016	0.011	0.0085	0.0084	0.0290
CCS	0.023	0.008	0.015	0.011	0.0073	0.0111	0.0480

In both GCS and CCS, most patients had larger movement rate in their tipping side than the rate in their translation side. Only two patients, Patient 11 and 13, had larger translation movement rate in GCS (Figure 4.11); while two patients, Patient 02 and 11, have larger translation movement rate in CCS (Figure 4.12). There is one patient, Patient

07, who has the same tipping and translation CCS movement rate (Figure 4.11). The average difference is 0.0085 mm/day in GCS, 0.0073 in CCS.

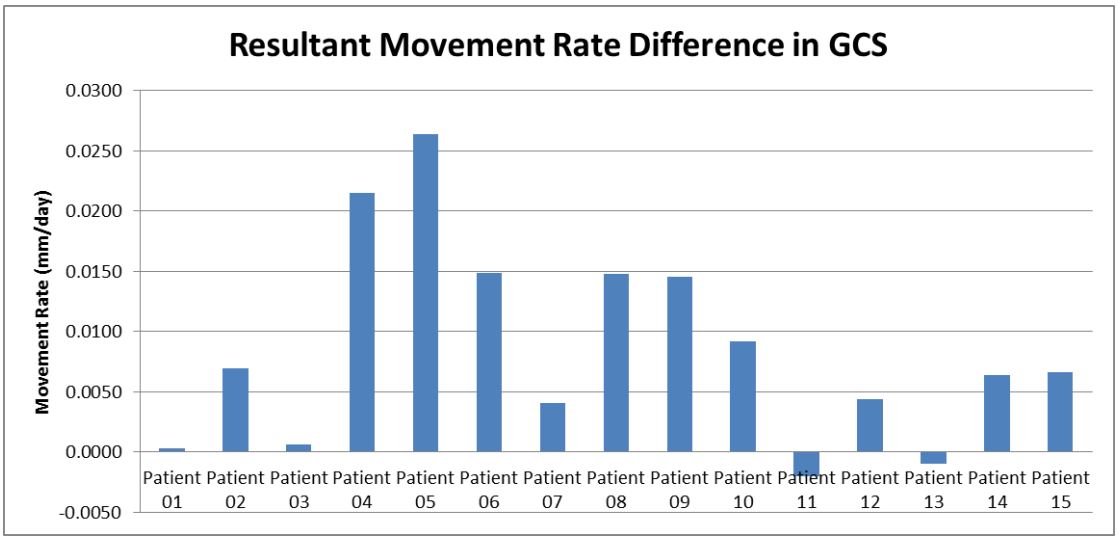

Figure 4.11. Movement rate difference in GCS.

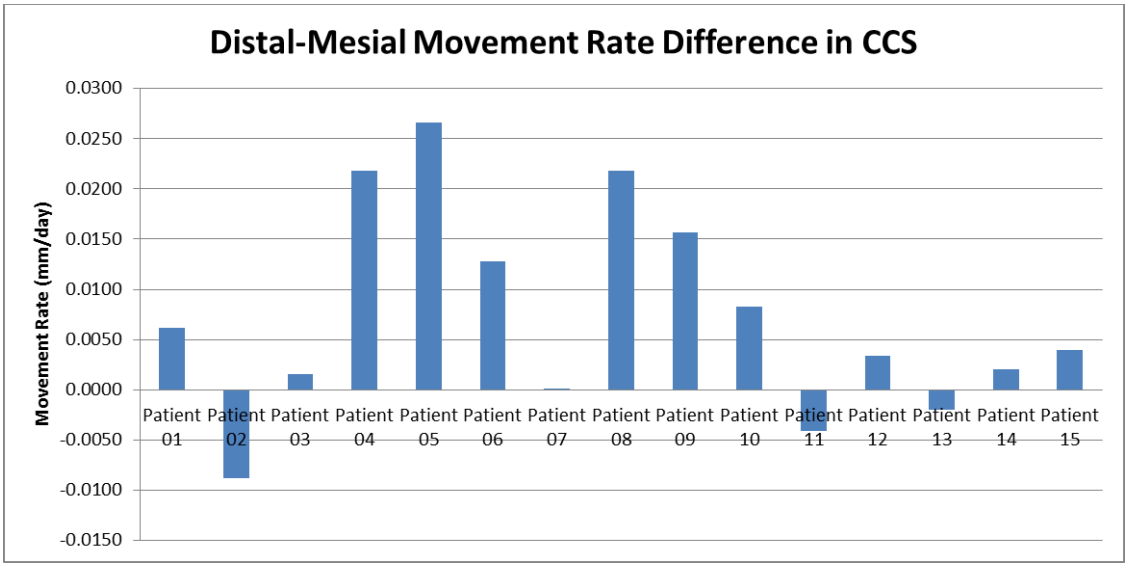

Figure 4.12. Movement rate difference in CCS.

The means and standard deviations of movement directions in GCS were shown in Table 4.8. Movement directions of translation side had much smaller mean and much greater standard deviation than controlled tipping side. This is because all the negative angles happened at translation side.

Table 4.8. Movement directions statistical analysis results (°).

	Tipping		Translation		Overall	
	Mean	Standard Deviation	Mean	Standard Deviation	Mean	Standard Deviation
GCS	30.21	17.09	4.36	32.69	17.29	28.81

The means and standard deviations of intrusion and extrusion values were shown in Table 4.9.

Table 4.9. Intrusion and extrusion statistical analysis results (mm).

Tipping		Translation		Overall	
Mean	Standard Deviation	Mean	Standard Deviation	Mean	Standard Deviation
-0.22	0.59	-0.27	0.74	-0.25	0.68

The maxillary canine retraction rates reported varied greatly. For frictionless mechanics, the largest value was more than 2.5 mm/month measured from ten patients by using a calibrated sectional archwire [71], while the smallest one was about 0.6 mm/month measured six patients using a vertical loop which can produce an application of a force rapidly declining in magnitude. [72] The average value was about 1.6 mm/month [46, 50, 71-75]. In this study, the average GCS movement rate was 0.672 mm/month for the tipping side, and 0.448 mm/month for the translation side (28 days per month). The values were relatively small compared to previous studies. The large variety of the movement rate may be caused by many factors, like sample size and retraction appliances. Previous studies quantified relative displacement between two landmarks on the moving and anchorage teeth, respectively. Anchorage loss occurs in the clinic, which affects the measurement. The displacement is commonly described on a point. Choosing

different points result in different displacement especially when a large tipping is involved. These factors were the reasons for the discrepancies in the reported displacement rates.

Description of tooth displacement with respect to a static reference helps clinician to quantify real tooth displacement and effects of various treatment strategies. Many previous studies reported tooth displacement relative to an anchorage tooth, which might move. Thus, the actual displacement was not obtained. The resultant movement rate results expressed in GCS provide absolute tooth displacement relative to the stable anatomical region (rugea area), which are accurate description of tooth movement. Displacement of the moving and anchorage teeth are decoupled so that they can be analyzed separately, which will allow clinicians to quantify the anchorage loss as well. Using this method, the intrusion/extrusion can be reliably quantified, which is not possible from the relative displacement. The direction of the tooth movement relative to the sagittal plan can also be clearly demonstrated. On the other hand, clinicians commonly used distal displacement to evaluate clinical outcomes in the space closure case. This can be done by using the CCS. For this proper, the distal displacement, y_c, was used to calculate movement rate.

When the last TI was included, the movement rates were decreased (Table 4.10). Tipping side decreases were slightly larger than translation side. This was because all the patients had their tipping side closed first. In the study's last treatment interval, tipping side canine completed retraction in the middle of the period, while translation side canine kept moving to close the space through the period. When the total number of days was used to calculate the movement rate, tipping side movement rate became smaller than its actual value.

Table 4.10. Movement rate results in GCS and CCS within the All TIs (mm/day).

	Tipping		Translation		Difference	
	GCS	CCS	GCS	CCS	GCS	CCS
With last interval (R1)	0.024	0.021	0.017	0.015	0.0072	0.0060
Without last interval (R2)	0.024	0.023	0.016	0.015	0.0085	0.0073
R2-R1	0.000	0.002	0.001	0.000	0.0013	0.0013

4.4.3. Conclusions

Corresponding to the first three hypotheses (**H4.1 - 4.3**), the conclusions related to canine movements were:

1. The relationship between canine displacement and treatment time was highly nonlinear. (**H4.1**)
2. The load system is not the only key factor controlling the canine displacement. (**H 4.2**)
3. Using segmental T-loop with a well-controlled load system, large variation in canine displacement can be expected.
4. With the same force magnitude, controlled tipping strategy moves canine faster than translation. This difference is statistically significant for both resultant movement rate in global coordinate system (GCS) and distal/mesial direction movement rate in canine coordinate system (CCS). (**H4.3**)

4.5. Quantification of Anchorage Teeth Movement

4.5.1. Anchorage Teeth Movement Quantification

Fourteen subjects' anchorage teeth movements were quantified by using CBCT maxillary tooth movement procedure (P2, Section 3.5). After obtained one patient's pre- and post-treatment scans, the first step was to standardize the head position in the CBCT scans. The second step was to separate the upper jaw and the 1st molar and 2nd premolars of the two sides from the rest of the image, and create 3D models. The third step was to

define upper jaw coordinate system (UCS, Section 3.2.2.1) on the pre-treatment upper jaw model. Next, the pre- and post-treatment models were superimposed on the anterior inner curve of the hard palate. Following superimposition, the two tooth models in pre- and post-treatment positions were aligned using the entire tooth surface points. Transformation matrix between the two positions was calculated. Then the 1st molar or 2nd premolar's six displacement components in terms of translation along and rotation about the three coordinate axes were computed from the entries of the transformation matrix, and expressed in UCS.

In this study, two types of anchorage reinforcement appliances were used, removable Trans-Palatal Arch (TPA) and fixed TPA. Within the fourteen subjects, eight had removable TPAs; and six had fixed TPAs (Figure 4.13).

Figure 4.13. Removable and fixed TPA.

The comparison between two strategies, controlled tipping (CT) and translation (TR) was done with paired t-test; and the comparison between two types of TPAs was done with two-sample t-test. The equal-variance and normality assumptions were checked using normal probability plots (Figure 4.14). The normal probability plot was performed by using Matlab®.

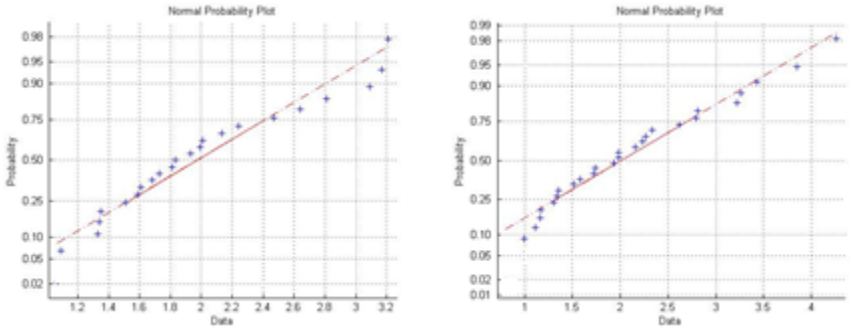

(a) (b)

Figure 4.14. Normal probability plots for anchorage teeth.
(a) 1st Molar; (b) 2nd Premolar

4.5.2. Results and Discussion

4.5.2.1. Anchorage Teeth Movement (**H4.4**)

The movements of two anchorage teeth, 1st molar and 2nd premolar, were shown in Figures 4.15-4.16 and Tables 4.11-4.12. The maximum x direction 1st molar displacement was 0.94 mm; and the maximum y direction 1st molar displacement was 3.16 mm. The maximum x direction 2nd premolar displacement was 1.16 mm; and the maximum y direction 1st molar displacement was 3.73 mm. The average 1st molar displacement in x direction was 0.01 mm (± 0.64 mm), and in y direction was 1.51 mm (± 0.72 mm). The average 2nd premolar displacement in x direction was 0.03 mm (± 1.28 mm), and in y direction was 1.72 mm (± 0.72).

Under the controlled retraction load system, the 1st molars and 2nd premolars moved generally mesially. Relatively large lingual/buccal displacement components existed. Figure 4.15 showed that all of the 1st molars moved in the directions within 45 ° to mesially direction. Figure 4.16 showed that 27 of 28 (14 subjects, each subject has 2 premolars) premolars moved in the directions within 45 ° to mesially direction. The x and y direction displacement for the only one premolar fell out of the 45 ° range were less than 0.5 mm, which was at the translational process error level.

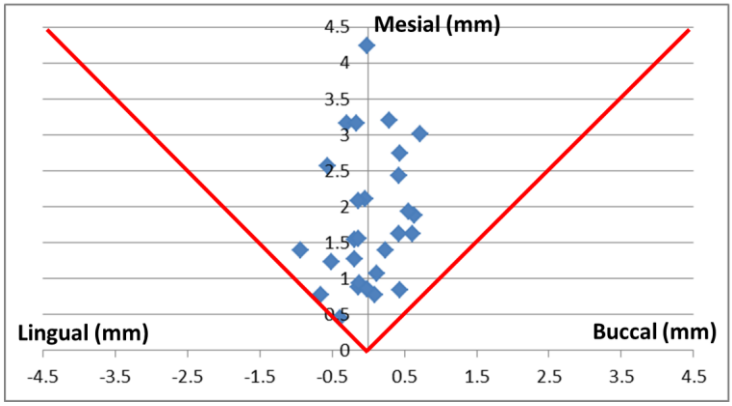

Figure 4.15. 1st Molar movement directions.

Table 4.11. 1st Molar controlled tipping and translation comparison.

	X-direction			Y-direction		
	CT	TR	Diff	CT	TR	Diff
Average	-0.01	-0.01	0.00	1.60	1.41	0.19
Standard Deviation	0.43	0.44	0.64	0.88	0.72	0.72
p-value	0.99			0.34		

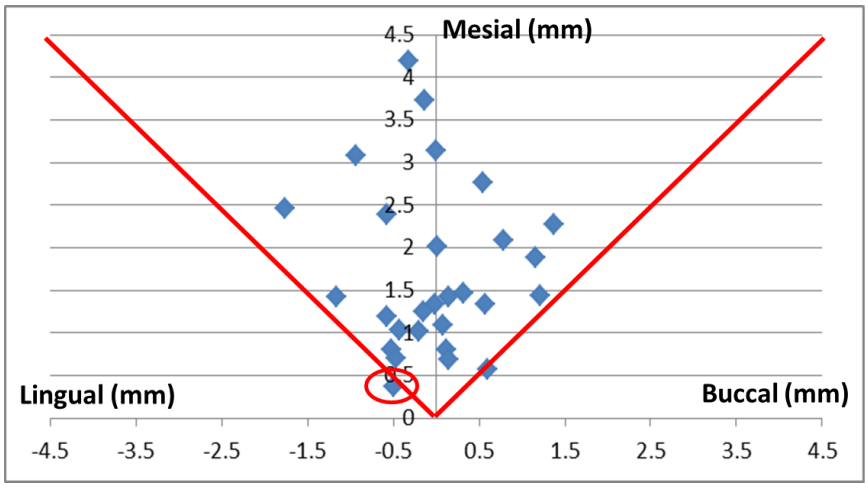

Figure 4.16. 2nd Premolar movement directions.

Table 4.12. 2nd Premolar controlled tipping and translation comparison.

(mm)	X-direction			Y-direction		
	CT	TR	Diff	CT	TR	Diff
Average	-0.10	0.06	-0.16	1.77	1.66	0.12
Standard Deviation	0.82	0.60	1.28	1.06	0.94	0.72
p-value	0.65			0.56		

Even with the reinforced anchorage appliances (removable and fixed TPAs), significant movements were still observed among anchorage teeth. These finds were in accordance with other studies [52-54]. The conclusion was that TPA did not effectively reinforce the posterior anchorage.

4.5.2.2. Comparison between Controlled Tipping and Translation (**H4.5**)

Figure 4.17 and Table 4.11 showed the 1st molar displacements in x and y directions. The data were separated into two groups, controlled tipping (CT) group and translation (TR) group. The averages x direction 1st molar displacements were -0.01 mm for both CT and TR. The *p* value for paired t-test between CT and TR data was 0.99, which was statistically insignificant. The average y direction 1st molar displacement was 1.61 mm (±0.88 mm) for CT, and 1.41 mm (±0.72 mm) for TR. The *p* value for paired t-test between CT and TR data was 0.34, which is also statistically insignificant.

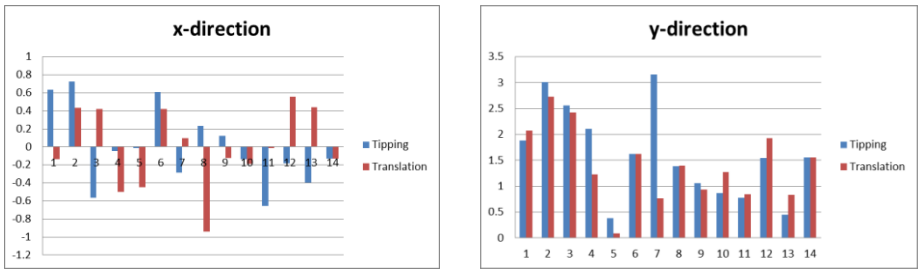

(a) (b)

Figure 4.17. 1st molar controlled tipping and translation comparison.
(a) x-direction (b) y-direction

Figure 4.18 and Table 4.12 showed the 2nd premolar displacements in x and y directions. The data were separated into two groups, controlled tipping (CT) group and translation (TR) group. The average x direction 2nd premolar displacements was -0.10 mm for CT, and 0.06 mm for TR. The *p* value for paired t-test between CT and TR data was 0.65, which was statistically insignificant. The average y direction 1st molar displacement was 1.77 mm (± 1.06 mm) for CT, and 1.66 mm (± 0.94 mm) for TR. The *p* value for paired t-test between CT and TR data was 0.56, which is also statistically insignificant.

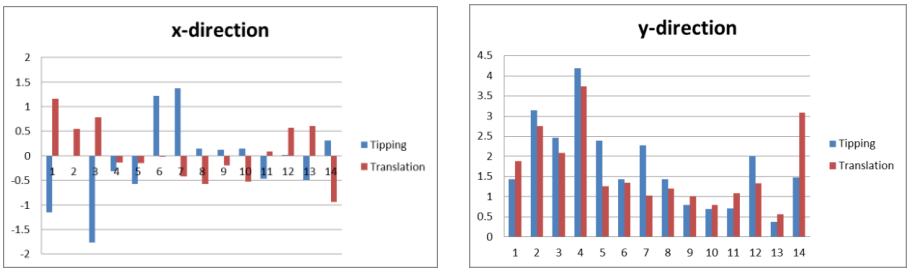

(a) (b)

Figure 4.18. 2nd premolar dontrolled tipping and translation comparison.
(a) x-direction, (b) y-direction

For both 1st molars and 2nd premolars, the teeth displacement differences between CT and TR were not significant (**H4.5**). A possible explanation was that there were large variations in the anchorage teeth movement. This was similar to the canine movement pattern results (Table 4.6).

Since a TPA was attached between two 1st molars, the two 1st molars should move in the same direction in order to keep the distance between the two teeth. However, the 1st molar x-direction displacement data (Figure 4.15 (a)) showed that 7 of 14 patients had different x-direction displacements. Among these patients, only two showed greater than 1 mm distance change between left and right 1st molars and both of the two patients had removable TPA.

Both 1st molars and 2nd premolars had larger variations in x direction displacement than in y direction displacement (Figures 4.15 and 4.16). One reason was that y direction force was the y direction force component was the main focus when the T-loop wire used in this study was designed. The other force components were only kept minimal. Thus, the movements in x direction were not as controlled as the movements in y direction.

For both CT group and TR group, 2nd premolars had larger displacements in both x and y directions than 1st molars did. There were two potential reasons for this observation. First is the geometry difference between 1st molar and 2nd premolar. 1st molars have three or four roots, and the average tooth length is 19.5 mm. 2nd premolars have one to two roots, and the average tooth length is 22.5 mm. 2nd premolar is longer with fewer roots than 1st molar. This made it easier to be moved. Second, the TPA was directly attached to the left and right 1st molars, which gave 1st molars stronger support.

4.5.2.3. Comparison between Removable and Fixed TPA (**H4.6**)

The anchorage data were separated again into two groups based on the type of TPAs, removable group and fixed group. Figure 4.13 showed the 1st molar and 2nd premolar displacements in x direction. The averages x direction 1st molar displacements were 0.07 mm (± 0.51 mm) for removable group, and -0.12 mm (± 0.27 mm) for fixed group. The *p* value for t-test between removable and fixed group data was 0.27, which was statistically insignificant. The averages x direction 2nd premolar displacements were -0.02 mm (± 0.79 mm) for removable group, and -0.03 mm (± 0.62 mm) for fixed group. The *p* value for t-test between removable and fixed group data was 0.80, which was also statistically insignificant.

Table 4.13. Comparison between removable and fixed group in x direction.

(mm)	1st Molar		2nd Premolar	
	Removable	Fixed	Removable	Fixed
Average	0.07	-0.12	-0.02	-0.03
Std	0.51	0.27	0.79	0.62
p-value	0.27		0.80	

Figure 4.14 showed the 1st molar and 2nd premolar displacements in y direction. The averages y direction 1st molar displacements were 1.75 mm (± 0.78 mm) for removable group, and 1.17 mm (± 0.71 mm) for fixed group. The *p* value for t-test between removable and fixed group data was 0.05, which was statistically significant. The averages x direction 2nd premolar displacements were 2.13 mm (± 0.93 mm) for removable group, and 1.16 mm (± 0.78 mm) for fixed group. The *p* value for t-test between removable and fixed group data was 0.001, which was also statistically significant.

Table 4.14. Comparison between removable and fixed group in y direction.

(mm)	1st Molar		2nd Premolar	
	Removable	Fixed	Removable	Fixed
Average	1.75	1.17	2.13	1.16
Std	0.78	0.71	0.93	0.78
p-value	0.05		0.001	

For both 1st molar and 2nd premolar, the differences between removable and fixed group in x direction displacements were statistically insignificant; while the differences in y direction displacements were statistically significant (**H4.6**). The reason was that x direction displacements were much smaller than y direction displacement. The average differences in x direction were only 0.19 mm for 1st molar and 0.01 mm for 2nd premolar, compared with 0.58 mm for 1st molar and 0.97 mm for 2nd premolar in y direction (Tables 4.13 and 4.14).

4.5.3. Conclusion

Corresponding to the last three hypotheses (**H 4.4-4.6**), the conclusions related to anchorage teeth movements were:

1. Anchorage losses were still observed in patients with removable or fixed TPA. (**H 4.4**)
2. No significant difference in anchorage loss was found between controlled tipping and translation strategies. (**H 4.5**)
3. Fixed TPA provided significant better anchorage control than removable TPA in mesial-distal direction. (**H 4.6**)

5. IMAGE ANALYSIS IN MANDIBULAR GROWTH STUDY

5.1. Introduction

Numerous children in the United States have excessive overjet (Figure 5.1), mainly caused by deficient mandibles. There is a fundamental lack of knowledge on effective approaches to stimulate mandibular growth and correct mandibular deficiency in growing individuals.

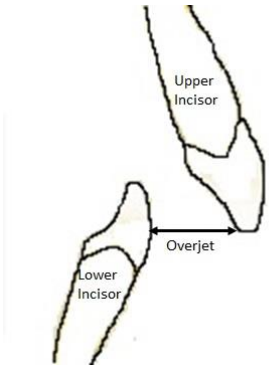

Figure 5.1. Overject.

Condylar changes in traditional two-dimensional (2D) cephalograms are obscure, which might cause misleading interpretation and lead to false clinical judgment. Three-dimensional (3D) Cone-beam Computed Tomography (CBCT) is capable of clearly evaluating the morphology of the condyle. In this study, the patients are treated using either Mandibular Anterior Reposition Appliance (MARA) or Herbst appliances (Figure 5.2). Herbst appliance (Figure 5.2a), are commonly used because of requiring no patient compliance. However, its oblique force vector (Figure 5.2b) pushes the mouth open, which rotates the mandible backward and impedes the treatment goal of “mandibular advancement”. MARA is a relative new appliance designed to avoid mandibular

backward rotation (Figure 5.2c). Because the MARA "positions" or "guides" the mandible forward instead of directly pushing the dentition, it advances the mandible without rotating mandible backward (Figure 2d and 2e). Although, in theory, MARA provides more favorable effects than the Herbst appliance, the effects have not been compared clinically.

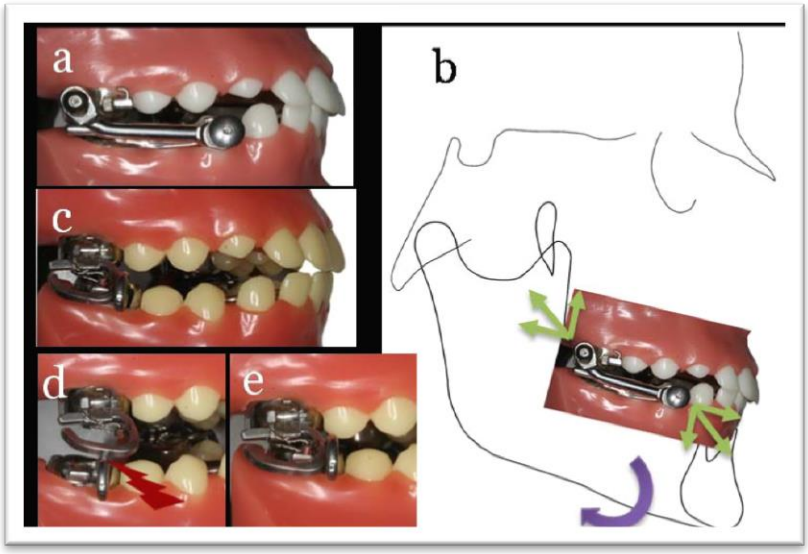

Figure 5.2. Herbst and MARA appliances.

The goal of this study was to (1) establish a novel and valid 3D analysis method to evaluate condylar growth and skeletal effects on patients treated by class II functional appliances; (2) compare the treatment outcomes and side effects of two different appliances.

5.2. Subjects

Total number of ten patients with large overject and retrusive mandible (mandible posterior to its normal position, Figure 5.3) were enrolled in this randomized controlled clinical trial. For each patient, before- and after-treatment 3D CBCT scans were taken using i-CAT®. The scan was 0.3 mm resolution with enhanced portrait mode. The images were saved as DICOM format files and processed with MIMICS®.

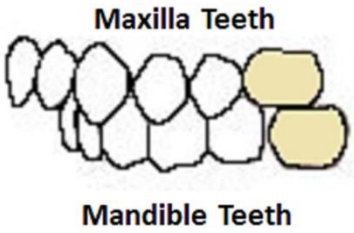

Figure 5.3. Retrusive mandible.

5.3. Hypotheses and Parameters

The hypotheses for this study are:

H5.1: Herbst appliance causes mandibular forward movement with backward rotation.

H5.2: MARA guides greater mandibular advancement and condylar growth, compared to Herbst appliance.

The hypotheses were tested with the following parameters:

Landmark displacement relative to cranial base is defined as the displacement obtained after the before- and after-treatment models are superimposed on cranial base. It is expressed in a rectangular coordinate system with six displacement components, three translations and three rotations. This displacement shows the effect of the mandible changes to the whole face.

Landmark displacement relative to mandibular stable structures is defined as the displacement obtained after the before- and after-treatment models are superimposed on mandibular stable structures. It is expressed in a rectangular coordinate system with six displacement components, three translations and three rotations. This displacement gives the actual mandibular landmark points movements during the treatment.

5.4. Quantification of Skeletal Landmark Movements

Selected skeletal landmark movements were quantified by using CBCT skeletal landmark procedure (P3, Section 3.6). After obtained one subject's pre- and post-treatment scans, the first step was to standardize the head position in the CBCT scans. Then, the whole skull digital model was isolated from the rest of the tissues, followed by separating the mandibular digital model from the skull. For each subject, two skull models, pre- (SK1) and post-treatment (SK2), and two corresponding mandible models (pre-treatment, MD1; post-treatment, MD2) were generated (Figure 5.4).

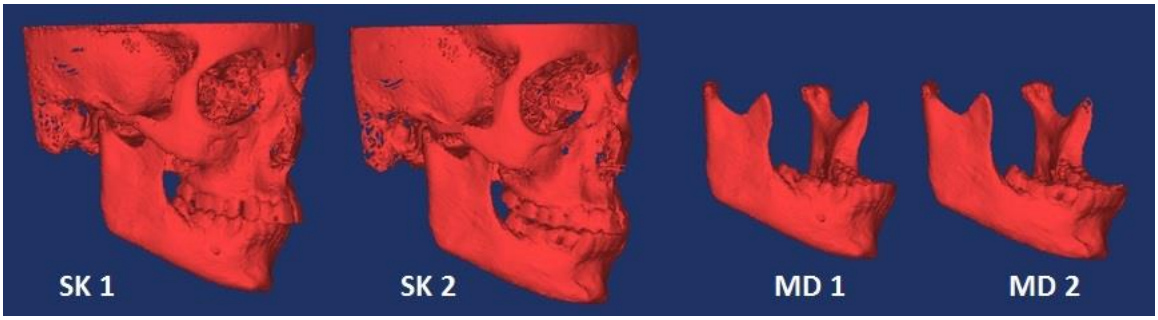

Figure 5.4. Whole skull and mandible digital models.

To quantify landmark movements relative to anterior cranial base, the first step was to define CBCS (Section 3.2.2.2) on SK1. Then SK1 and SK2 were superimposed on anterior cranial base (Figure 5.5). After SK1 and SK2 were in the comparable position, the coordinates of the selected landmarks in both SK1 and SK2 needed to be identified in CBCS. The landmark movements relative to anterior cranial base were calculated based on the coordinates of landmarks in CBCS (Section 3.4.2).

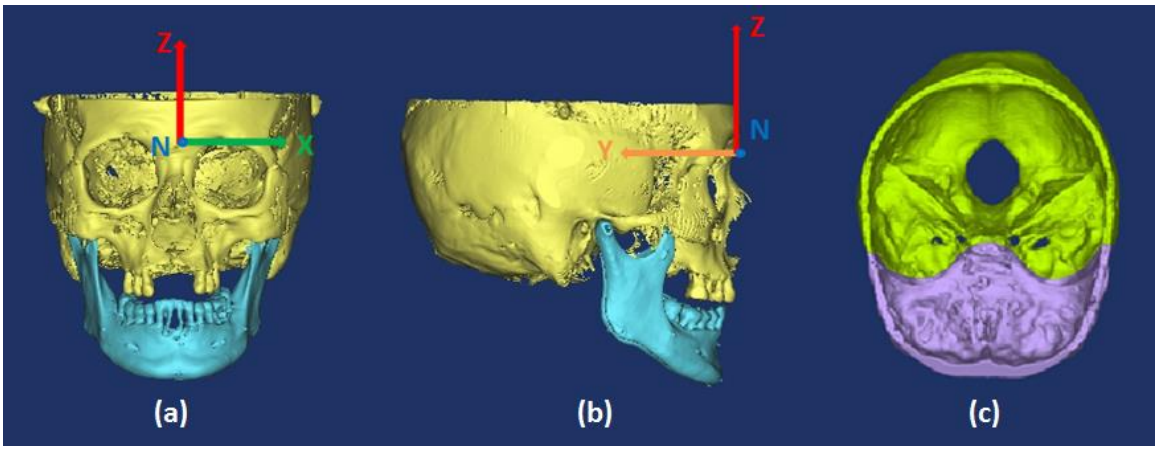

Figure 5.5. CBCS and superimposition on anterior cranial base.
(a) and (b) CBCS; (c) superimposition on anterior cranial base

Similar procedure was used for quantifying landmark movements relative to mandible stable structure. The first step was to define MCS (Section 3.2.2.2, Figure 3.12) on MD1. Then MD1 and MD2 were superimposed on mandible (Figure 5.6). After MD1 and MD2 were in the comparable position, the coordinates of the selected landmarks in both MD1 and MD2 needed to be identified in MCS. The landmark movements relative to mandible were calculated based on the coordinates of landmarks in MCS (Section 3.4.2).

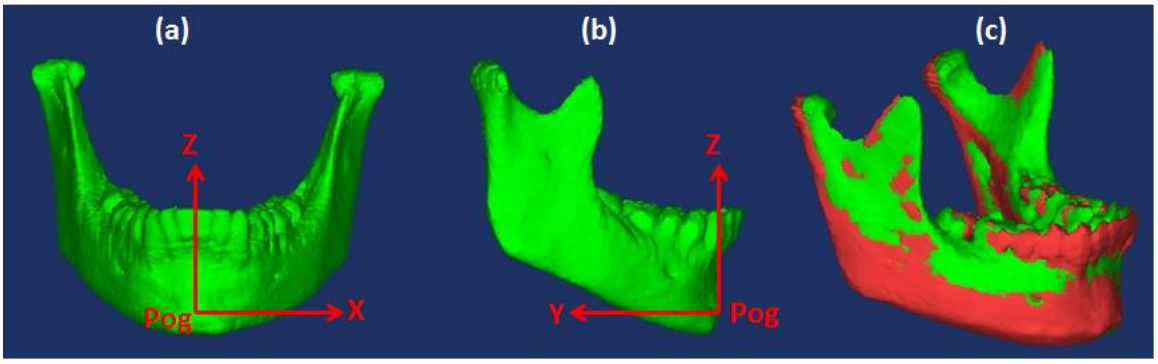

Figure 5.6. MCS and superimposition on mandible.
(a) and (b) MCS; (c) superimposition on mandible

Twelve skeletal landmarks were selected for calculation (Table 5.1, Figure 5.7). Three of them (ANS, PNS and A) was on upper jaw, and the other nine were on lower jaw. Among the nine lower jaw landmarks, four (Con_L, Con_R, ML Con_L, and ML Con_R) were on the tips of the condyles; three (B, Pog, and Me) were on the lower mandible body; and the other two (Go_L and Go_R) were at the midpoints of the contour connecting the ramus and mandible body.

Table 5.1. Skeletal landmarks definition.

ANS	Anterior nasal spine	**Go_L**	Left gonion
PNS	Posterior nasal spine	**Go_R**	Right gonion
A	A point	**Con_L**	Left condylion
B	B point	**Con_R**	Right condylion
Pog	Pogonion	**ML Con_L**	Left medial and lateral pole
Me	Menton	**ML Con_R**	Right medial and lateral pole

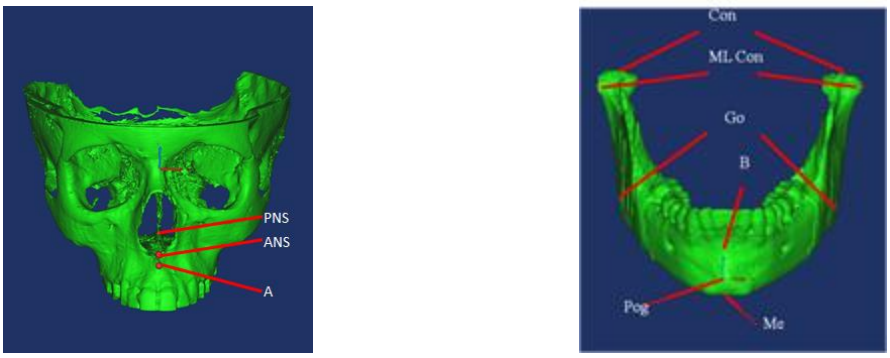

(a) (b)

Figure 5.7. Selected skeletal landmarks location.

5.5. Results and Discussion

5.5.1. Skeletal Landmarks Displacement for Herbst Appliance

Skeletal landmark displacements relative to cranial base for Herbst appliance were shown in Tables 5.2, 5.3. For translational displacement components, the maximum x direction average translation magnitude was 1.20 mm (± 1.30 mm) at Me and B points; the maximum y direction average translation magnitude was 3.50 mm (± 2.68 mm) at Me point; and the maximum z direction average translation magnitude was 3.38 mm (± 4.51 mm) at B point (Table 5.2). All upper jaw landmarks (A, ANS, PNS) had less than 1 mm translational displacement components in three directions. For rotational displacement components, the maximum x direction average rotation magnitude was 2.72 ° (± 3.29 °) at A point; the maximum y direction average rotation magnitude was 0.90 ° (± 0.42 °) at Con_R point; and the maximum z direction average rotation magnitude was 21.26 ° (± 35.98 °) at A point (Table 5.3).

Table 5.2. Skeletal landmarks translational displacement relative to cranial base (Herbst group).

(mm)	x		y		z	
	Ave.	Std.	Ave.	Std.	Ave.	Std.
Pog	1.07	1.26	-2.69	1.96	-1.47	4.71
Me	1.20	1.30	-3.50	2.86	-1.55	4.51
B	1.20	1.30	-2.23	1.91	-3.38	4.51
Go_R	-0.91	1.15	-1.37	1.42	-1.13	2.16
Go_L	1.11	0.99	-1.19	2.09	-0.35	2.47
Con_R	-0.91	2.44	0.27	1.02	0.63	3.62
ML Con_R	0.03	0.07	0.27	0.81	0.61	2.43
Con_L	-0.04	0.58	0.32	0.92	0.06	2.33
ML Con_L	0.40	0.55	0.67	1.38	0.07	1.62
ANS	0.36	1.22	0.06	1.43	0.52	3.09
PNS	0.39	1.16	0.71	1.09	-0.26	2.45
A	0.48	1.02	-0.89	3.48	-0.41	2.65

Table 5.3. Skeletal landmarks rotational displacement relative to cranial base (Herbst group).

(°)	x		y		z	
	Ave.	Std.	Ave.	Std.	Ave.	Std.
Pog	1.53	1.39	-0.63	0.77	-10.79	25.51
Me	1.70	1.82	-0.71	0.83	16.28	32.74
B	1.43	1.46	-0.76	0.80	-14.68	42.54
Go_R	-0.57	1.18	-0.11	0.99	0.71	0.88
Go_L	-1.07	0.67	-0.35	0.65	-1.01	1.12
Con_R	0.84	2.10	0.90	0.42	0.76	1.76
ML Con_R	0.96	1.70	0.10	1.82	0.01	0.62
Con_L	-0.03	1.46	0.17	1.68	0.24	0.66
ML Con_L	-0.04	1.18	0.12	1.03	0.08	0.50
ANS	0.18	1.88	-0.27	1.24	-5.19	21.25
PNS	0.62	1.17	-0.39	1.26	1.75	3.51
A	2.72	3.29	-0.32	0.97	21.26	35.98

Based on the definitions for CBCS (Section 3.2.2.2, Figures 3.10), YZ plane was the sagittal plane in the coordinate system. In mandibular growth treatment, the displacement components on sagittal plane (y-, z-direction translations and x direction rotation) were more important for orthodontists to evaluate the treatment outcomes. The y- and z-direction translations and x-direction rotations relative to cranial base for herbst group were shown in Figures 5.8 and 5. 9. The mandible landmarks (Pog, Me, and B) had negative values in both y- and z-direction translations. As Figure 5.5 (b) shown, negative y and z values means that mandible pushed forward and downward relative to cranial base. Figure 5.9 showed that mandible landmarks also had positive x-direction rotations, which means that mandible had backward rotations (Figure 5.10) (**H5.1**).

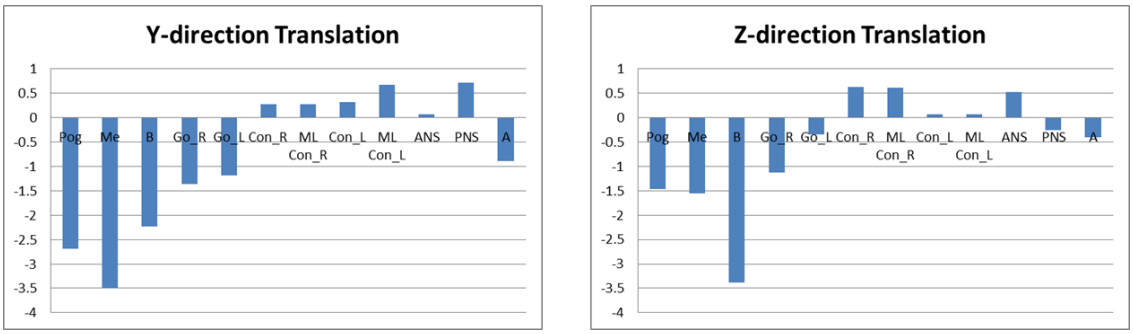

Figure 5.8. Y- and Z-direction translations relative to cranial base (Herbst group).

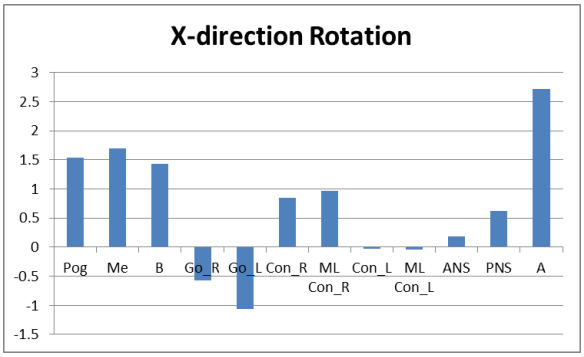

Figure 5.9. Z-direction rotations relative to cranial base (Herbst group).

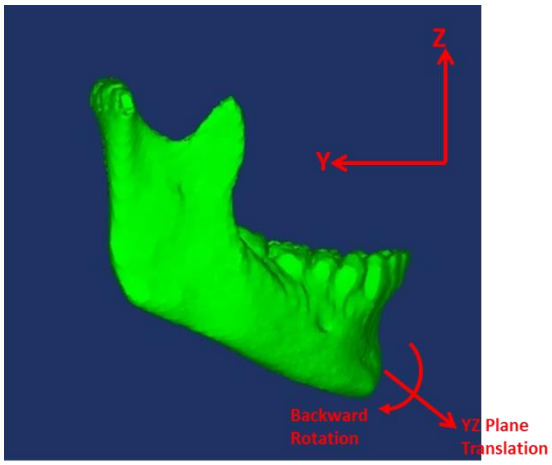

Figure 5.10. Mandible landmarks movement relative to cranial base (Herbst group).

Skeletal landmark displacements relative to mandible for Herbst appliance were shown in Tables 5.4 and 5.5. For translational displacement components, the maximum x direction average translation magnitude was 2.28 mm (± 2.54 mm) at Con_R point; the maximum y direction average translation magnitude was 2.41 mm (± 1.77 mm) at ML Con_R point; and the maximum z direction average translation magnitude was 3.28 mm (± 1.36 mm) at Con_L point (Table 5.4). For rotational displacement components, the maximum x direction average rotation magnitude was 14.07 ° (± 29.38 °) at Go_R point; the maximum y direction average rotation magnitude was 15.53 ° (± 31.98 °) at Con_L point; and the maximum z direction average rotation magnitude was 30.95 ° (± 36.27 °) at Me point (Table 5.5).

Table 5.4. Skeletal landmarks translational displacement relative to mandible (Herbst).

(mm)	x		y		z	
	Ave.	Std.	Ave.	Std.	Ave.	Std.
Me	0.72	1.05	-0.76	0.75	-0.46	0.54
B	-0.50	0.99	0.18	1.04	-2.26	2.39
Go_R	-0.82	1.46	1.60	0.97	0.78	1.67
Go_L	1.16	0.51	0.74	1.27	2.50	1.22
Con_R	-2.28	2.54	2.35	2.70	2.80	1.90
ML Con_R	-0.33	0.88	2.41	1.77	2.71	1.38
Con_L	-0.40	1.00	1.27	1.52	3.28	1.36
ML Con_L	0.06	0.72	1.75	1.71	3.27	0.65

Table 5.5. Skeletal landmarks rotational displacement relative to mandible (Herbst).

(°)	x		y		z	
	Ave.	Std.	Ave.	Std.	Ave.	Std.
Me	-8.49	13.68	-6.59	8.05	-30.95	36.27
B	-1.11	3.16	3.45	3.35	-10.55	18.52
Go_R	14.07	29.38	15.32	32.63	-9.42	20.95
Go_L	1.49	0.84	7.82	19.66	13.46	31.29
Con_R	1.31	2.13	14.12	31.64	-12.41	29.84
ML Con_R	0.53	0.92	1.74	1.90	-0.70	2.08
Con_L	0.78	1.35	-15.53	31.98	13.28	29.58
ML Con_L	0.92	0.85	-1.41	2.01	0.50	1.66

Based on the definitions for MCS (Section 3.2.2.2, Figures 3.11), YZ plane was the sagittal plane in the coordinate system. Like Figures 5.8 and 5.9, the y- and z-direction translations and x-direction rotations relative to mandible for herbst group were shown in Figures 5.11 and 5.12. The condyle landmarks (Con_R, Con_L, ML Con_R, and ML Con_L) had positive y- and z-direction translations and positive x-direction rotation. The positive translations means that the condyle growth backward and upward (Figure 5.13). The x-direction rotation for all condyle landmarks were less than 1.5 °.

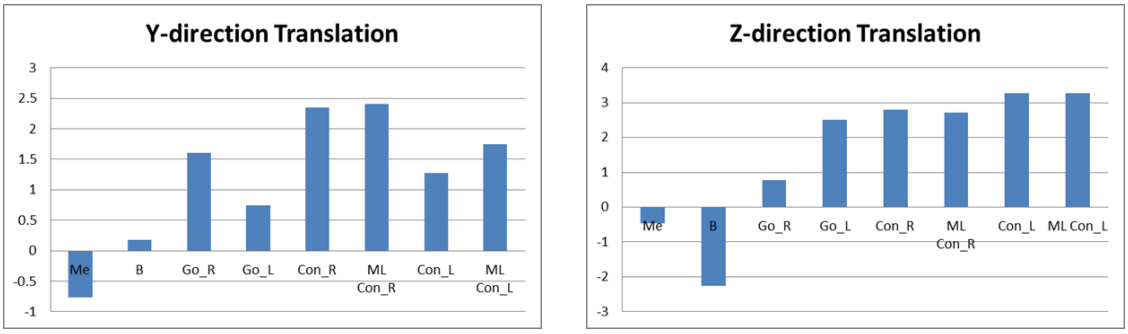

Figure 5.11. Y- and Z-direction translations relative to mandible (Herbst group).

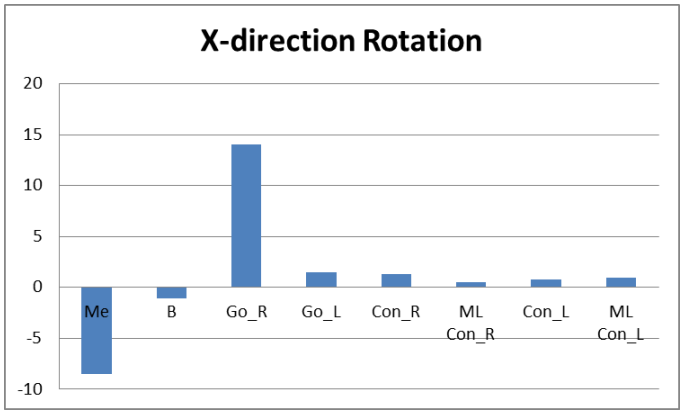

Figure 5.12. Z-direction rotations relative to mandible (Herbst group).

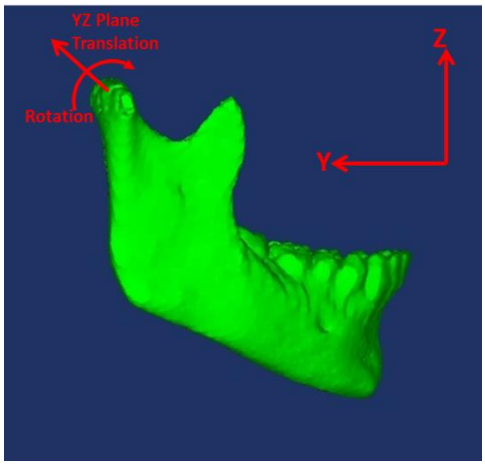

Figure 5.13. Condyle landmarks movement relative to mandible (Herbst group).

5.5.2. Comparison on Landmark Displacements between Herbst and MARA Appliances

Skeletal landmark displacements relative to cranial base for MARA appliance were shown in Tables 5.6 and 5.7. For translational displacement components, the maximum x direction average translation magnitude was 1.34 mm (± 2.60 mm) at Pog point; the maximum y direction average translation magnitude was 3.44 mm (± 3.29 mm) at Me point; and the maximum z direction average translation magnitude was 2.83 mm (± 1.51 mm) at Pog point (Table 5.6). All upper jaw landmarks (A, ANS, PNS) had less than 0.2 mm translational displacement components in three directions. For rotational displacement components, the maximum x direction average rotation magnitude was 1.63 ° (± 0.84 °) at B point; the maximum y direction average rotation magnitude was 0.76 ° (± 0.77 °) at Con_R point; and the maximum z direction average rotation magnitude was 27.17 ° (± 32.67 °) at A point (Table 5.7).

Table 5.6. Skeletal landmarks translational displacement relative to cranial base (MARA group).

(mm)	x		y		z	
	Ave.	Std.	Ave.	Std.	Ave.	Std.
Pog	-1.34	2.60	-2.33	3.05	-2.83	1.51
Me	-1.18	2.59	-3.44	3.29	-1.76	0.90
B	-1.28	2.59	-2.54	3.52	-1.68	1.56
Go_R	-0.28	1.82	-1.59	3.77	-1.41	1.69
Go_L	-0.31	1.01	-2.02	3.73	-2.27	1.23
Con_R	1.29	2.65	0.49	3.45	-0.17	1.14
ML Con_R	-0.43	0.61	0.59	3.76	-0.01	0.76
Con_L	-0.82	2.98	0.00	3.64	-0.39	1.42
ML Con_L	0.04	0.71	-0.98	3.89	-0.32	1.46
ANS	0.36	0.94	-0.07	0.80	-0.69	1.90
PNS	0.15	1.12	-0.16	0.34	-0.45	0.91
A	-0.53	1.32	-0.16	1.13	0.23	2.21

Table 5.7. Skeletal landmarks rotation displacement relative to cranial base (MARA group).

(°)	x		y		z	
	Ave.	Std.	Ave.	Std.	Ave.	Std.
Pog	-1.19	0.98	0.03	1.96	18.93	23.46
Me	-1.62	1.35	0.05	1.86	-10.32	36.71
B	-1.63	0.84	0.13	2.30	27.17	32.67
Go_R	-1.33	1.53	-0.09	1.35	1.08	1.47
Go_L	-1.23	0.92	0.76	0.77	-0.44	0.99
Con_R	-0.13	1.24	0.07	2.97	0.47	3.01
ML Con_R	-0.34	0.32	0.20	0.59	0.72	0.81
Con_L	-0.04	1.39	0.65	2.58	0.69	1.72
ML Con_L	-0.46	1.26	0.45	1.34	-0.04	0.73
ANS	0.15	0.79	-1.40	1.46	5.81	11.86
PNS	-0.52	0.44	-1.47	1.70	3.62	10.17
A	-0.88	0.98	-0.23	1.74	-0.52	2.08

Similar to the Herbst group results, the y- and z-direction translations were shown in Figure 5.14; and the x-direction rotations were shown in Figure 5.15. The mandible landmarks (Pog, Me, and B) had negative values in both y- and z-direction translations. As Figure 5.5 (b) shown, negative y and z values means that mandible pushed forward and downward relative to cranial base. Figure 5.15 showed that mandible landmarks had negative x-direction rotations, which means that mandible had forward rotations (Figure 5.16).

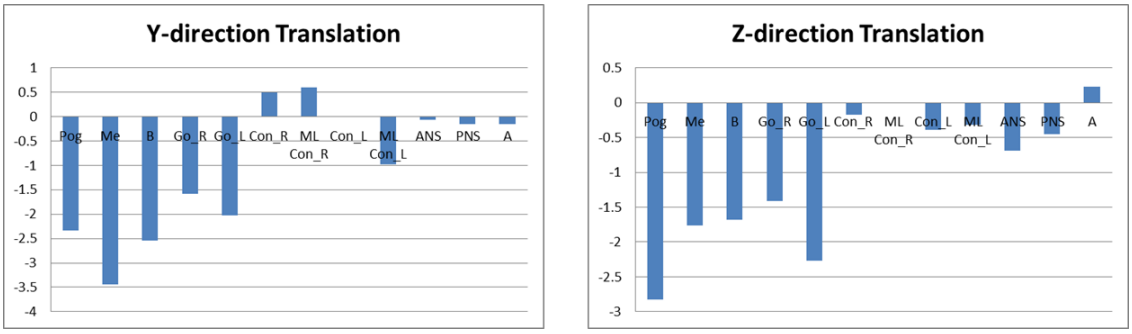

Figure 5.14. Y- and Z-direction translations relative to cranial base (MARA group).

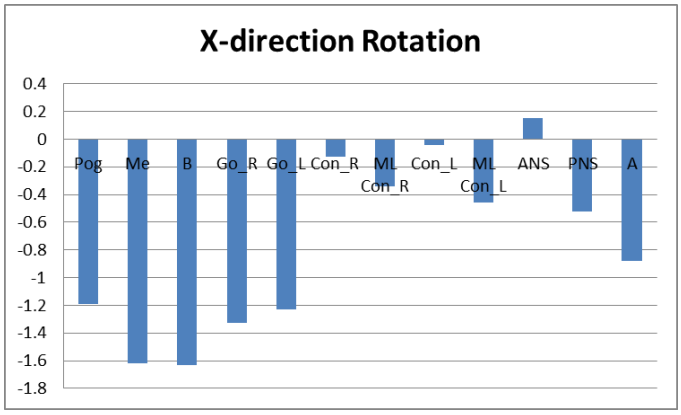

Figure 5.15. Z-direction rotations relative to cranial base (MARA group).

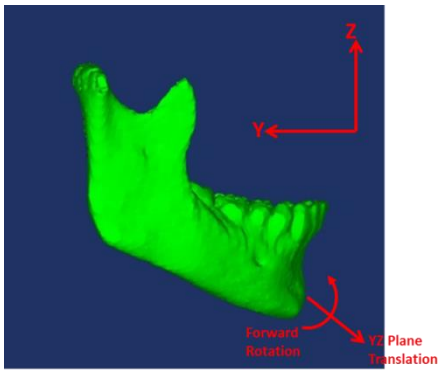

Figure 5.16. Mandible landmarks movement relative to cranial base (MARA group).

Skeletal landmark displacements relative to mandible for MARA appliance were shown in Tables 5.8 and 5.9. For translational displacement components, the maximum x direction average translation magnitude was 1.52 mm (± 2.04 mm) at B point; the maximum y direction average translation magnitude was 2.63 mm (± 4.59 mm) at Con_R point; and the maximum z direction average translation magnitude was 3.59 mm (± 3.17 mm) at Go_L point (Table 5.8). For rotational displacement components, the maximum x direction average rotation magnitude was 7.32 ° (± 38.59 °) at Me point; the maximum y direction average rotation magnitude was 16.91 ° (± 40.65 °) at Go_R point; and the maximum z direction average rotation magnitude was 13.78 ° (± 27.97 °) at Con_L point (Table 5.9).

Table 5.8. Skeletal landmarks translational displacement relative to mandible (MARA group).

(mm)	x		y		z	
	Ave.	Std.	Ave.	Std.	Ave.	Std.
Me	-1.51	1.53	1.07	4.41	1.01	2.99
B	-1.52	2.04	0.78	3.10	1.32	2.58
Go_R	-0.65	1.66	0.68	2.01	-2.23	4.82
Go_L	-1.52	1.76	0.21	1.47	-3.95	3.17
Con_R	0.22	1.21	2.63	4.59	-1.59	3.92
ML Con_R	-0.20	0.43	2.38	4.14	-1.13	4.22
Con_L	-0.02	1.89	1.75	2.71	-2.80	4.10
ML Con_L	-0.17	1.64	1.83	0.90	-2.52	4.03

Table 5.9. Skeletal landmarks rotational displacement relative to mandible (MARA group).

(°)	x		y		z	
	Ave.	Std.	Ave.	Std.	Ave.	Std.
Me	7.32	38.59	-7.26	31.67	12.72	35.23
B	1.48	6.26	-2.90	12.54	-2.97	28.15
Go_R	-1.36	3.20	16.91	40.65	-6.88	13.79
Go_L	-2.50	1.61	7.21	9.04	13.75	31.15
Con_R	-2.18	1.44	14.34	31.60	-13.61	25.85
ML Con_R	-1.98	1.91	0.72	2.36	-2.52	0.90
Con_L	-2.28	1.07	-14.22	33.80	13.78	27.97
ML Con_L	-1.59	0.91	0.35	2.67	1.19	2.47

Similar to the Herbst group results, the y- and z-direction translations were shown in Figure 5.17; and the x-direction rotations were shown in Figure 5.18. The condyle landmarks (Con_R, Con_L, ML Con_R, and ML Con_L) had positive y-direction translations, negative z-direction translations, and negative x-direction rotations. The positive y-direction and negative z-direction translations means that the condyle growth backward and downward (Figure 5.19). The negative x-direction rotation means that condyle growth counter clockwise (Figure 5.19).

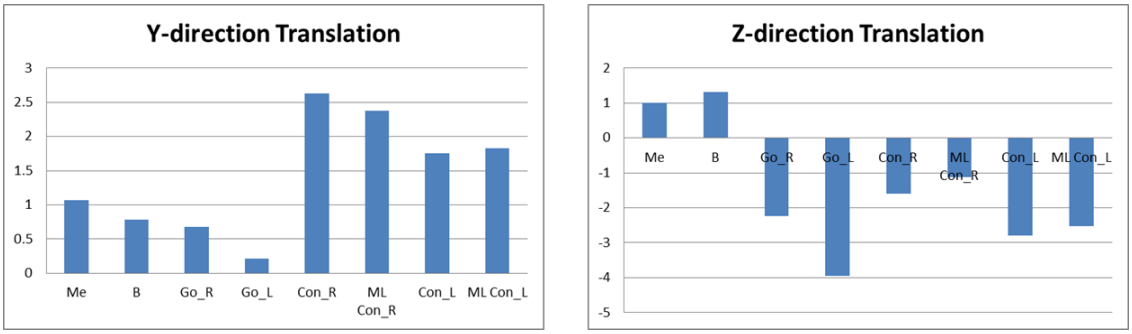

Figure 5.17. Y- and Z-direction displacements relative to mandible (MARA group).

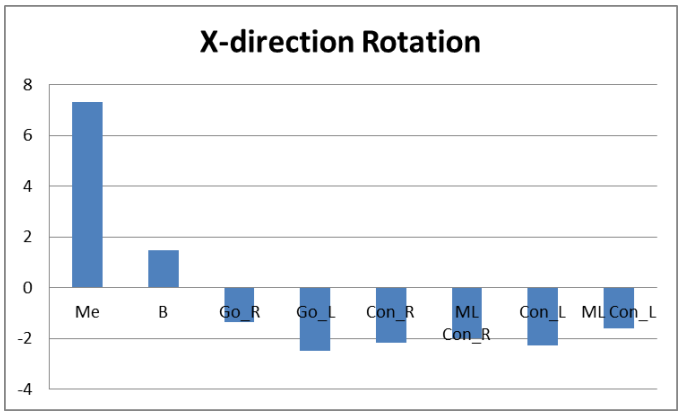

Figure 5.18. Z-direction rotations relative to mandible (MARA group).

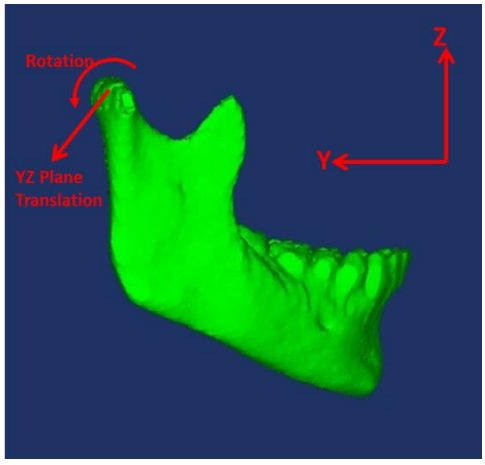

Figure 5.19. Condyle landmarks movement relative to mandible (MARA group).

Results of comparison on landmark translational displacement relative to cranial base were shown in Tables 5.10, 5.11 and Figure 5.20. For translational displacements, only the x direction translation at Go_L showed statistically significant the difference between Hebst and MARA group. For rotational displacements, the x direction rotation at Con_L and ANS, the y direction rotation at Go_L and the z direction rotation at Go_L and ML Con_R showed statistically significant the difference between Hebst and MARA group.

Table 5.10. Comparison on landmark translational displacement relative to cranial base.

(mm)	x		y		z	
	Diff	*p*-value	Diff	*p*-value	Diff	*p*-value
Pog	2.41	0.16	-0.36	0.66	1.35	0.62
Me	2.38	0.15	-0.06	0.94	0.22	0.93
B	2.48	0.14	0.31	0.54	-1.71	0.53
Go_R	-0.62	0.20	0.23	0.80	0.28	0.74
Go_L	1.42	0.05	0.84	0.53	1.92	0.25
Con_R	-2.20	0.23	-0.22	0.83	0.80	0.66
ML Con_R	0.46	0.16	-0.32	0.79	0.62	0.64
Con_L	0.77	0.59	0.32	0.68	0.44	0.65
ML Con_L	0.36	0.48	1.65	0.05	0.39	0.73
ANS	0.01	0.99	0.13	0.86	1.21	0.21
PNS	0.24	0.77	0.86	0.17	0.19	0.85
A	1.01	0.21	-0.73	0.66	-0.64	0.57

Table 5.11. Comparison on landmark rotational displacement relative to cranial base.

(°)	x		y		z	
	Diff	*p*-value	Diff	*p*-value	Diff	*p*-value
Pog	-0.34	0.53	-0.66	0.56	-29.72	0.10
Me	-0.08	0.85	-0.76	0.48	26.61	0.28
B	0.20	0.70	-0.88	0.51	-41.85	0.14
Go_R	0.76	0.13	-0.03	0.97	-0.37	0.67
Go_L	0.16	0.77	-1.11	0.02	-0.57	0.01
Con_R	0.97	0.28	0.83	0.81	0.29	0.89
ML Con_R	1.30	0.12	-0.10	0.92	-0.71	0.01
Con_L	0.01	0.99	-0.48	0.76	-0.45	0.60
ML Con_L	0.41	0.66	-0.33	0.74	0.12	0.70
ANS	0.03	0.97	1.13	0.37	-11.00	0.47
PNS	1.14	0.16	1.08	0.37	-1.87	0.73
A	3.61	0.12	-0.09	0.93	21.78	0.27

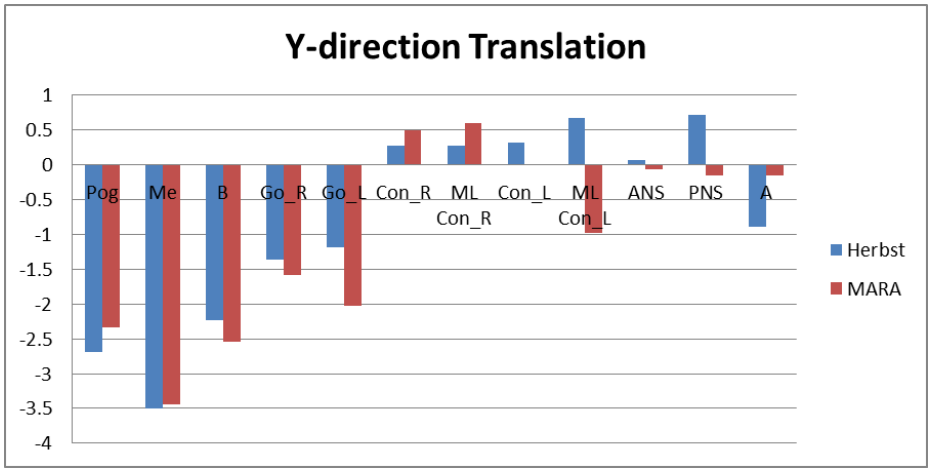

(a)

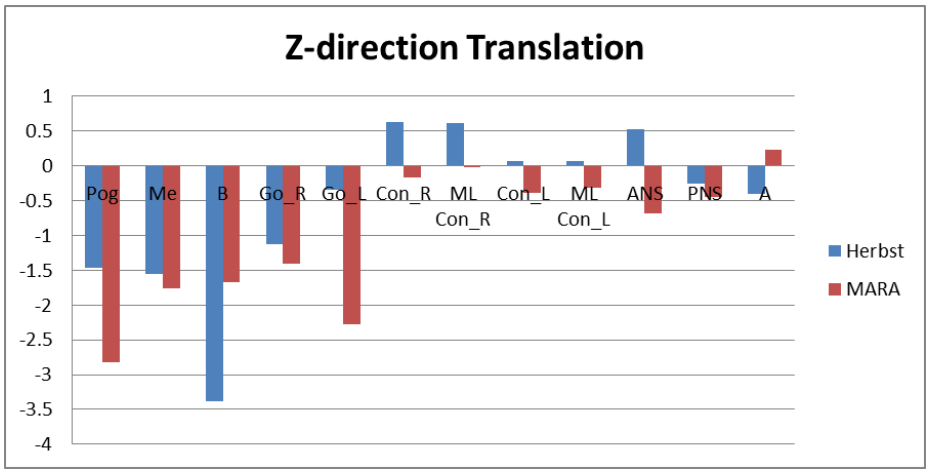

(b)

Figure 5.20. Comparison on landmark translational displacement relative to cranial base.

Results of comparison on landmark translational displacement relative to cranial base were shown in Tables 5.12 and 5.13. For translational displacements, the x direction translation at Go_L, and the z direction translation at Go_L, Con_R, Con_L, and ML Con_L showed statistically significant the difference between Hebst and MARA group. For rotational displacements, the x direction rotation at Go_L, Con_R, ML Con_R, Con_L and ML Con_L showed statistically significant the difference between Hebst and MARA group.

Table 5.12. Comparison on landmark translational displacement relative to mandible.

(mm)	x		y		z	
	Diff	*p*-value	Diff	*p*-value	Diff	*p*-value
Me	2.23	0.09	-1.82	0.46	-1.47	0.39
B	2.01	0.14	-0.59	0.75	-3.58	0.12
Go_R	-0.17	0.89	0.92	0.34	3.00	0.25
Go_L	2.67	0.02	0.54	0.53	6.45	0.02
Con_R	-2.51	0.07	-0.28	0.86	4.39	0.01
ML Con_R	-0.13	0.83	0.03	0.98	3.84	0.09
Con_L	-0.38	0.75	-0.48	0.64	6.07	0.01
ML Con_L	0.22	0.83	-0.08	0.88	5.79	0.04

Table 5.13. Comparison on landmark rotational displacement relative to mandible.

(°)	x		y		z	
	Diff	*p*-value	Diff	*p*-value	Diff	*p*-value
Me	-15.81	0.45	0.67	0.96	-43.68	0.10
B	-2.59	0.43	6.35	0.30	-7.58	0.70
Go_R	15.43	0.32	-1.60	0.95	-2.54	0.85
Go_L	3.99	0.00	0.61	0.96	-0.30	0.99
Con_R	3.49	0.02	-0.21	0.99	1.21	0.95
ML Con_R	2.52	0.04	1.02	0.48	1.81	0.09
Con_L	3.06	0.00	-1.31	0.96	-0.50	0.98
ML Con_L	2.51	0.00	-1.76	0.35	-0.69	0.60

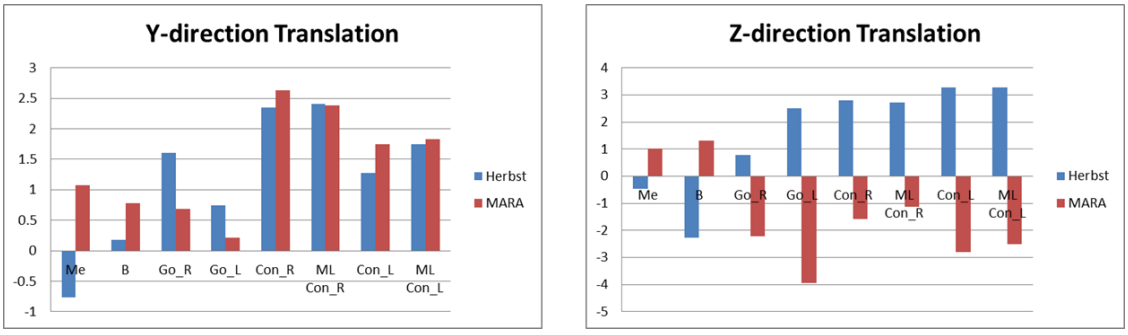

Figure 5.21. Comparison on landmark translational displacement relative to mandible.

When considering the landmark movements relative to cranial base, 2.8% translational displacement components and 11% rotational displacement components showed statistically significant difference between Herbst and MARA group. For landmark movements relative to mandible, 13.9% translational displacement components and 13.9% rotational displacement components showed statistically significant difference between Herbst and MARA group. Most of the significant differences showed at the condyle tip landmarks. One of the potential explanations was that the main purpose of Herbst and MARA appliances was to stimulate the condyle to grow. If there were difference treatment effects between the two appliances, the landmarks on condyle should have more significant responds.

The purposes of Herbst and MARA appliances were to push the mandible forward and stimulate the condyle to grow backward for adapting back to the cranial base. The amount of mandible forward was quantified with displacements relative to cranial base. Based on the definition of CBCS (Figure 5.6 (a) and (b)), y-direction displacements in CBCS represented the forward-backward movement. The y-direction displacements of mandible landmarks in CBCS showed no significant differences between Herbst and MARA appliances (Table 5.10). In order to insure the relation between condyle and cranial base (i.e., have the condyle adapt back to the cranial base), the displacements of condyle landmarks in CBCS should be small enough. Table 5.2 and 5.6 showed that y- and z-direction translations of all condyle landmarks in CBCS were less than 1 mm for both appliances.

The amount of condyle backward growth was quantified with displacements relative to mandible. Base on the definition of MCS (Figure 5.7 (a) and (b)), y-direction displacements in MCS represented the forward-backward movement. The y-direction displacements of condyle landmarks in MCS showed no significant differences between Herbst and MARA appliances, either (Table 5.12). Thus, **H5.2** is not true.

5.6. Conclusions

After evaluating condylar growth and skeletal effects on patients treated by class II functional appliances using a 3D analysis method, the following conclusions can be drawn:

1. Herbst appliance causes mandibular forward movement with backward rotation; while MARA appliance causes mandibular forward movement with forward rotation. (**H5.1**)
2. There were no evidence showed that MARA guides greater mandibular advancement and condylar growth, compared to Herbst appliance. (**H5.2**)

6. DISCUSSION AND CONCLUSIONS

6.1. Discussion

The main advantage of the methods is that they do real 3D analysis. The inputs of the methods are 3D images, and the outputs of the methods are 3D displacement components. Two different kinds of dental records are selected, one is the dental cast, and the other is the Cone-Beam Computed Tomography (CBCT) images. The dental cast is the most widely used 3D record in orthodontic clinic and the CBCT becomes increasingly used. During an orthodontic treatment, a set of dental casts are made at each important milestone. These casts can help the orthodontists to trace and monitor the treatment outcomes. The method using dental casts will have broad applications. CBCT is a relatively new technology to obtain the digital 3D models of the patients' jaws. With CBCT images, doctors are able to not only evaluate the crown as in the cast case, but also check the roots of the teeth. Currently, the images are used primarily for qualitative evaluation. However, more meaningful information can be collected from the images if parameters can be quantified. The methods developed in this study can be used for this purpose.

CBCT images have advantages than the dental casts. The methods proposed require stable anatomical structures used as the references to align two models. Certain bony structures in the CBCT are more stable, thus are better than the palatal region as reference in the cast method. In some orthodontic treatments such as palatal expansion, the palatal region changes, shifting the reference area, which disqualifies it. However, even though CBCT method has its advantages, its radiation exposure dose is still of concern, especially for young patients. Therefore, a better way to use 3D images in clinic is to integrate the two methods as presented in the canine retraction application.

The methods have been applied in two different types of orthodontic treatments, canine retraction and mandibular growth. In both applications, the 3D methods are used to quantify the treatment outcomes and evaluation side effects. In the canine retraction study, two commonly used treatment strategies, controlled tipping and translation, were compared. Both the canine displacement results and the anchorage loss results showed very large variations in both displacement magnitude and movement pattern, even though the initial forces and moments were well controlled. This study revealed an important fact that tooth displacements are not uniquely controlled by the initial load system. There should be more factors which affect the treatment outcome, such as initial alignment of the tooth to the alveolar bone, the alveolar bone quality, the bone modeling and remodeling cycles, genotype, and personal biological reaction to the load. Further studies will be needed to identify the dominant parameters affecting the tooth movement rate and pattern. These findings are essential for optimizing treatment and new appliances design. In the mandibular growth study, two widely used appliances, Herbst and MARA, were compared. Even though, theoretically, MARA can provide more favorable effect to stimulate condyle growth and avoid dental and condylar relapse, there were no enough evidences to suggest that MARA appliance can give better treatment results.

6.2. Conclusions

Orthodontic treatment outcomes, tooth displacement and bony changes, can be quantified by using systematic 3D image analysis methods developed in this study. The methods have proper accuracy and consistency for clinical use. The results obtained from the 3D methods can be used to test orthodontic hypotheses.

The findings from the two clinical studies are listed below. In canine retraction treatment,

- The relationship between canine displacement and treatment time was highly nonlinear;

- The load system is not the only key factor controlling the canine displacement;
- Using segmental T-loop with a well-controlled load system, large variation in canine displacement can be expected;
- With the same force magnitude, controlled tipping strategy moves canine faster than translation. This difference is statistically significant for both resultant movement rate in global coordinate system (GCS) and distal/mesial direction movement rate in canine coordinate system (CCS);
- Anchorage losses were still observed in patients with removable or fixed TPA;
- No significant difference in anchorage loss was found between controlled tipping and translation strategies;
- Fixed TPA provided significant better anchorage control than removable TPA in mesial-distal direction.

In mandibular growth treatment,

- Herbst appliance causes mandibular forward movement with backward rotation;
- There were no evidence showed that MARA guides greater mandibular advancement and condylar growth, compared to Herbst appliance.

LIST OF REFERENCES

LIST OF REFERENCES

[1] C. A. Hurst, *et al.*, "Surgical cephalometrics: applications and developments," *Plast Reconstr Surg*, vol. 120, pp. 92e-104e, Nov 2007.

[2] W. J. Updegrave, "The Role of Panoramic Radiology in Diagnosis," *Oral Surg*, vol. 22, pp. 49-57, 1966.

[3] P. S. Horton, *et al.*, "Panoramic radiography--an adjunct," *Oral Surg Oral Med Oral Pathol*, vol. 43, pp. 473-7, Mar 1977.

[4] G. A. Zach, Langland, O. E., and Sippy, F. H., "The Use of the Orthopantomogrpha in Longitudinal Studies," *Oral Surg*, vol. 39, pp. 42-50, 1969.

[5] K. O. Turner, "Limitations of panoramic radiography," *Oral Surg Oral Med Oral Pathol*, vol. 26, pp. 312-20, Sep 1968.

[6] M. M. Alattar, *et al.*, "A survey of panoramic radiographs for evaluation of normal and pathologic findings," *Oral Surg Oral Med Oral Pathol*, vol. 50, pp. 472-8, Nov 1980.

[7] H. E. Lyon, "Reliability of panoramic radiography in the diagnosis of maxillary sinus pathosis," *Oral Surg Oral Med Oral Pathol*, vol. 35, pp. 124-8, Jan 1973.

[8] W. B. Downs, "Analysis of the dentofacial profile," *Angle Orthodontist*, vol. 26, pp. 191-212, 1956.

[9] C. Steiner, "The use of cephalometrics as an aid to planning and assessing orthodontic treatment," *American Journal of orthodontics*, vol. 46, pp. 721-735, 1960.

[10] R. M. Rcketts, "Cephalometric analysis and synthesis," *Angle Orthodontist*, vol. 31, pp. 141-156, 1961.

[11] W. R. Proffit, D. M. Sarver, *Contemporary Orthodontics 4th Edition*: Elsevier Health Sciences, 2006.

[12] I. L. Nielsen, "Maxillary superimposition: a comparison of three methods for cephalometric evaluation of growth and treatment change," *Am J Orthod Dentofacial Orthop,* vol. 95, pp. 422-31, May 1989.

[13] Z. M. Arat, *et al.*, "The displacement of craniofacial reference landmarks during puberty: a comparison of three superimposition methods," *Angle Orthod,* vol. 73, pp. 374-80, Aug 2003.

[14] C. Steiner, "Cephalometrics in clinical practice," *Angle Orthod,* vol. 29, pp. 8-29, 1959.

[15] B. Broadbent, "Bolton Standards and Technique in Orthodontic Practice," *Angle Orthod,* vol. 7, pp. 209-33, 1937.

[16] W. R. Proffit, *et al.*, *Contemporary orthodontics*, 4th ed. St. Louis, Mo.: Mosby Elsevier, 2007.

[17] A. Bjork, "Facial growth in man, studied with the aid of metallic implants," *Acta Odontol Scand,* vol. 13, pp. 9-34, Jun 1955.

[18] A. Bjork, "Variations in the growth pattern of the human mandible: longitudinal radiographic study by the implant method," *J Dent Res,* vol. 42(1)Pt 2, pp. 400-11, Jan-Feb 1963.

[19] A. Bjork and V. Skieller, "Facial development and tooth eruption. An implant study at the age of puberty," *Am J Orthod,* vol. 62, pp. 339-83, Oct 1972.

[20] A. Bjork, "Prediction of mandibular growth rotation," *Am J Orthod,* vol. 55, pp. 585-99, Jun 1969.

[21] A. Bjork and V. Skieller, "Normal and abnormal growth of the mandible. A synthesis of longitudinal cephalometric implant studies over a period of 25 years," *Eur J Orthod,* vol. 5, pp. 1-46, Feb 1983.

[22] M. Lamichane, *et al.*, "Accuracy of reconstructed images from cone-beam computed tomography scans," *Am J Orthod Dentofacial Orthop,* vol. 136, pp. 156 e1-6; discussion 156-7, Aug 2009.

[23] P. Commer, *et al.*, "Construction and testing of a computer-based intraoral laser scanner for determining tooth positions," *Med Eng Phys,* vol. 22, pp. 625-35, Nov 2000.

[24] J. L. Ashmore, *et al.*, "A 3-dimensional analysis of molar movement during headgear treatment," *Am J Orthod Dentofacial Orthop,* vol. 121, pp. 18-29; discussion 29-30, Jan 2002.

[25] L. Keilig, *et al.*, "Applications of surface-surface matching algorithms for determination of orthodontic tooth movements," *Comput Methods Biomech Biomed Engin,* vol. 6, pp. 353-9, Oct-Dec 2003.

[26] B. K. Cha, *et al.*, "Analysis of tooth movement in extraction cases using three-dimensional reverse engineering technology," *Eur J Orthod,* vol. 29, pp. 325-31, Aug 2007.

[27] J. F. Sherrard, *et al.*, "Accuracy and reliability of tooth and root lengths measured on cone-beam computed tomographs," *Am J Orthod Dentofacial Orthop,* vol. 137, pp. S100-8, Apr 2010.

[28] B. Hassan, *et al.*, "Influence of scanning and reconstruction parameters on quality of three-dimensional surface models of the dental arches from cone beam computed tomography," *Clin Oral Investig,* vol. 14, pp. 303-10, Jun 2010.

[29] L. H. Cevidanes, *et al.*, "Three-dimensional cone-beam computed tomography for assessment of mandibular changes after orthognathic surgery," *Am J Orthod Dentofacial Orthop,* vol. 131, pp. 44-50, Jan 2007.

[30] L. H. Cevidanes, *et al.*, "Superimposition of 3-dimensional cone-beam computed tomography models of growing patients," *Am J Orthod Dentofacial Orthop,* vol. 136, pp. 94-9, Jul 2009.

[31] J. H. Choi and J. Mah, "A new method for superimposition of CBCT volumes," *J Clin Orthod,* vol. 44, pp. 303-12, May 2010.

[32] K. Tai, *et al.*, "Using superimposition of 3-dimensional cone-beam computed tomography images with surface-based registration in growing patients," *J Clin Pediatr Dent,* vol. 34, pp. 361-7, Summer 2010.

[33] R. M. Nada, *et al.*, "Accuracy and reproducibility of voxel based superimposition of cone beam computed tomography models on the anterior cranial base and the zygomatic arches," *PLoS One,* vol. 6, p. e16520, 2011.

[34] H. Lee and H. Hong, "Hybrid surface- and voxel-based registration for MR-PET brain fusion," *Image Analysis and Processing - Iciap 2005, Proceedings,* vol. 3617, pp. 930-937, 2005.

[35] J. Chen, *et al.*, "Quantification of tooth displacement from cone-beam computed tomography images," *Am J Orthod Dentofacial Orthop,* vol. 136, pp. 393-400, Sep 2009.

[36] M. Alves, Jr., *et al.*, "Assessment of mini-implant displacement using cone beam computed tomography," *Clin Oral Implants Res,* vol. 22, pp. 1151-6, Oct 2011.

[37] H. J. Cho, "A three-dimensional cephalometric analysis," *J Clin Orthod,* vol. 43, pp. 235-52, discussion 235; quiz 273, Apr 2009.

[38] J. J. Pilon, *et al.*, "Magnitude of orthodontic forces and rate of bodily tooth movement. An experimental study," *Am J Orthod Dentofacial Orthop,* vol. 110, pp. 16-23, Jul 1996.

[39] T. Kohno, *et al.*, "Experimental tooth movement under light orthodontic forces: rates of tooth movement and changes of the periodontium," *J Orthod,* vol. 29, pp. 129-35, Jun 2002.

[40] E. J. Van Leeuwen, *et al.*, "Rate of orthodontic tooth movement after changing the force magnitude: an experimental study in beagle dogs," *Orthod Craniofac Res,* vol. 13, pp. 238-45, Nov 2010.

[41] E. J. van Leeuwen, *et al.*, "Tooth movement with light continuous and discontinuous forces in beagle dogs," *Eur J Oral Sci,* vol. 107, pp. 468-74, Dec 1999.

[42] Y. Ren, *et al.*, "Optimum force magnitude for orthodontic tooth movement: a mathematic model," *Am J Orthod Dentofacial Orthop,* vol. 125, pp. 71-7, Jan 2004.

[43] P. Owman-Moll, *et al.*, "Effects of a doubled orthodontic force magnitude on tooth movement and root resorptions. An inter-individual study in adolescents," *Eur J Orthod,* vol. 18, pp. 141-50, Apr 1996.

[44] P. Owman-Moll, *et al.*, "The effects of a four-fold increased orthodontic force magnitude on tooth movement and root resorptions. An intra-individual study in adolescents," *Eur J Orthod,* vol. 18, pp. 287-94, Jun 1996.

[45] J. A. Yee, *et al.*, "Rate of tooth movement under heavy and light continuous orthodontic forces," *Am J Orthod Dentofacial Orthop,* vol. 136, pp. 150 e1-9; discussion 150-1, Aug 2009.

[46] K. Hayashi, *et al.*, "Comparison of maxillary canine retraction with sliding mechanics and a retraction spring: a three-dimensional analysis based on a midpalatal orthodontic implant," *Eur J Orthod,* vol. 26, pp. 585-9, Dec 2004.

[47] M. Mezomo, *et al.*, "Maxillary canine retraction with self-ligating and conventional brackets," *Angle Orthod,* vol. 81, pp. 292-7, Mar 2011.

[48] K. D. Dholakia and S. R. Bhat, "Clinical efficiency of nonconventional elastomeric ligatures in the canine retraction phase of preadjusted edgewise appliance therapy: an in-vivo study," *Am J Orthod Dentofacial Orthop,* vol. 141, pp. 715-22, Jun 2012.

[49] B. Thiruvenkatachari, *et al.*, "Comparison of rate of canine retraction with conventional molar anchorage and titanium implant anchorage," *Am J Orthod Dentofacial Orthop,* vol. 134, pp. 30-5, Jul 2008.

[50] R. P. Martins, *et al.*, "Changes over time in canine retraction: an implant study," *Am J Orthod Dentofacial Orthop,* vol. 136, pp. 87-93, Jul 2009.

[51] A. Hart, *et al.*, "The effectiveness of differential moments in establishing and maintaining anchorage," *Am J Orthod Dentofacial Orthop,* vol. 102, pp. 434-42, Nov 1992.

[52] M. Sharma, *et al.*, "Mini-screw implant or transpalatal arch-mediated anchorage reinforcement during canine retraction: a randomized clinical trial," *J Orthod,* vol. 39, pp. 102-10, Jun 2012.

[53] P. E. Benson, *et al.*, "Midpalatal implants vs headgear for orthodontic anchorage--a randomized clinical trial: cephalometric results," *Am J Orthod Dentofacial Orthop,* vol. 132, pp. 606-15, Nov 2007.

[54] H. L. Zablocki, *et al.*, "Effect of the transpalatal arch during extraction treatment," *Am J Orthod Dentofacial Orthop,* vol. 133, pp. 852-60, Jun 2008.

[55] E. J. Clemmer, Hayes, E. W., "Paatient cooperation in wearing heardgear.," *Am J Orthod,* vol. 75, pp. 517-524, 1975.

[56] R. H. Samuels, *et al.*, "A national survey of orthodontic facebow injuries in the UK and Eire," *Br J Orthod,* vol. 23, pp. 11-20, Feb 1996.

[57] G. N. Holland, Wallance, D. A., Mondino, B.J., Cole, S.H. Ryan, S.J., "Severe ocular injuries from orthodontic headgear," *Arch Ophthalmol,* vol. 103, pp. 649-651, 1985.

[58] G. Dickson, "Contact dermatitis and vervical headgear," *Br Dent J,* vol. 155, p. 112, 1983.

[59] J. Odman, Lekholm, U., Jemt, T., Thilander, B., "Osseointegrated implants as orthodontic anchorage in the treatment of partially edentulous adult patients," *Eur J Orthod,* vol. 31, pp. 763-767, 1997.

[60] W. E. Roberts, *et al.*, "Rigid endosseous implant utilized as anchorage to protract molars and close an atrophic extraction site," *Angle Orthod,* vol. 60, pp. 135-52, Summer 1990.

[61] M. S. Block and D. R. Hoffman, "A new device for absolute anchorage for orthodontics," *Am J Orthod Dentofacial Orthop,* vol. 107, pp. 251-8, Mar 1995.

[62] J. S. Lee, *et al.*, "Micro-implant anchorage for lingual treatment of a skeletal Class II malocclusion," *J Clin Orthod,* vol. 35, pp. 643-7; quiz 620, Oct 2001.

[63] H. M. Kyung, *et al.*, "Development of orthodontic micro-implants for intraoral anchorage," *J Clin Orthod,* vol. 37, pp. 321-8; quiz 314, Jun 2003.

[64] L. H. Cevidanes, *et al.*, "Three-dimensional quantification of mandibular asymmetry through cone-beam computerized tomography," *Oral Surg Oral Med Oral Pathol Oral Radiol Endod,* vol. 111, pp. 757-70, Jun 2011.

[65] "Optix 400S Laser Scanner Parameters," in *http://www.3ddigitalcorp.com/Products/optix.shtml*, Last accessed: Jul 20, 2011.

[66] I. T. Inc., "RapidForm 2006 Help Documentation," 2006.

[67] M. Group, "Mimics 10.11 Help Documentation," 2007.

[68] B. R. Hoggan and C. Sadowsky, "The use of palatal rugae for the assessment of anteroposterior tooth movements," *Am J Orthod Dentofacial Orthop,* vol. 119, pp. 482-8, May 2001.

[69] M. A. Almeida, *et al.*, "Stability of the palatal rugae as landmarks for analysis of dental casts," *Angle Orthod,* vol. 65, pp. 43-8, 1995.

[70] P. J. Besl and N. D. Mckay, "A Method for Registration of 3-D Shapes," *Ieee Transactions on Pattern Analysis and Machine Intelligence,* vol. 14, pp. 239-256, Feb 1992.

[71] K. Tanne, *et al.*, "Biomechanical behavior of the periodontium before and after orthodontic tooth movement," *Angle Orthod,* vol. 65, pp. 123-8, 1995.

[72] J. Daskalogiannakis and K. R. McLachlan, "Canine retraction with rare earth magnets: an investigation into the validity of the constant force hypothesis," *Am J Orthod Dentofacial Orthop,* vol. 109, pp. 489-95, May 1996.

[73] R. Hasler, *et al.*, "A clinical comparison of the rate of maxillary canine retraction into healed and recent extraction sites--a pilot study," *Eur J Orthod,* vol. 19, pp. 711-9, Dec 1997.

[74] B. W. Lee, "The force requirements for tooth movement, Part I: Tipping and bodily movement," *Aust Orthod J,* vol. 13, pp. 238-48, Mar 1995.

[75] M. A. Darendeliler, *et al.*, "The drum spring (DS) retractor: constant and continuous force for canine retraction," *Eur J Orthod,* vol. 19, pp. 115-30, Apr 1997.

VITA

VITA

Name: SHUNING LI Email: li33@iupui.edu

EDUCATIONAL BACKGROUND

Ph.D. Mechanical Engineering Purdue University, May 2013

M.S. Mechanical Engineering Purdue School of Engineering and Technology, IUPUI, May 2008

M.S. Mechanical Engineering Tsinghua University, China, Jul 2005

B.S. Mechanical Engineering Hebei University of Technology, China, Jul 2002

AWARDS AND HONORS

- 2008-2009: IUPUI University Fellowship Award
- Jun 2008: Third Place Award in the MS student paper competition in 2008 Summer Bioengineering Conference
- Apr 2008: Aydin Ungan Award for Outstanding Mechanical Engineering Graduate Student

RESEARCH AREAS AND INTERESTS

- Biomechanics
- Medical Image Processing
- Information System Modeling Technology and Implementation Methodology

PUBLICATIONS

Z. Xia, J. Chen, F. Jiang, **S. Li**, R. Viecilli, and S. Liu, "Load System of Segmental T-Loops for Canine Retraction," American Journal of Orthodontics & Dentofacial Orthopedics, 2013 (Submitted).

J. Chen, **S. Li**, and S. Fang, "Quantification of tooth displacement from cone-beam computed tomography images," American Journal of Orthodontics & Dentofacial Orthopedics, vol. 136, pp. 393-400, Sep 2009.